NASA CONTRACTOR REPORT

NASA CR-842

HIGH-PERFORMANCE "ONCE-THROUGH" BOILING OF POTASSIUM IN SINGLE TUBES AT SATURATION TEMPERATURES OF 1500° TO 1750° F

by J. R. Peterson

Prepared by
GENERAL ELECTRIC COMPANY
Cincinnati, Ohio
for Lewis Research Center

NATIONAL AERONAUTICS AND SPACE ADMINISTRATION • WASHINGTON, D. C. • AUGUST 1967

HIGH-PERFORMANCE "ONCE-THROUGH" BOILING OF POTASSIUM IN SINGLE TUBES AT SATURATION TEMPERATURES OF 1500° TO 1750° F

By J. R. Peterson

Prepared under Contract No. NAS 3-2528 by
GENERAL ELECTRIC COMPANY
Missile and Space Division
Cincinnati, Ohio

for Lewis Research Center

NATIONAL AERONAUTICS AND SPACE ADMINISTRATION

For sale by the Clearinghouse for Federal Scientific and Technical Information
Springfield, Virginia 22151 – CFSTI price $3.00

FOREWORD

The work described in this report is part of an alkali metal boiling and condensing heat transfer program conducted by the General Electric Company under NASA Contract NAS 3-2528. The work was done under the technical management of Ruth N. Weltmann, Space Power Systems Division, NASA Lewis Research Center.

ABSTRACT

The results of boiling potassium experiments conducted with a sodium-heated Haynes-25 alloy test facility at temperatures to 1750° F are presented. The results include data and correlations for the critical heat flux, transition boiling heat transfer coefficient and boiling pressure loss, as well as a few values of the superheated vapor heat transfer coefficient. Potassium heat transfer coefficients averaged over the entire tube length in boiling are also presented. The data are applied to the design of a large power boiler, which is analyzed with respect to uncertainties in the design variables.

TABLE OF CONTENTS

LIST OF FIGURES

LIST OF FIGURES (Cont'd)

LIST OF FIGURES (Cont'd)

LIST OF TABLES

NOMENCLATURE

Latin Letter Symbols

A	Area	ft^2
a_R	Radial Acceleration developed by the inserts	g's
B	Constant in Equation (5)	$(°F)^2$
b	Constant in Equation (5)	dimensionless
C	Constant pressure heat capacity	$Btu/(lb_m-°F)$
c	Constant in Equation (5)	dimensionless
D	Tube diameter	inches
E	Thermocouple error	°F
f	Darcy-Weisbach friction factor	dimensionless
G	Mass velocity	$lb_m/(ft^2-sec)$
g	Acceleration due to gravity	$ft/(sec^2)$
g_c	Conversion factor	$32.2\ (ft-lb_m)/(sec^2-lb_f)$
H	Enthalpy	Btu/lb_m
h	Heat transfer coefficient	$Btu/(hr-ft^2-°F)$
h_{fg}	Latent heat of vaporization	$Btu/(lb_m)$
J	Conversion factor	$778\ (ft-lb_f)/Btu$
K	Slip ratio; ratio of average vapor velocity to average liquid velocity	dimensionless
k	Thermal conductivity	$Btu/(hr-ft-°F)$
L	Boiler tube length	inches
P	Static pressure	psia
P/D	Insert twist ratio, tube diameters per 360° revolution of helix	dimensionless
Q	Rate of heat transfer	Btu/sec
q	Heat flux	$Btu/(hr-ft^2)$
R	Thermal resistance	$(hr-ft^2-°F)/Btu$
T	Temperature	°F
t	Time	seconds
U	Overall heat transfer coefficients	$Btu/(hr-ft^2-°F)$
V	Velocity	ft/sec
W	Mass flow rate	lb_m/sec
w	Angular velocity	radians/sec
x	Flowing quality	dimensionless
z	Distance along boiler tube from potassium inlet	inches

Greek Letter Symbols

α	Void fraction	dimensionless
Δ	Difference	
Δ_T	Insert tape thickness	inches
θ	Angular displacement	radians
θ_R	Vapor residence time in superheated vapor region	sec
μ	Viscosity	$lb_m/(ft\text{-}hr)$
ρ	Density	lb_m/ft^3
Φ	Two-phase frictional pressure loss multiplier integrated with respect to quality from 0 to x	dimensionless
ϕ	Local two-phase frictional pressure loss multiplier	dimensionless
δ_{SH}	Degrees of vapor superheat, $(T-T_{sat})$	°F

Subscripts

a	Axial or axial component
B	Boiling
c	Refers to point of critical heat flux
cb	Centerbody of helix insert
e	Equivalent
F	Flow, friction
f	Refers to the liquid phase
G	Refers to pressure gages
g	Refers to the vapor phase
H	Helical
i	Inside, inlet
IS	Refers to the point where bulk vapor superheating commences
IB	Refers to the point where boiling commences
K	Potassium
L	Losses

Subscripts (Continued)

M	Refers to momentum component of two-phase pressure loss
m	Measured
Na	Sodium
NB	Nucleate boiling
O	Overall
o	Outlet, outside
p	Primary fluid
R	Radial
s	Shell
sat	Refers to the saturation curve
si	Refers to the inside of the boiler shell
sc	Refers to the subcooled heating region
SH	Refers to the vapor superheating region
T	Total, Tape, Tangential
t	Tube
TB	Refers to the transition boiling region
TP	Two-phase
TPF	Two-phase friction
v	Refers to vapor phase
w	Wall

Dimensionless Groups

N_{Nu}	Nusselt number, $\frac{hD}{k}$
N_{Pe}	Peclet number, $\frac{DGC}{k}$
N_{Pr}	Prandtl number, $\frac{C\mu}{k}$
N_{Re}	Reynolds number, $\frac{DG}{\mu}$

SUMMARY

Boiling potassium heat transfer results obtained in a two-fluid Haynes 25 alloy facility are presented. The single-tube test section used is a shell and tube heat exchanger, approximately eight feet long, in which boiling potassium in vertical upflow in the tube is heated by sodium flowing in the annulus. Boiler tubes of 0.92-inch and 0.67-inch inside diameter were tested, both with and without instrumented vortex generator inserts. Boiling heat transfer and pressure loss data were obtained from 10% quality to over 200°F of vapor superheat at the test section exit over the boiler exit temperature range from 1500°F to 1750°F with average heat fluxes up to more than 300,000 Btu/hr-ft^2. The results include data and correlations for the critical heat flux, transition boiling heat transfer coefficient and boiling pressure loss, as well as a few values for the superheated vapor heat transfer coefficient. Potassium heat transfer coefficients averaged over the entire length of the tube in boiling are also presented.

The results obtained demonstrate the feasibility of high-performance "once-through" boiling of potassium in tubes containing vortex generator inserts. The boiling heat transfer and pressure loss data and correlations presented provide a reasonable basis for thermal design of "once-through" potassium boilers for space power application. In illustration of this, design procedures based upon the experimental results and an example thermal analysis of a large power boiler producing potassium vapor at 2150°F with 150°F of superheat are presented, together with an analysis of the significance to design of uncertainties in the main design variables.

I INTRODUCTION

Since 1961 an experimental program has been conducted by the General Electric Company for the National Aeronautics and Space Administration to clarify some of the problems associated with forced convection vaporization and condensation of potassium and to provide basic heat transfer information needed for development of Rankine cycle space power systems using potassium as the working fluid. One concept under consideration for the boilers of Rankine cycle space power systems is the "once-through" boiling process, in which a subcooled liquid is transformed into a saturated or superheated vapor in one continuous pass through heated tubes. This concept is attractive for space power application because it removes the need for a boiler recirculation loop, which results in increased reliability and reduced weight by elimination of the additional pump, flow control and separate superheater required by recirculating boilers.

A Haynes-25 test facility, employing a sodium-heated single-tube boiler, was used to approximate the two-fluid boiling conditions anticipated in space power systems. This facility was employed to investigate the forced convection vaporization of potassium, as applied to the "once-through" concept, in several single tube geometries, both with and without vortex generator inserts, at potassium temperatures to 1750°F. Data from these experiments include boiling potassium heat transfer data as a function of vapor quality up to more than 200°F of vapor superheat at the boiler exit, heat transfer coefficients in the various boiling regimes comprising the once-through boiling process, two-phase pressure drop measurements and critical heat flux values.

Descriptions of the experimental equipment, measurement techniques and data reduction procedures used, the experimental data, and associated analyses and correlations obtained are presented in following sections of this report.

II BACKGROUND

Balzhiser, who summarizes the liquid metal literature up to 1961 (Reference 14), points out that very little information is available for boiling liquid metal systems. Considerable work has been done in the last twenty years with the more common fluids, but the understanding of two-phase phenomena even for simple fluids is far from complete because of the complex nature of boiling and two-phase flow, which involves several flow regimes and types of boiling in forced convection systems. Collier (Reference 15) summarizes the two-phase literature up to 1957, and the MIT Two-Phase Summer Symposium of 1964 (Reference 16) provides up-to-date summary of the status of the field. Parker and Grosh (Reference 17) provide an excellent literature survey for the high quality flow regimes in their study of mist flow.

There is no general agreement in the field on the nomenclature and description of the complex structure of the various heat transfer and flow regimes which may occur in once-through forced convection boiling. Based upon the two-phase literature, however, Figure 1 is presented as a conceptual model of the local conditions thought to occur in a two-fluid once-through potassium boiler, defining the terminology employed in this work.

Entering subcooled, the potassium bulk temperature is increased by single phase heat transfer in the "subcooled heating region" until boiling is initiated. The point of net boiling inception marks the beginning of the "nucleate boiling region", whose main characteristic is a relatively large heat transfer coefficient. It is believed that the wall is completely wetted in the nucleate boiling regime. In the higher quality regions of the regime, it is thought that part of the liquid flows as a continuous liquid film on the tube wall, the remainder being entrained in the vapor core. Heat can be transferred in the nucleate boiling region by conduction through the postulated liquid film and subsequent evaporation into the vapor core ("film evaporation"), and by boiling with bubble formation from nucleation sites in the boiler tube wall.

The point of "critical heat flux", (sometimes called "dry-out", "DNB" or "burn-out") where the thin liquid film is thought to be destroyed, terminates the high performance nucleate boiling region and marks the onset of the lower performance "transition boiling" region. The lower heat transfer coefficients determined for the transition region are thought to be caused by the heat transfer surface being only partially wetted. Heat transfer in this region is visualized as a combination of heat transfer to patches or droplets on the boiler tube wall and vapor phase heat transfer from the dry areas. The transition region is terminated by the onset of "film boiling", at which point the liquid droplets and patches, thought to wet the wall in the transition region, become insulated from the heat transfer surface by a superheated vapor film. The film boiling region extends to the point at which bulk superheating commences, and the subsequent "superheat region" is the final step in the once-through boiling process.

Several investigators (References 11, 18, 19) have reported in the literature that considerable bulk liquid superheat is attained before boiling commences in the liquid metals. Converse (Reference 12), however, employing an extension of the bubble nucleation analysis utilized by Bergles and Rohsenow with water (Reference 20), has shown that boiling in potassium may be initiated over a range of bulk temperatures, depending upon the local conditions. He presents calculated results for potassium, allowing predictions of the bulk temperature at boiling initiation to be made. Boiling is predicted to be initiated at bulk potassium temperatures subcooled with respect to the saturation temperature at high heat fluxes and high saturation temperatures, whereas boiling is predicted to be initiated at superheated potassium bulk temperatures at low heat fluxes and low saturation temperatures.

Potassium, due to its relatively large liquid to vapor density ratio at the temperatures of interest, has a large void fraction for flow in pipes at low qualities. At a quality of 5%, for example, the void fraction calculated

(Reference 12) for a temperature range of 1500°F to 2100°F varies from 75% to 50% respectively, increasing with increase in quality. It is expected, therefore, that the bubbly and slug flow regimes characteristic of low void fractions will be very short or absent in high performance once-through boiling. The flow regime thought to be characteristic of the nucleate boiling region is the annular-mist regime, which consists of a continuous liquid film wetting the boiler tube wall with some of the liquid entrained in the vapor core. Converse (Reference 12) has examined two of the vaporization mechanisms possible under these conditions, a film evaporation model, which supposes heat transfer by conduction through the liquid film with subsequent evaporation from its surface, and a boiling model, based upon boiling from nucleation sites in the boiler tube wall. The heat transfer coefficient predicted by the film evaporation model decreases with increasing temperature level, increases with increasing quality and is virtually independent of heat flux level. The heat transfer coefficient predicted by the boiling model, on the other hand, increases with both increasing heat flux and temperature level but is independent of quality. Both of the models predict relatively high heat transfer coefficients under the conditions of interest (in excess of 5,000 Btu/hr-ft^2-°F) at heat fluxes above 75,000 Btu/(hr-ft^2) and qualities above 20%, and generally of the order 10,000 Btu/(hr-ft^2-°F). The large magnitude of the nucleate boiling coefficient is confirmed by the experimental results of Berenson (Reference 21) and the data of Bond (Reference 60) for forced convection vaporization of potassium in the annular flow or nucleate boiling regime.

Very few critical heat flux data have been reported for potassium. In addition to the values obtained in the present investigation, Colver (Reference 22) has reported pool boiling critical heat flux data over the pressure range 0.1 to 20 psia, and both Hoffman (Reference 19) and Bond (Reference 12) have recently reported values for the forced convection boiling of potassium in the net quality region. Tippets (Reference 23) and Janssen (Reference 24), among others, have obtained forced convection critical heat flux data in the net quality region for

water, and Tippets (Reference 25) has correlated these and additional data with a theoretical model which predicts the critical heat flux to decrease with increasing vapor quality, increasing mass velocity and increasing tube diameter.

Several investigators (Reference 26, 27, 28, 29) have studied transition and film boiling for the forced convection vaporization of water in controlled heat flux test sections, and Bond (Reference 60) has recently obtained exploratory measurements of transition and film boiling for the forced convection vaporization of potassium in vertical upflow, also under controlled heat flux conditions. Transition boiling was characterized in these controlled heat flux experiments by rather large oscillations of the heater surface temperature (over 600°F fluctuations were reported in Reference 27), as compared to the small fluctuations (about 5°F) characteristic of nucleate boiling, and the steady surface temperature characteristic of film boiling. The investigators found the transition boiling heat transfer coefficient to be intermediate in value between the nucleate boiling heat transfer coefficient and the film boiling coefficient, the latter being of the same order as calculated for the vapor phase alone.

The temperature fluctuations observed for transition boiling in the controlled heat flux tests support the hypothesis of a partially wetted wall. At constant heat flux, the wall temperature can assume a high value characteristic of film boiling or a low value characteristic of nucleate boiling, depending upon the local absence or presence of a droplet or patch of liquid. In a two-fluid or controlled temperature test, however, the temperature fluctuations are thought to be less in magnitude, as the local heat flux decreases when a local dry spot occurs. In fact, the maximum possible fluctuation of inside tube wall temperature in a two-fluid boiler is equal to the radial temperature drop through the tube wall and primary fluid, which is generally less than 100°F in liquid metal boilers. There is no such limit on the temperature fluctuations in a controlled heat flux boiler.

The change from transition to film boiling is characterized in the conceptual picture of once-through boiling as occurring when the individual droplets of liquid become insulated from the heat transfer surface by a vapor film. Drew and Mueller (Reference 30) describe the film boiling condition for individual droplets as the "spheroidal state" (sometimes called the Leidenfrost effect), and present values measured by various investigators of the critical temperature necessary for existence of the film-boiling or spheroidal state. Recent results obtained by investigators at Geoscience (Reference 31) regarding the vaporization lifetimes of single potassium droplets on heated surfaces indicate that the critical temperature difference for the spheroidal state of potassium droplets at the conditions of their test is approximately 300°F. These results suggest that film boiling may not have occurred in the two-fluid potassium boiler used in the present experiments, since no tube wall-to-potassium temperature differences as large as 300°F were employed in the tests. In a controlled heat flux boiler, on the other hand, at high heat fluxes film boiling may occur immediately after onset of critical heat flux conditions, due to the rapid decrease in the heat transfer coefficient and resulting rapid increase in wall temperature after the critical heat flux.

The effect of vortex-generator inserts upon the heat transfer and pressure losses in single phase flow and upon the critical heat flux in subcooled boiling has been extensively studied by Gambill (References 32, 33), who employed twisted tapes. Gambill was able to correlate the single phase friction factors measured with twisted tape inserts within approximately 20% by defining swirl-flow friction factors and Reynolds numbers based upon the helical velocity and path length and the equivalent diameter obtained with the inserts. This procedure is employed in Appendix D of this report to correlate water pressure drop data obtained with helical inserts in support of the boiling potassium data. Gambill also measured the critical heat flux for subcooled water flowing in tubes containing twisted tapes, and determined an increase in critical heat flux above that for tubes without inserts as high as three-fold. Viskanta (Reference 34), in his forced convection boiling experiments with water, found a similar substantial

increase of the critical heat flux with inserts in the net quality region.

The effect of the vortex-generator inserts upon the heat transfer in single-phase flow is indicated by Gambill to be more complicated than the effect upon pressure drop, since there is an effect of the acceleration produced by the inserts upon the intensity of natural convection in addition to the velocity and equivalent diameter effects. The few single phase heat transfer data available in the literature for helical inserts similar to those employed in the boiling potassium tests, however, are also correlated as discussed in Appendix D by use of the helical flow parameters.

It is expected that vortex generator inserts will increase the heat transfer performance obtained in the transition region, since the radial acceleration produced by the insert will tend to force the liquid droplets entrained in the vapor core to the partially wetted tube wall. Blatt and Adt (Reference 35) present forced convection boiling data for Freon-11, obtained with twisted tapes, which indicate that a substantial improvement in heat transfer coefficient beyond the critical heat flux is obtained.

A knowledge of the pressure losses occurring during the flow of a boiling mixture is necessary for the design of forced convection boilers. This knowledge is necessary not only to size the pump required, but also in the thermal design, since the fluid pressure and temperature are related by the saturation curve. The pressure drop during the flow of a boiling fluid includes, in addition to the frictional loss, a loss resulting from the change in momentum of the mixture as it flows through the tube and vaporizes. The momentum pressure drop may be significant in relation to the frictional drop in plain tubes, but is generally less than the frictional drop in tubes containing vortex generator inserts, since the inserts increase the frictional loss considerably. The methods of Martinelli, in which the ratio of two-phase to single phase pressure gradients are correlated, are widely used for the prediction of two-phase frictional pressure losses. Lockhart and Martinelli (Reference 36) provide a method for

the prediction of two-phase pressure loss under isothermal non-boiling conditions. Martinelli and Nelson (Reference 37) give a procedure for the calculation of the two-phase frictional pressure losses during the forced convection boiling of water.

Converse (Reference 8) has modified the Martinelli-Nelson curves of Reference 37 for application to potassium, and has also developed a homogeneous model, based upon quality-weighted viscosities and densities, for the prediction of the frictional pressure losses for the forced convection boiling of potassium. The resulting curves of two-phase friction pressure drop multipliers for potassium are given in Figures 2 and 3.

References 36 and 37 also provide correlations useful in the prediction of the momentum pressure losses for water. Converse, however, found these predictions difficult to generalize to potassium, and recommends that the boiling momentum pressure losses for potassium be computed from the following equations, derived in Reference 6.

$$\left(\frac{dP}{dz}\right)_M = \frac{G^2}{g_c}\, d/dz \left[\left(\frac{1}{\hat{\rho}}\right)\right] \qquad (1)$$

$$1/\hat{\rho} = \frac{1}{\rho_g}\left[(1-x)\ \rho_g/\rho_f + \frac{x}{K}\right]\left[1 + x\ (K-1)\right] \qquad (2)$$

The parameter K in the above equations is the ratio of average vapor velocity to average liquid velocity for two-phase flow, and is called the slip ratio. The proper value of the slip ratio to employ in equation (2) is at present uncertain. Converse (Reference 6) has shown its value to be between the square root of the liquid-to-vapor density ratio and 1.0. Fauske (Reference 38) found the slip ratio to be equal to the square root of the liquid-to-vapor density ratio in his studies. Polomik (Reference 39) determined the slip ratio to be equal to the cube root of the liquid-to-vapor density ratio

in an analytical study of an idealized model. Levy (Reference 40) derived the slip ratio from a momentum exchange model of two-phase flow, predicting values which are approximated at intermediate and high qualities by the square root of the liquid-to-vapor density ratio for potassium.

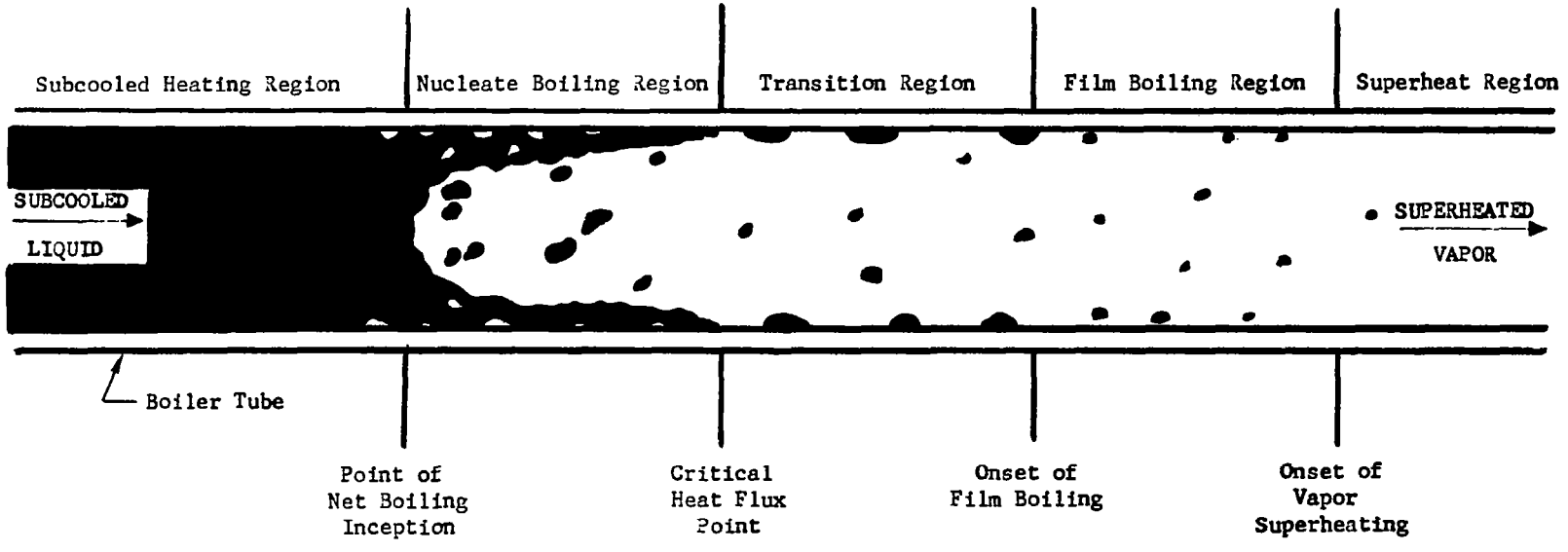

Figure 1. Conceptual Illustration of Once-Through Boiling

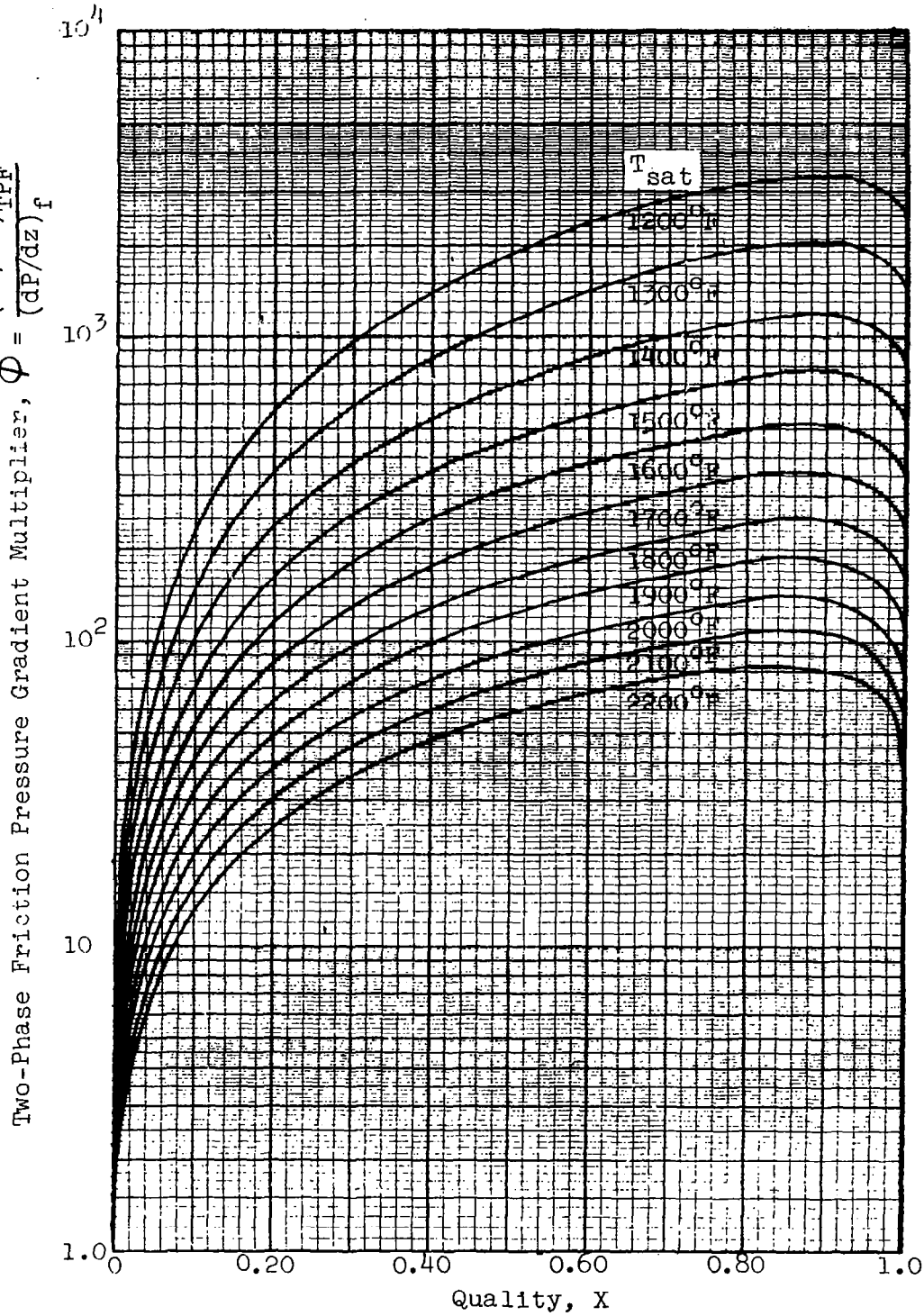

Figure 2. Two-Phase Friction Pressure Gradient Multipliers for Potassium From Modified Martinelli Model of Reference 8

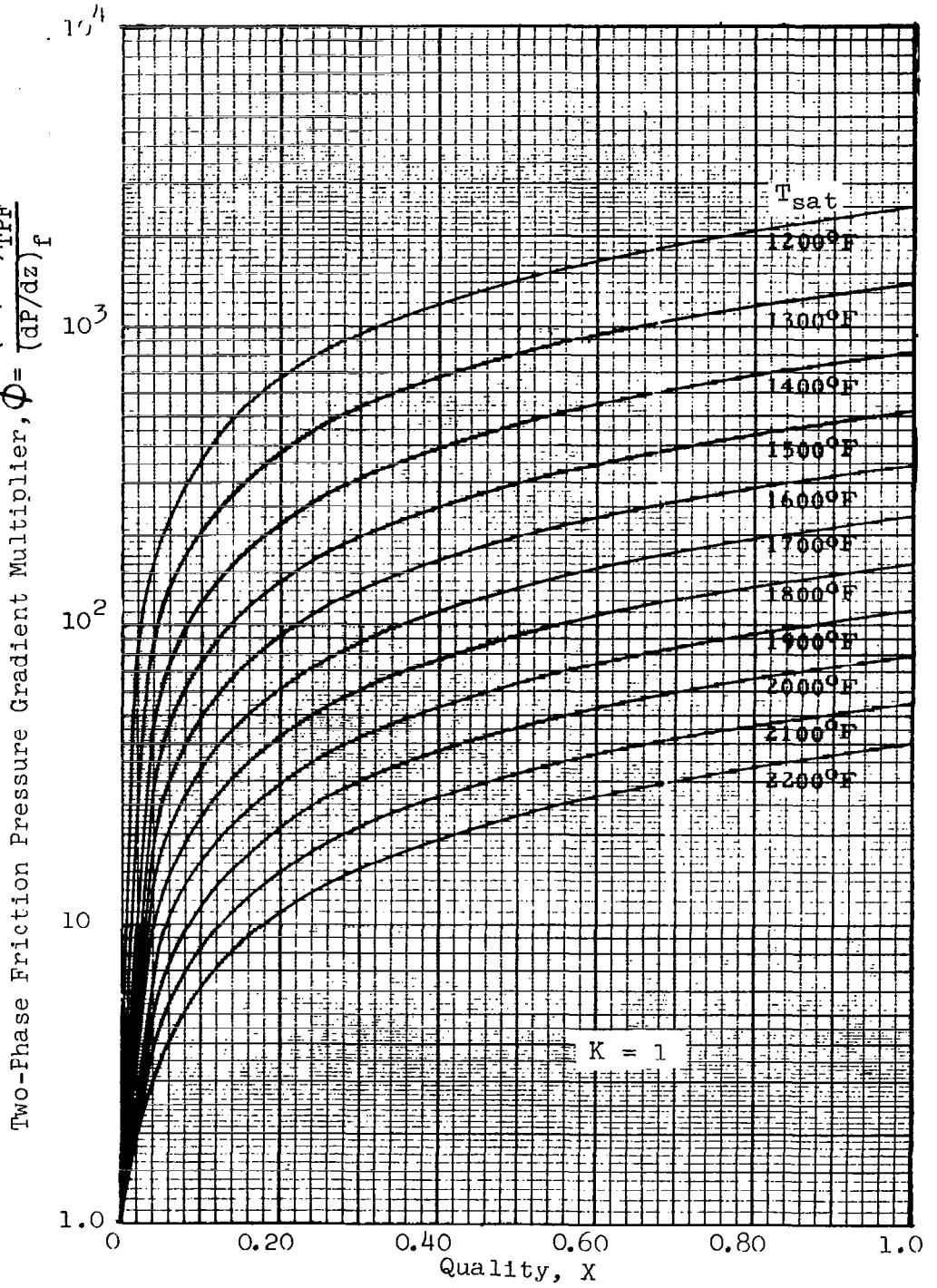

Figure 3. Two-Phase Friction Pressure Gradient Multipliers for Potassium From Homogeneous Model of Reference 8

III APPARATUS

Liquid Metal Test Facility

The two-fluid liquid metal test facility employed in the experiments is shown schematically in Figure 4. Figure 5 is a photograph of the facility during construction. The entire facility is constructed of Haynes-25 alloy, a cobalt-nickel-tungsten superalloy which permits continuous operation with alkali metals to 1850°F. The alloy is resistant to air oxidation, thus no special containment or atmosphere is required for the piping and components.

The sodium primary loop of the facility, which represents the reactor loop of an actual power plant, accepts heat from a gas fired furnace and rejects heat to boiling potassium in the secondary loop. A reversible helical induction pump is used in the single phase primary loop and the sodium flow rate is determined with an electromagnetic flowmeter. The sodium level is indicated by a "J" type resistance probe positioned in the standpipe located at the loop high point and is controlled by inert gas pressurization of the dump tank.

Potassium flowing in the secondary loop is boiled in vertical upflow in the sodium-heated test section and is condensed in a horizontal air-cooled single tube condenser. The vertical condenser shown in Figure 4 was not activated for the tests. The vapor-liquid interface is maintained in a head tank fitted with level probes, positioned immediately downstream of the horizontal condenser. The liquid potassium flows through a helical induction pump, an electromagnetic flowmeter, and finally a throttling valve upon its return to the test section from the head tank.

The gas fired furnace employed as the prime source of heat is shown schematically in Figure 6. The furnace is designed for a nominal heat load of 300 KW at a sodium exit temperature of 1850°F. One hundred twenty square feet of heat transfer area are provided in the furnace by thirty 1.0-inch ID tubes with 0.210-inch wall thickness, connected by toroidal headers formed from 5-inch

diameter pipe. The heater shell is air-tight and the flue is valved, so that alkali metal fumes may be contained in the event of a tube failure. An alternate vent line to a scrubber system insures that no caustic fumes will be released to the atmosphere. Outside of initial adjustments of the fuel-air ratio, no difficulties were encountered in the operation of the gas fired furnace. The furnace tubes showed no deterioration over the time of operation.

The liquid metal pumps utilized in both loops are of the helical induction type, as shown schematically in Figure 7. The pumps consist essentially of a polyphase stator, a pump duct made up of two concentric tubes with spiral passages in the annulus and suitable enclosing and supporting framework. The design point of the primary pump is 20 psi developed head at 200 gpm with sodium at 1850°F, and the design point of the secondary pump is 100 psi developed head at 3.5 gpm with potassium at 1850°F. No difficulty whatsoever was encountered in the operation of the helical induction pumps.

The use of valves in the test facility was limited to those locations requiring throttling or isolation obtainable in no other way, due to the inherent lack of reliability in high temperature liquid metal valves. As shown in the facility schematic (Figure 4), a throttling valve is employed in the liquid potassium line upstream of the boiler test section and an isolation valve is provided between the potassium loop and the secondary dump tank. A vapor valve located in the potassium line downstream of the test section, before the vertical condenser, was originally provided in the anticipation of a need for vapor throttling. This anticipated need did not materialize, thus the vapor valve was dismantled after a failure of the valve bellows during shakedown operation. The valves were originally designed with Haynes-25 alloy bellows in order to provide temperature capabilities comparable to the remainder of the facility. The liquid throttling and potassium dump tank isolation valves, however, never reached temperatures above 1600°F during facility operation, thus their Haynes-25 bellows were replaced by more ductile stainless steel units near the end of the

test program. The use of stainless steel reduced the failure rate of the valve bellows considerably.

Oxide and impurity control in the sodium and potassium loops was achieved by a combination of hot flushing and hot trapping. Upon startup or following an inter-loop failure, such as failure of the bellows at the test boiler inlet, gross impurities in the two loops were eliminated by hot flushing with several charges of alkali metal, which were discarded. Oxygen content during operation was maintained at less than 50 ppm by hot-trapping the alkali metals at 1200°F with zirconium gettering grids in their respective dump tanks between test runs and by hot-trapping during operation with a gettering grid located in the potassium head tank. In early stages of operation, a continuous flow hot trap of columbium-1% zirconium was located in the primary loop. This hot trap was unsatisfactory, however, in that a sodium-columbium-oxygen alloy was formed in the trap which was transported throughout the sodium loop. The in-line hot trap was not used after the initial shake-down operation for this reason.

The liquid metal test facility and its components are discussed in greater detail in Reference 1, in which the design bases and calculations are also presented.

Boiler Test Sections

Figure 8 is a disassembled view of a typical boiling test section employed in the two-fluid boiling facility, also showing one of the vortex-generator inserts utilized. The test section is a shell and tube heat exchanger with the potassium flowing inside the tube being heated by sodium flowing in the annulus. Relative expansion between the boiler tube and the shell of the heat exchanger is accommodated by a bellows positioned near the potassium inlet end of the test section. The tube is maintained concentric within the shell by means of centering pins located at three axial positions.

Figure 9 is a schematic view of the test section, showing the instrumentation employed. Three 0.095-inch OD platinum-platinum 10% rhodium thermocouples sheathed in Haynes-25 and insulated with MgO, are positioned in each of four thermocouple wells located at the inlet and exit of both the sodium and the potassium streams. Eleven rings containing five 0.062-inch OD inconel sheathed platinum-platinum 10% rhodium thermocouples each are positioned at various locations along the outside of the boiler shell to provide information regarding the axial variation of sodium temperature. As shown in Figure 10, the shell thermocouples are held in contact with the boiler shell by metal foil tabs. These thermocouples are held in contact with the shell for approximately 50 thermocouple diameters from the junctions in order to minimize errors due to heat conduction through the leads.

Slack diaphragm Taylor absolute pressure transducers located at the potassium inlet and exit (Figure 9) are employed to measure the two-phase pressure losses. Figure 11 shows the potassium inlet pressure transducer as installed in the facility. The pressure tap at the potassium exit is located in the boiler tube itself to avoid correction for the pressure change from the boiler tube to the exit plenum.

The vortex-generator inserts employed in several of the tests consist of a 1/4-inch OD tube having a 0.050-inch thick wall, around which is wound a ribbon so as to form a helical flow path when the insert is placed inside the boiler tube. The potassium temperature as a function of axial distance is determined directly in tests with inserts from seven 0.040-inch OD inconel sheathed chromel-alumel thermocouples positioned inside the insert support tube. Figure 12 is a photograph of a typical insert, showing the thermocouple leads. The primary seal between the thermocouples and the insert tube is provided by a braze, with a secondary seal being provided by a Conax thermocouple gland. The space between the two seals is filled with argon, pressurized so that argon will leak into the loop in the event of a primary seal failure, rather than potassium leaking to the atmosphere.

Table I shows the combinations of boiler tube diameter and helical insert pitch-to-diameter ratio (P/D) tested for which data are presented in this report. The potassium was in vertical up-flow in all cases. The sodium flow was countercurrent to the potassium flow in all tests except case IV, for which both countercurrent and cocurrent sodium flows were employed. The boiler tube heat transfer length was 91.5 inches and the shell inside diameter was 2.07-inches in all cases.

TABLE I

BOILER TEST GEOMETRIES

Case	Boiler Tube O.D., inches	Boiler Tube I.D., inches	Helical Insert P/D
I	1.00	0.92	2.2
II	1.00	0.92	6.0
III	0.75	0.67	6.0
IV	0.75	0.67	No Insert

The sodium inlet and potassium exit well thermocouples were used as primary standards for the in-loop calibration of the remaining thermocouples. The well thermocouples were calibrated periodically within $\pm$ 1°F in a melting point apparatus at several temperatures bracketing the range of test operation. A technique employing two sodium flow rates at several temperatures with the potassium loop evacuated, described in Appendix A, was employed to determine the test section heat losses and to calibrate the sodium exit well thermocouples relative to the sodium inlet well. The heat losses so determined are 1 to 3 KW, depending upon the temperature level. The primary well thermocouples are judged accurate to within $\pm$ 1°F relative to each other and within $\pm$ 2°F on an absolute basis. The higher precision obtained in the relative calibration is important, since the total amount of heat transferred in boiling runs is determined from the temperature change in the sodium stream.

The shell thermocouples were calibrated relative to the sodium well thermo-

couples at two temperatures with the potassium loop evacuated, at maximum sodium flow rate, under which conditions the temperature change between sodium inlet and exit is less than 1°F. The corrections to the shell thermocouples made in this manner were generally about 10°F and are believed accurate to approximately ± 2°F.

The insert thermocouples were calibrated against the potassium exit well thermocouples with low quality, low power boiling runs in which the temperature change due to two-phase pressure loss is small. The corrections applied were approximately 10°F and are believed accurate to ± 2°F.

The Taylor pressure transducers were calibrated versus a standard gas gage by inert gas pressurization of the secondary loop. The calibration of the Taylor gages was found to be dependent upon the diaphragm temperature. Thus the transducers were maintained at a constant temperature during test operation by means of auxiliary heating wire.

The pressure gage calibrations obtained by both decreasing and increasing the pressure, and before and after a test run, generally agreed within ± 1 psi. Thus the accuracy obtained in the two-phase pressure measurements is judged to be about ± 3/4 psi. In addition to the measurement of two-phase pressure loss, the potassium exit pressure gage was used in conjunction with the exit temperature measurement as one means to detect vapor superheat in the boiling runs. Figure 13 shows the measured potassium exit pressure versus the measured exit temperature for the superheated vapor runs obtained from Test Cases I, II and III. Also plotted for Test Case I are data for which the calculated exit quality is between 10% and 90%. The latter results are generally within ± 1 psi of the potassium saturation curve as determined by the Naval Research Laboratories (Reference 41). This is a further indication of the accuracy of the pressure measurements.

The relationships between flow rate and output signal from the electro-

magnetic flowmeters in both loops of the facility were obtained by theoretical calculation (Reference 61). In order to minimize errors inherent in this procedure, measured values of the field strength of the magnets, which were maintained at low temperatures, were used for the calculations. An indication of the resulting accuracy in flow determination was obtained through inter-calibration of the two flowmeters by heat balance around the test section, using liquid-liquid runs. The disagreement obtained was 2%, which is believed to be also representative of the probable error in the individual flow determinations.

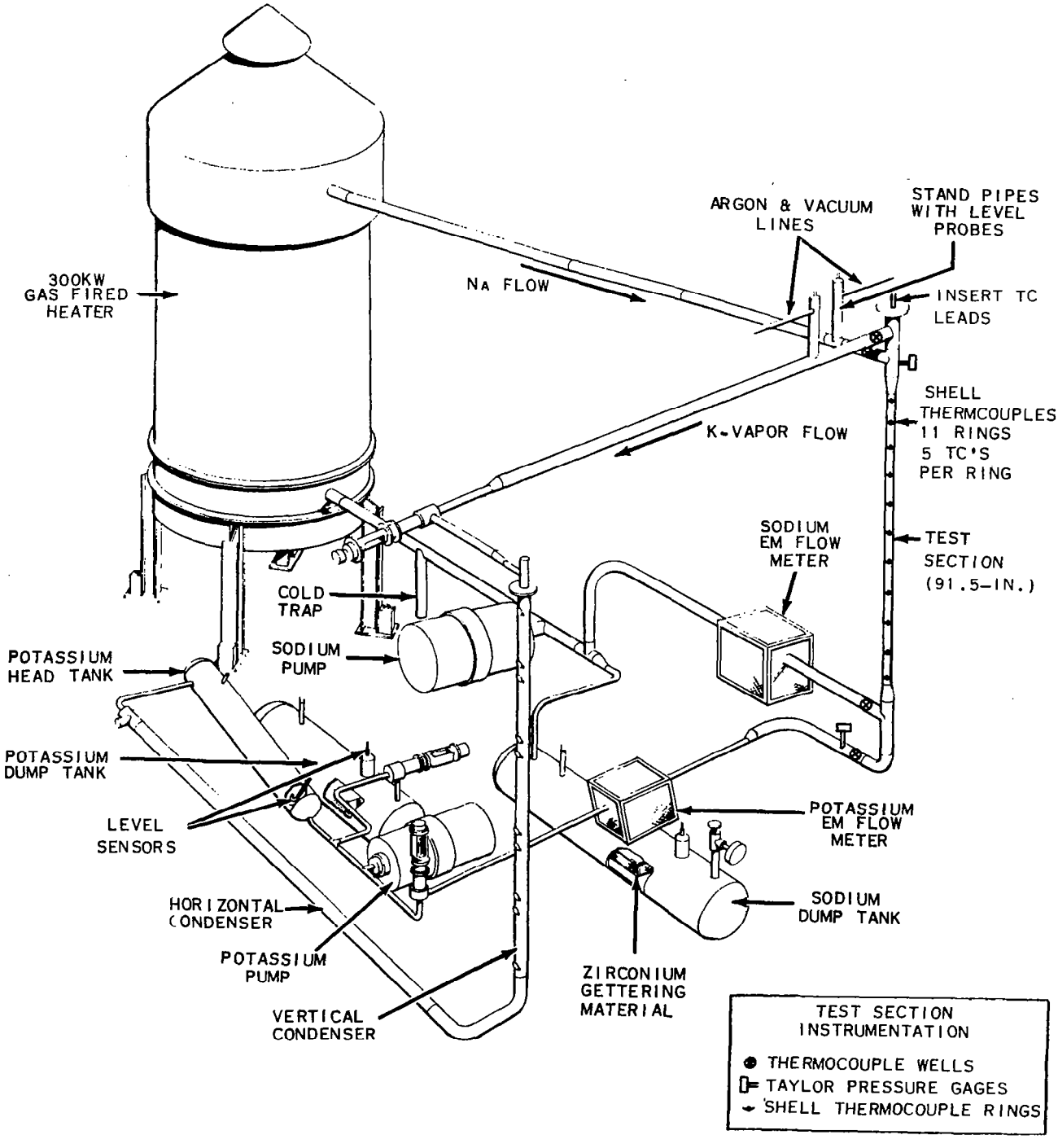

Figure 4. Two-Fluid Heat Transfer Facility

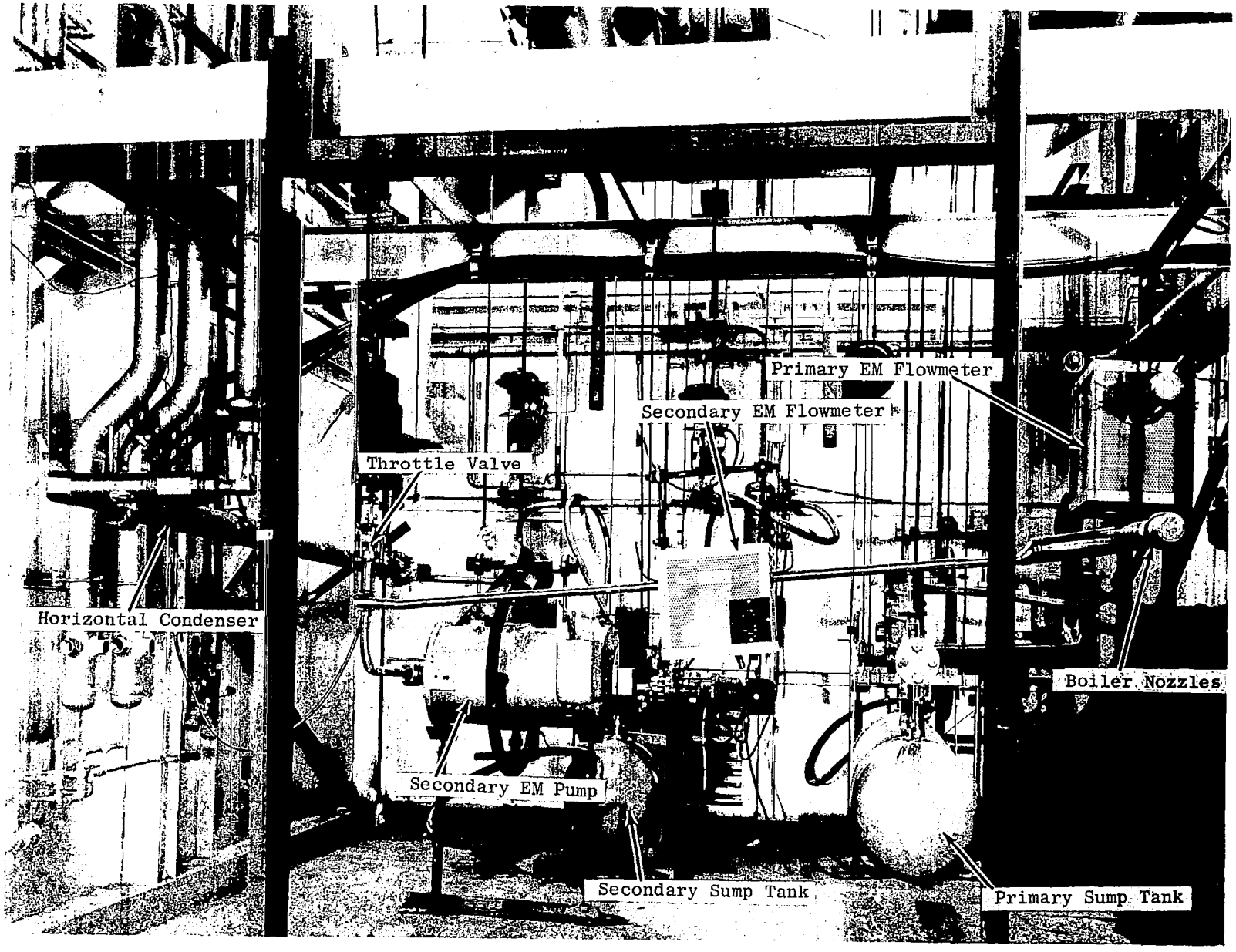

Figure 5. - Facility piping and components during construction.

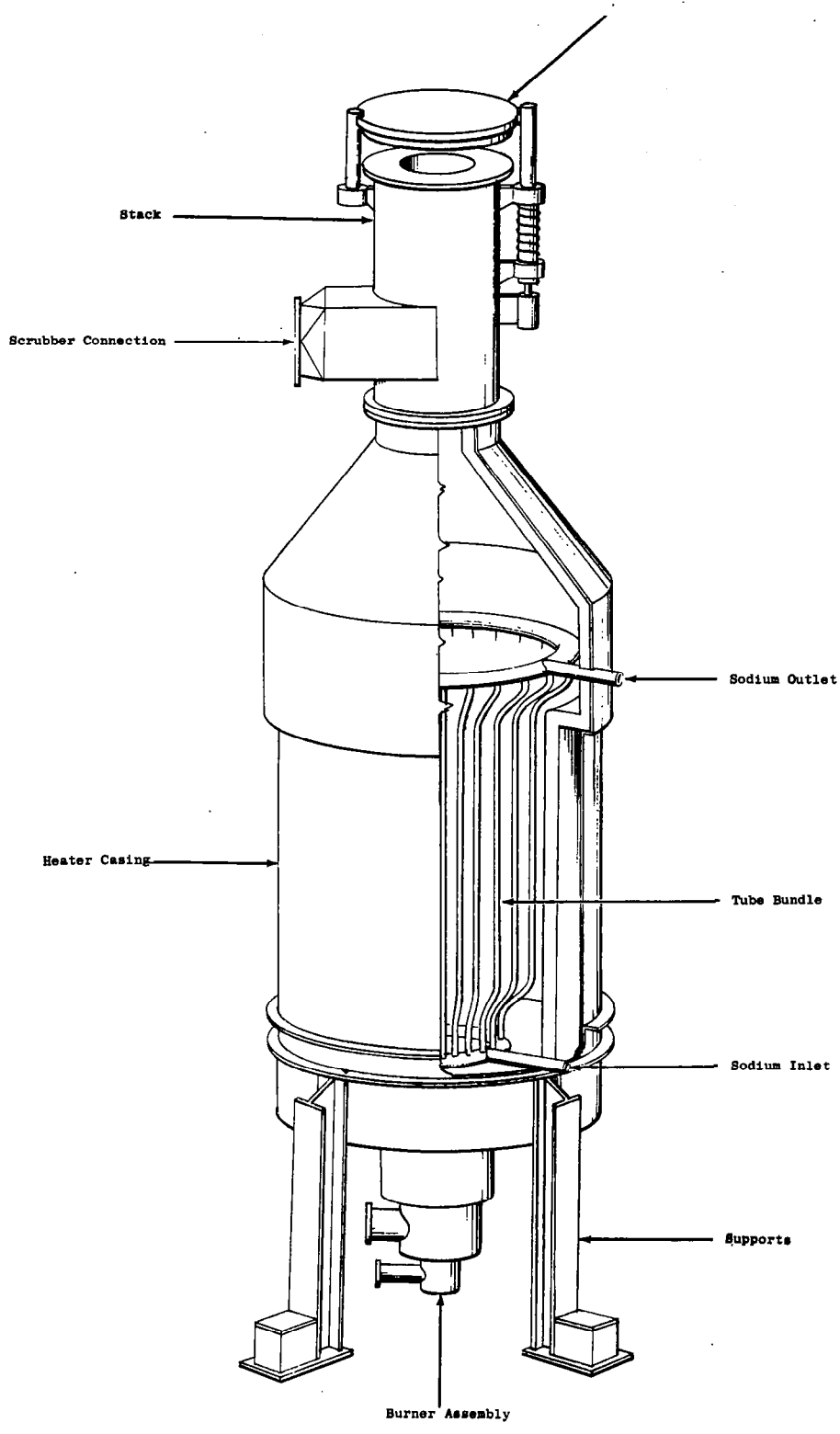

Figure 6. Schematic of Facility Gas Fired Sodium Heater.

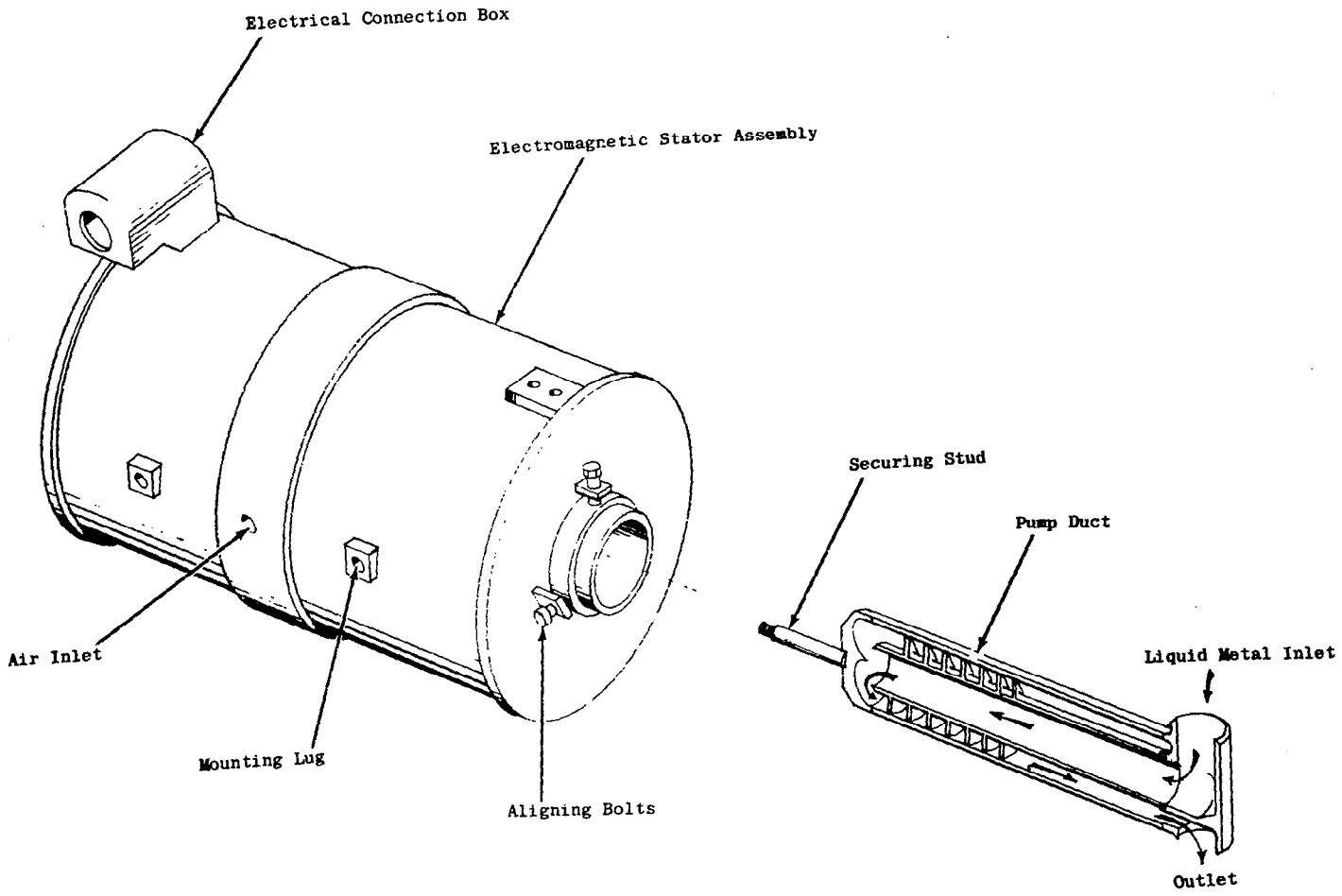

Figure 7. Facility Primary Loop EM Pump and EM Pump Duct.

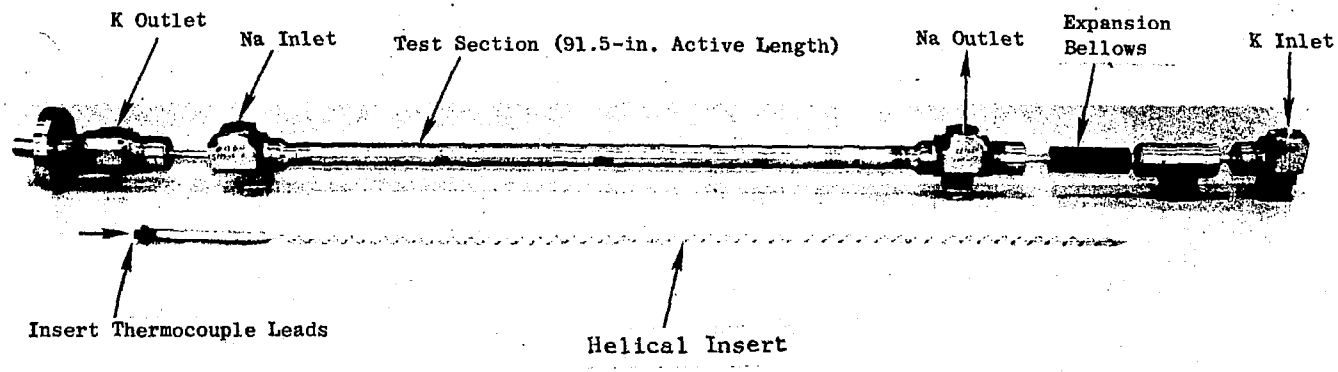

Figure 8. - Boiling test section with instrumented helical insert.

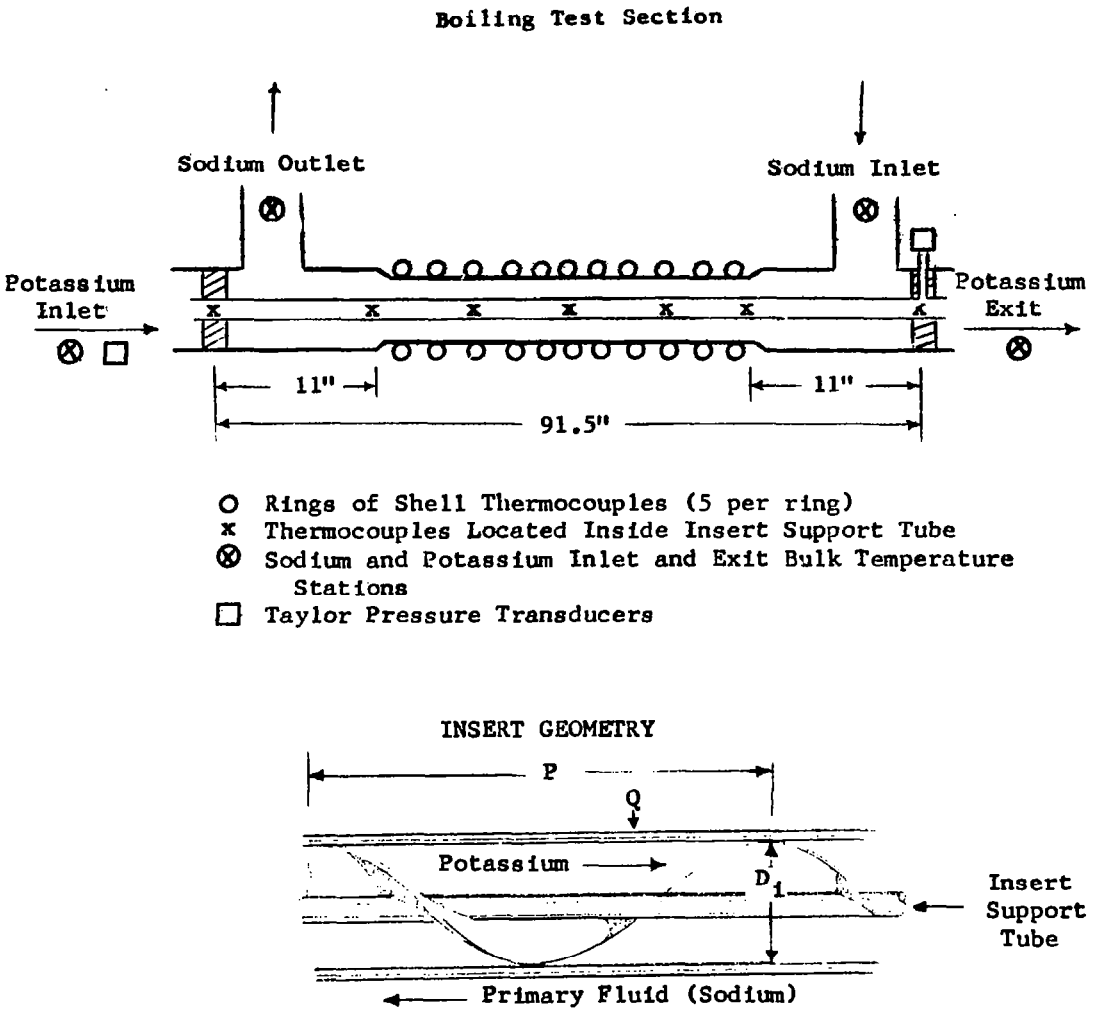

Figure 9. Instrumentation of Boiling Test Section.

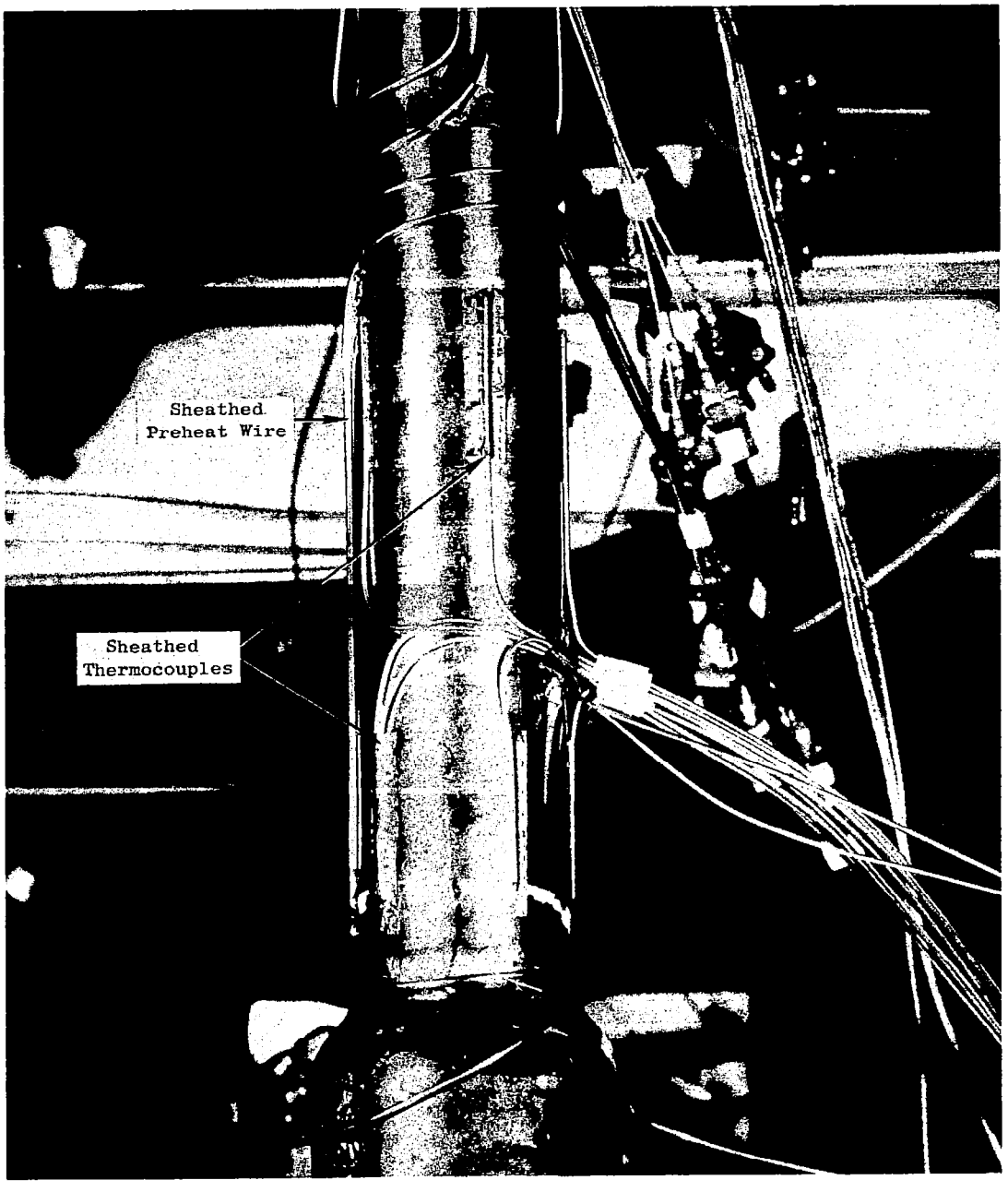

Figure 10. - Shell thermocouple attachment on boiling test section.

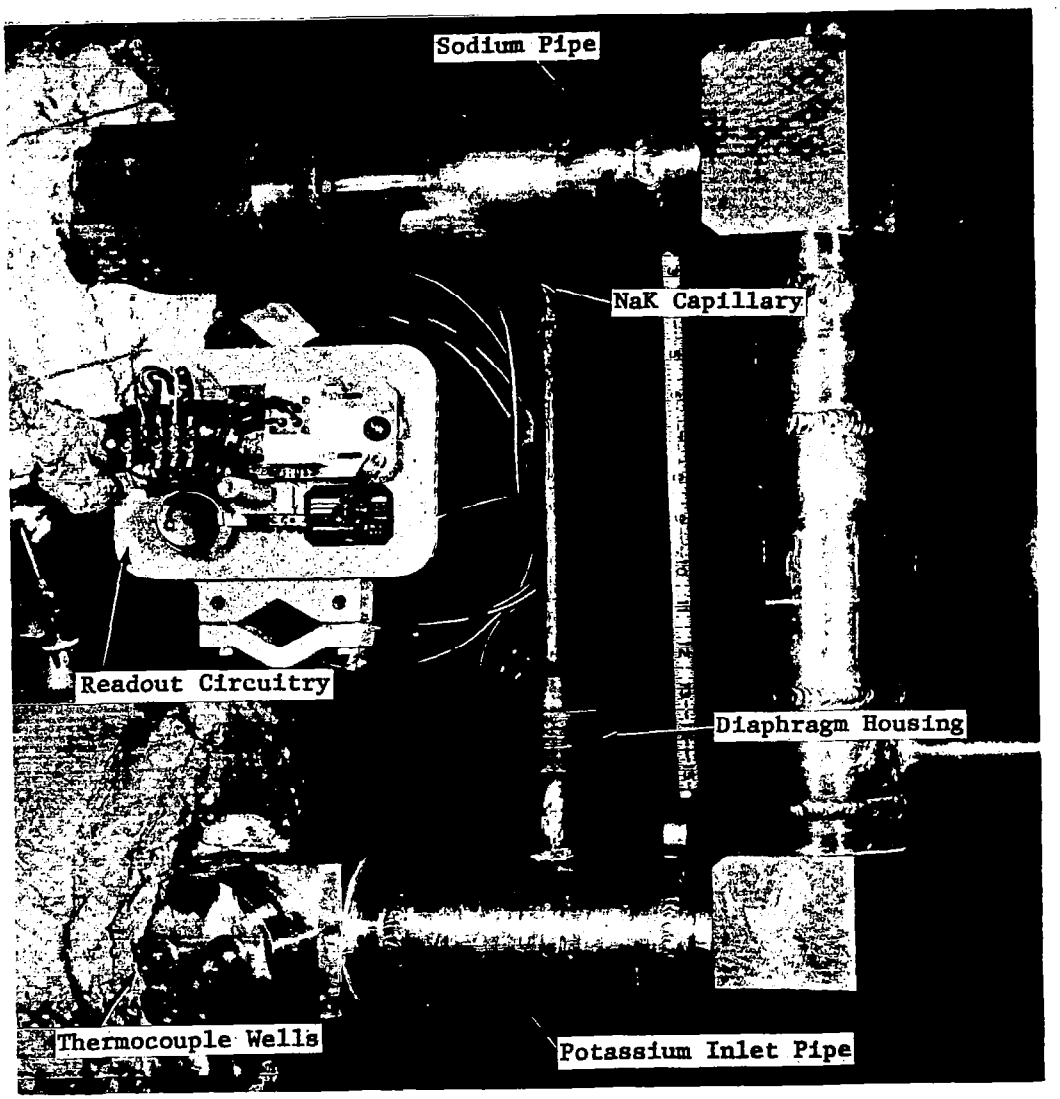

Figure 11. Typical Installation of a Diaphragm Type Pressure Gage.

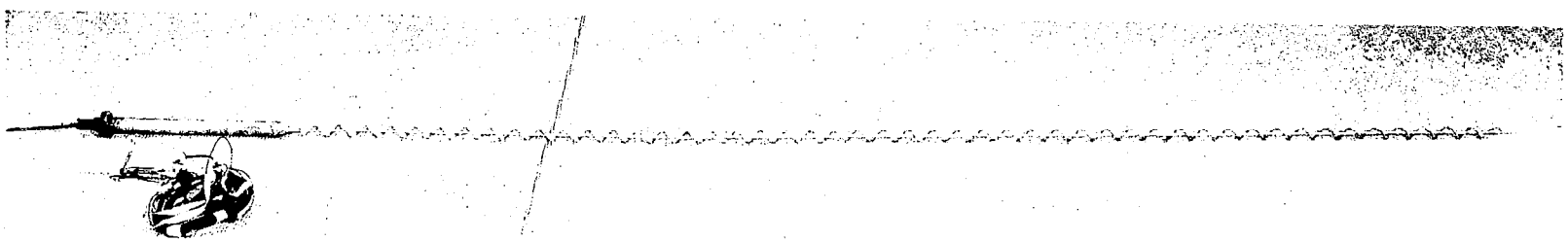

Figure 12. - Photograph of typical insert, showing thermocouple leads.

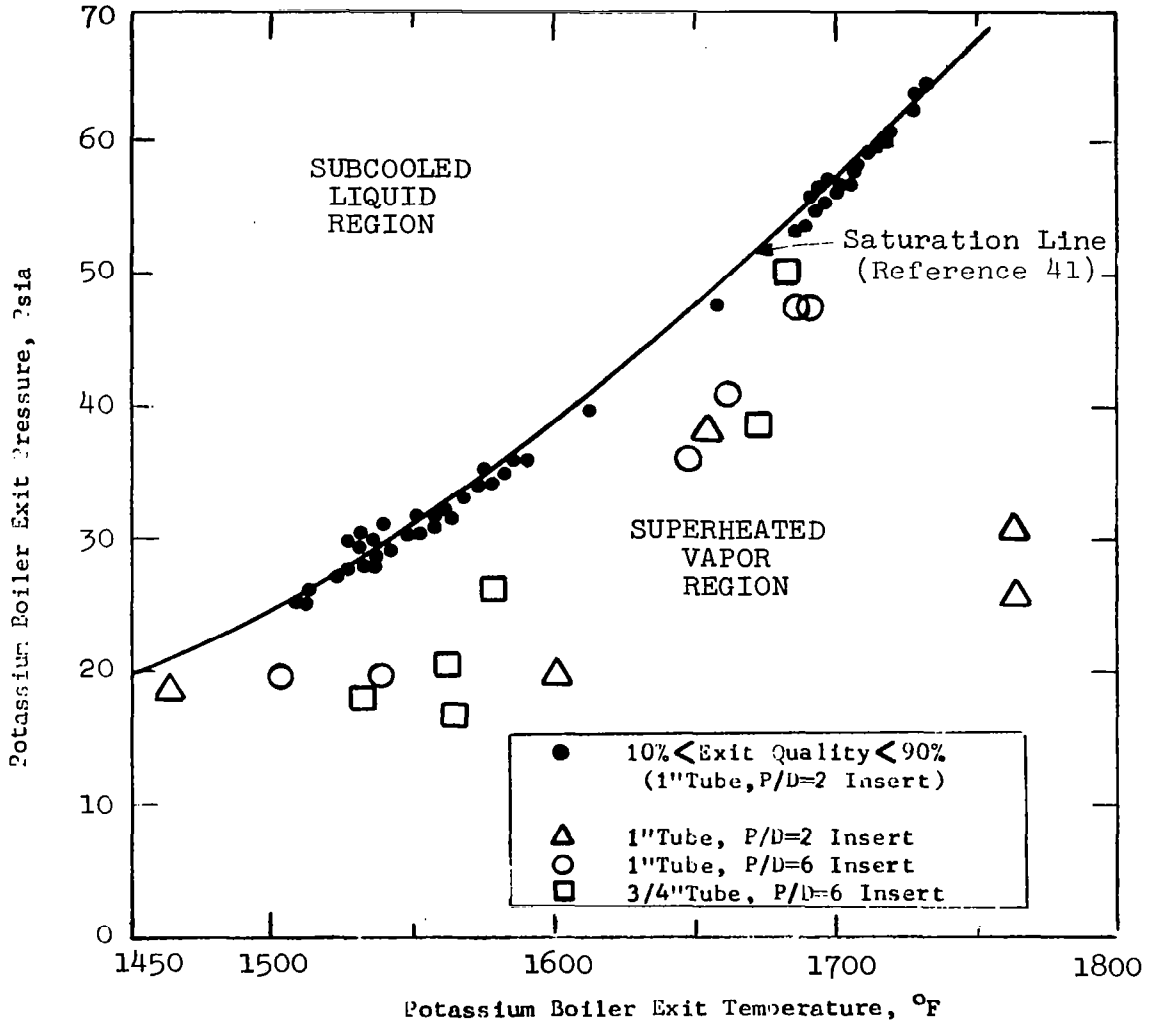

Figure 13. Comparison of Saturation Properties With Measured Potassium Pressures and Temperatures

IV FACILITY OPERATION, STARTUP AND TEST PROCEDURE

The operation and performance of the test facility, although complex in detail, is rather simple from an overall viewpoint. The prime variables under the control of the operator are the primary and secondary loop liquid metal flow rates, the amount of fuel to the gas fired furnace (and thus the power level), and finally, the cooling air flow rate to the potassium vapor condensers.

The cooling air to the condensers is supplied at essentially room temperature, and its temperature rises as it passes through the condenser by accepting heat from the condensing potassium. The air temperature rise, and thus the average air temperature, increases as the air flow rate is reduced at a particular facility heat load. The potassium temperature level in the condenser at a particular power level is therefore controlled by the condenser air flow rate, since the condenser potassium temperature is related to the average air temperature by the heat transfer characteristics of the condenser. This also constitutes control of the potassium temperature at the boiler exit, as the temperature change between the boiler and condenser, which is generally small, is determined by the two-phase pressure losses in the connecting piping. The cooling air flow rate controls the two-phase potassium pressure as well as the temperature, since the pressure and temperature are related together at saturation conditions.

The sodium temperature in the boiler at a particular power level is similarly set by the heat transfer characteristics of the boiler and the temperature of the boiling potassium.

The test facility has no auxiliary preboiler, thus the vapor quality of the potassium at the boiler exit cannot be set independently of the heat load and the potassium flow rate. At a set heat load, the quality is increased by decreasing the potassium flow rate and at a set potassium flow rate, the potassium

quality is increased by increasing the heat load.

The facility was operated at fixed potassium inventory, that is, with the valve connecting the potassium dump tank and the secondary loop in the closed position. Stable operation was more easily achieved with the dump tank valve closed, presumably because the tank was partially filled with argon and acted as a compressible volume. It was also found during early shakedown tests that the facility tended to be unstable if the potassium vapor-liquid interface was held inside the horizontal condenser, whereas stable operation was achieved when this interface was maintained in the head tank immediately following the condenser (Figure 4). With the interface located in the condenser, small fluctuations in potassium flow rate could change the position of the interface in the condenser, resulting in a change in the condensing length and therefore causing a perturbation in the instantaneous rate of heat rejection, which would tend to propagate the disturbance. Maintaining the interface in the head tank, however, may have eliminated propagation of the disturbances, since the condensing length remained constant. Flow fluctuations do not change the liquid level in the relatively large diameter head tank to any significant degree, which further reduced propagation of flow disturbances. All test operation of the facility was conducted with the potassium vapor-liquid interface located in the head tank for these reasons.

Test operation of the facility is restricted by the limitations of the individual components. In particular, the gas fired furnace is limited to a heat load of 300 KW at a sodium temperature of 1850°F. The condensing capability of the facility is not limiting. The calculated capacity of the horizontal condenser alone is 410 KW at a potassium temperature of 1200°F and 595 KW at a potassium temperature of 1600°F.

Determination of the performance of the boiler was the prime purpose of the experiments. An upper limit to the boiler power capability can be calculated for test planning purposes by assuming the thermal resistance of the boiling potassium

to be negligible. The maximum amount of heat which can be transferred by the boiler under these conditions is set by the thermal resistances of the boiler tube and the sodium primary fluid, and the average temperature difference between the sodium and potassium. The maximum amount of heat transferred by the boiler is zero at a potassium temperature of 1850°F, corresponding to the maximum allowable sodium temperature, and increases as the potassium temperature is lowered. Another limitation of the heat transfer capability of the boiler at low potassium temperatures is determined by a maximum vapor velocity equal to the sonic velocity (Mach number equal to one). The potassium vapor velocity corresponding to a given flow rate and quality is higher at lower potassium temperatures, since the vapor density decreases with decreasing temperature. The Mach 1 or choking limitation, therefore, is most severe at low potassium boiling temperatures.

Figure 14 shows the facility operational limitations determined as described above and plotted versus the potassium temperature at the boiler exit. It is seen that the boiler is the limiting component in the facility, a maximum possible heat transfer rate of 220 KW being predicted at a potassium temperature of 1500°F. It is emphasized that the curves shown represent the maximum possible performance of the boiler, since the boiling potassium heat transfer resistance was assumed negligible. This assumption is realistic for low potassium qualities, when the high-performance nucleate boiling region extends over the entire length of the boiler tube. At high potassium qualities, however, the potassium thermal resistance is appreciable due to the onset of the low-performance transition boiling and vapor superheat regions; thus at high qualities, the actual heat transfer limitations are more severe than indicated.

Also shown on Figure 14 are the two temperatures selected for the test plan employed in the boiling experiments. Test temperatures as high as possible, consistent with a reasonable allowable range of power levels, were selected. The higher range is of most interest in relation to the probable operating temperatures of a space power system. In addition, the large temperature differencesoccurring in operation at low potassium temperatures place large

thermal stresses upon the test section expansion bellows, which failed several times during the course of the experiments. Finally, the ductility of Haynes-25 Alloy is a minimum at 1200°F, maximizing the effects of thermal stress. Low temperature operation was avoided for these additional reasons.

At each of the two potassium exit temperatures selected (1550°F and 1700°F), boiling data were obtained for at least two values of the potassium flow rate. The potassium boiler exit quality for each flow rate was varied by changing the boiler power. Data were obtained as the boiler power was increased in steps effected by changes in the fuel rate to the gas-fired heater. These increases in power caused the boiler exit quality to increase proportionally. The sodium temperature also increased under these conditions due to the increased sodium-to-potassium temperature difference required at the higher power levels. The maximum boiler exit quality obtained at a particular potassium flow rate and temperature was determined by the sodium temperature reaching 1850°F, the maximum allowable sodium temperature. The sodium flow rate was held constant during these tests by adjustments made to the sodium pump. The potassium flow rate was held constant by adjustments made to the potassium pump. The potassium boiler exit temperature was held constant by adjustments made to the condenser cooling air flow rate, which affects the potassium boiler temperature as described previously. The potassium liquid throttle valve was employed during these experiments to minimize fluctuations in the potassium flow rate. If fluctuations in the potassium flow rate were observed at a particular test point, the throttle valve was closed until the fluctuations were minimized.

The test procedure described above, in which the sodium and potassium flow rates and the potassium exit temperature were held constant while the potassium quality was changed by changes in power, was followed for most of the boiling data obtained. Towards the end of the test program, however, a few additional data were obtained according to a second test plan. In the second plan the sodium flow rate and potassium boiler exit temperature were held constant as well as the boiler power. Under these conditions, the boiler potassium exit

quality was varied by changes made in the potassium flow rate. The sodium flow rate and the potassium exit temperature were maintained constant by adjustments to the sodium pump and the condenser air flow rate as before. The power was maintained constant by holding the fuel rate to the gas fired furnace constant.

Startup of the test facility proceeded from a condition in which both primary and secondary loops were evacuated with the facility mechanical vacuum pumps and were heated to approximately 600°F by means of auxiliary electrical heating wire. The alkali metals were contained in their respective dump tanks prior to startup, also heated to 600°F or above with auxiliary heating wire.

The primary loop was filled by pressurizing the sodium dump tank with argon, thereby forcing the sodium into the evacuated loop. Level sensors located in the loop standpipe indicated when the proper inventory was obtained. A small compressible volume of argon was maintained above the sodium level in the standpipe to allow for thermal expansion of the sodium during operation. The sodium pump was activated and the gas fired furnace was turned to minimum heat prior to filling of the primary loop.

The potassium loop was filled in a similar manner, in that potassium was forced to flow into the evacuated secondary loop by argon pressurization of the potassium dump tank. For boiling runs, however, the secondary loop was only partially filled, the proper inventory being determined by level probes located in the potassium head tank. When the desired inventory was attained, the valve between the secondary loop and dump tank was closed, the secondary pump was activated and cooling air flow to the potassium condensers was initiated. Boiling was initiated as the potassium was pumped into the sodium-heated boiler test section.

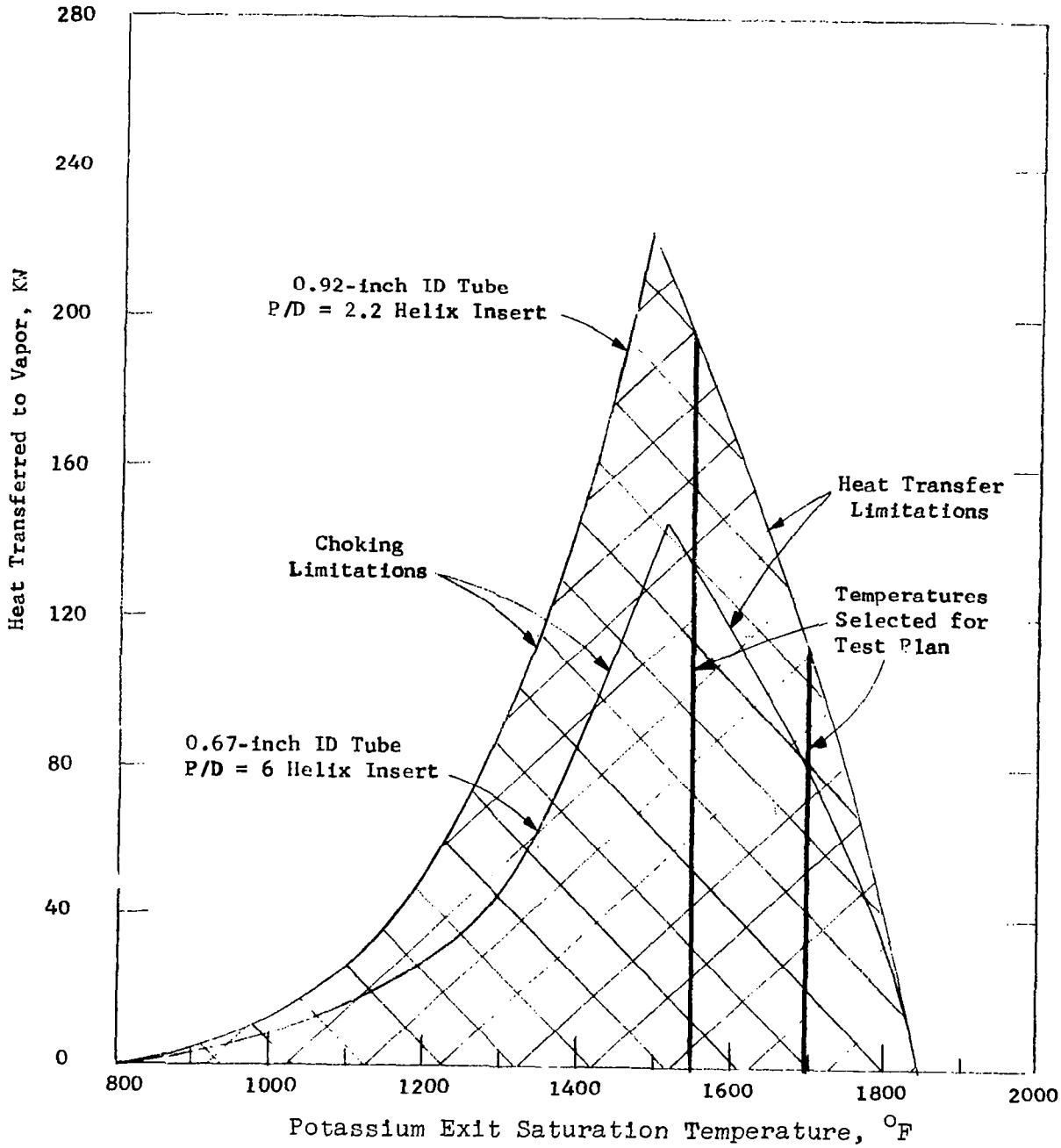

Figure 14. Facility Operating Limitations

V EXPERIMENTAL RESULTS

Several types of heat transfer and pressure loss parameters have been derived from the two-fluid boiling potassium experiments conducted in the test facility:

1. Overall Results, which consist of the measured flow rates and temperatures of sodium and potassium, the boiling pressure drop, the power level and the potassium exit quality, were obtained. The overall results illustrate the gross performance obtained and permit the design of multiple-tube boilers using approximately the same tube sizes and geometries as those tested by direct scale-up.

2. Average Boiling Potassium Heat Transfer Coefficients (obtained as averages over the entire boiling length of the tube) are presented, and were calculated by subtraction of the subcooled heating region and the sodium and tube wall thermal resistances from the overall boiling thermal resistance. The average coefficients may be applied to boiler designs with boiler tube materials and lengths, primary fluids, boiling pressure losses and potassium subcoolings different from those obtained of any particular test point. They are in general, however, averaged over more than one heat transfer regime of the once-through boiling process and cannot be extrapolated with confidence beyond the range of local potassium conditions tested.

3. Local Results for the individual boiling regimes and values for the critical heat flux were obtained from the data and correlated. These results enhance understanding of the once-through boiling process and provide the greatest generality for extrapolation beyond the range of test conditions.

4. The Boiling Pressure Loss data have been corrected for the momentum pressure loss, and the frictional component has been compared to values predicted for potassium.

The procedures employed to calculate the various parameters are presented in detail in Appendix A of this report. Tabulated results are given in Appendix B.

Overall and Average Results

The pressure and temperature measurements made and the overall results obtained for two typical once-through boiling data runs with exit superheat are shown in Figure 15. The two cases presented were obtained with the 0.92-inch ID boiler tube and have similar values of the sodium inlet temperature, potassium exit pressure and mass velocity but have helical inserts of different twist ratio (P/D). It can be seen from the figure that considerably more exit superheat is obtained in the run with the tighter twist ratio. The payment for this performance increase is made in terms of an increased boiling pressure drop; the measured potassium pressure drop for the P/D = 2 case is 10 psi compared to 4 psi for the P/D = 6 case. The overall performance obtained in these cases with inserts is impressive in view of the fact that the maximum potassium exit quality obtained in tests at similar conditions in the same test boiler, but without inserts, was less than 90%.

Overall results of the type presented in Figure 15 are useful in that they indicate the feasibility of compact once-through boilers, and permit the design of multiple-tube boilers by direct scale-up. It is unlikely, however, that a potassium boiler for power system application would be operated under conditions identical to the test conditions. It is therefore necessary to separate the thermal resistance of the primary fluid and of the boiler tube wall from the overall thermal performance of the test boiler, so that the effects due to the potassium alone may be studied and generalized.

A first step in this direction was taken by computation of "average" boiling potassium heat transfer coefficients for the data obtained. The details of the computational procedures employed are given in Appendix A. In brief, the liquid or subcooled heating region was removed by calculation

and an overall heat transfer coefficient was computed for the boiling length of the tube by employing a logarithmic average of the overall sodium-to-potassium temperature differences at the initiation of boiling and at the potassium exit. The subcooled potassium region is generally 10% of the total boiler tube length, the curves of Figure 15 being typical in this respect. The average boiling potassium heat transfer coefficient was calculated from the overall thermal resistance by subtraction of the sodium and tube wall thermal resistances. Lyon's equation (Reference 42) for an annulus was used to compute the sodium resistance and the tube wall resistance was calculated from its thermal conductivity (Reference 43) and thickness.

Values of the average boiling heat transfer coefficient obtained with the 0.67-inch inside diameter boiler tube containing no insert are shown in Figures 16 and 17 for both cocurrent and countercurrent flow of the sodium heating fluid with respect to the boiling potassium. Figure 16 shows the effect of boiler exit quality and mass velocity, and Figure 17 indicates the effect of quality and potassium temperature level. Results obtained with the 0.67-inch ID tube containing a P/D = 6 helical insert are plotted in Figure 18 versus quality with both mass velocity and temperature as parameters. In Figure 19, the non-insert results for both cocurrent and countercurrent sodium flow are compared with the insert values.

The effect of tube diameter upon the average heat transfer coefficients with inserts is shown in Figure 20, in which data for both the 0.67-inch ID and 0.92-inch ID tubes containing P/D = 6 helical inserts are plotted. Figures 21 and 22 present the average boiling heat transfer coefficients obtained with two different twist ratios in the 0.92-inch ID boiler tube, showing the effect of insert twist ratio at two different boiling temperatures.

The following observations can be made from the results presented in Figures 16 through 22.

1. The average boiling heat transfer coefficient, both with and without insert, increases with increasing temperature over the range covered (Figures 17 and 18). This effect is less pronounced with inserts at qualities near 100% and apparently disappears or even reverses for superheated exit conditions (Figure 18).

2. At qualities up to approximately 60%, the average heat transfer coefficient without insert increases with both increasing quality and increasing mass velocity (Figure 16). These effects are not well defined for the data with inserts, and apparently are absent for the 0.67-inch ID tube with P/D = 6 insert (Figure 18).

3. The results presented indicate that there is a quality at which the average boiling heat transfer coefficient is maximum and above which the heat transfer coefficient decreases rapidly with further increases in quality. Figure 16 indicates the quality at the point of maximum coefficient increases with decreasing mass velocity under both cocurrent and countercurrent flow conditions for the tube without insert.

4. Figure 19 shows that higher qualities are reached before the decrease in heat transfer coefficient under cocurrent flow conditions than with countercurrent flow at the same mass velocity.

5. The results presented for the 0.67-inch ID boiler tube (Figure 19) show helical inserts to be clearly effective in that exit superheat was obtained with inserts whereas without insert a maximum quality of only about 90% was obtained. The overall results of Figure 15 and the heat transfer coefficients of Figure 21 for the 0.92-inch ID tube with inserts confirm the high performance that can be obtained with helical inserts. Figures 19, 21 and 22, however, show that the insert apparently

decreases the heat transfer coefficient in the intermediate region of exit quality. This effect is especially apparent in Figure 22 at the higher mass velocity and lower temperature, where the heat transfer coefficient at 70% quality is approximately 12,000 Btu/(hr-ft^2-°F) for the P/D = 6 insert and 4,000 Btu/(hr-ft^2-°F) for the P/D = 2 insert. The effect is less at the lower mass velocity and higher temperature of Figure 21, the coefficient being approximately 8,000 Btu/(hr-ft^2-°F) for the P/D = 6 insert and 6,000 Btu/(hr-ft^2-°F) for the P/D = 2 insert at 70% exit quality.

Local Heat Transfer Results

In order to further enhance the understanding of the once-through boiling process for potassium, thereby aiding the application of the data to boiler design, a considerable effort was devoted to the analysis of the two-fluid boiling data on a local basis. Figure 23 shows the measurements made for a typical once-through boiling run to exit superheat conditions with a helical insert in the test section. Figure 24 shows the calculated local heat fluxes, qualities and heat transfer coefficients as a function of boiler length for the same run. This run exhibits four distinct heat transfer regimes; namely, subcooled heating, nucleate boiling, transition boiling and vapor superheating.

It should be noted in Figure 23 that there is no clear evidence of a distinct film boiling regime at the end of the transition boiling regime prior to beginning of bulk superheated vapor conditions. It is thought that this may be due to the controlled temperature characteristics of the two-fluid boiler, which results in an upper limit to the wall-to-coolant temperature difference that, at the test conditions used, was not sufficiently high to cause the wall to become completely dry as is required for fully-established film boiling.

The discontinuity of slope in the sodium temperature profile indicated by the shell temperature measurements shown in Figure 23 is assumed to be the critical heat flux point and the beginning of transition boiling. The position at which the potassium temperature begins to rise near the tube exit is assumed to mark the beginning of the superheated vapor region. The amount of heat

transferred in the superheat region is calculated from an energy balance using the measured potassium temperature rise to the exit. The point of boiling inception and the amount of heat transferred in the subcooled liquid region are similarly calculated from energy balances using the local potassium temperatures given by the insert thermocouples. For runs in which no insert was used, superheated vapor exit conditions were not attained and, consequently, only the subcooled heating region and nucleate and transition boiling regions were present. For these runs without insert, the potassium temperature at boiling inception was obtained using the inlet pressure gage in conjunction with saturation temperature-pressure properties, and the subcooled heating length was determined by single-phase heat transfer calculations.

The average heat flux in the nucleate boiling region is calculated from the axial shell temperature gradient in this region, which is assumed to be equal to the sodium axial temperature gradient. From the average heat flux and the length of the nucleate boiling region, the amount of heat transferred in the region is calculated. The heat transferred in the transition boiling region is determined as the difference between the total heat input to the boiler and that transferred in the other regions. The average heat flux in the transition region is then calculated from the length of the region indicated by the shell and insert thermocouples.

The local quality and local sodium temperature at various points along the tube, including the critical heat flux point, are calculated by heat balances, employing the values of heat flux and length determined for the various regions. The local potassium temperature, obtained from the insert thermocouples, and the calculated local sodium temperature are utilized to calculate overall heat transfer coefficients for the various regions. From these coefficients, a potassium heat transfer coefficient for each region is obtained by subtracting the thermal resistance of the sodium and boiler tube wall from the overall thermal resistance.

The nucleate boiling heat transfer coefficients calculated in the above manner are large compared to the tube-wall and sodium coefficients and therefore represent a small fraction of the overall thermal resistance in the nucleate boiling region. This fact precludes their accurate determination in the two-fluid facility utilized. The overall heat transfer coefficient in the nucleate boiling region, which includes the average nucleate boiling heat transfer coefficient and the effective coefficients for the tube wall and the sodium, can be employed, however, to calculate with good accuracy values of the local heat flux in the nucleate boiling region. In particular, the critical heat flux can be readily calculated as the product of the overall nucleate boiling heat transfer coefficient and the sodium-to-potassium temperature difference at the critical heat flux point.

A more detailed description of the calculational procedures utilized to obtain the local results is given in Appendix A. All of the local results obtained, including those plotted for the sample run in Figure 24, are tabulated in Appendix B. The critical heat flux data, transition boiling coefficient data, and the superheated vapor coefficient data obtained are presented graphically following.

Critical Heat Flux Results

Figure 25 shows a critical heat flux parameter plotted as a function of quality for the data obtained with the 3/4-inch nominal diameter boiler tube both with and without insert. Experiments in pool boiling have indicated that the critical heat flux is proportional to the fourth root of the local acceleration (Reference 44, 45); therefore, the forced convection critical heat flux values obtained for potassium with inserts have been divided by the fourth root of $(1 + a_R)$ to give a critical heat flux parameter. The radial acceleration of the fluid in g's (a_R) developed by the insert is given by Equation (3) as a function of the insert and fluid constants. This equation is derived in Appendix C and is as follows:

$$a_R = \left[\frac{x_c \, G_K \, \frac{\pi}{P/D}}{\rho_g \sqrt{\rho_f / \rho_g}} \right]^2 \frac{24}{g \, D_i} \qquad (3)$$

Figure 25 shows that the critical heat flux parameter data obtained with the insert are in fair agreement with the values obtained without insert, indicating a decrease in critical heat flux with increasing quality. For the insert data presented, the calculated radial acceleration varies from 65 to 90 g's. Figure 25 is presented as two plots of the same data, one with temperature shown as parameter and the second with mass velocity as parameter. No definite grouping of the data with respect to either parameter is observed. This indicates that the effects of temperature and mass velocity upon the critical heat flux parameter are less than the data scatter of about ± 30% over the ranges covered, when plotted as shown.

All of the critical heat flux data obtained from the two-fluid facility experiments, including values from the 0.67-inch ID tube, with and without P/D = 6 helical insert, and from the 0.92-inch ID tube with P/D = 2 and P/D = 6 helical inserts are plotted in Figure 26 and tabulated in Appendix B. Also shown on Figure 26 are some of the critical heat flux measurements of Bond (Reference 60), which were obtained for potassium in forced convection flow at higher saturation temperatures in a controlled heat flux facility, both with and without a helical insert of P/D = 6. The data in Figure 26 are correlated reasonably well by the following empirical equation:

$$q''_c = \frac{(1 + a_R)^{\frac{1}{4}} \times 10^6}{1 + 2\left(\frac{x}{1-x}\right)}, \quad \frac{\text{Btu}}{\text{hr-ft}^2} \qquad (4)$$

Equation (4) correlates the critical heat flux data within a probable error* of 26%. The data upon which the equation is based encompass the following range of variables:

*The probable error is that deviation whose probability of being exceeded is one-half (Reference 46).

Saturation temperature	1522 to 2106°F
Mass Velocity	15 to 101 lb/(ft^{2}sec)
Heat Flux	50,000 to 532,000 Btu/(hr-ft^2)
Quality	0.40 to 0.93
Radial Acceleration	0.0 to 117 g's
Tube Internal Diameter	0.42 to 0.92 inches

Transition Boiling Heat Transfer Coefficients

A correlation of the transition boiling heat transfer coefficients was attempted, based upon the following reasoning:

1. The results from potassium droplet vaporization experiments by Geoscience (Reference 31) show that the vaporization lifetimes of single droplets increase rapidly with increasing temperature difference between the heated surface and the droplet before the onset of film boiling. These data suggest that the wall-to-coolant temperature difference ΔT is an important parameter affecting the heat transfer coefficient in transition boiling.

2. The local vapor quality x must be a significant variable, since the amount of liquid which can be in contact with the heat transfer surface decreases with increasing quality.

3. The transition boiling heat transfer coefficient h_{TB} should reduce to the vapor phase heat transfer coefficient h_v at 100% quality.

4. The radial acceleration generated by a helical insert, a_R, given by Equation (3) should increase the transition boiling heat transfer coefficient, because the centrifugal force generated tends to increase the fraction of liquid in contact with the heat transfer surface. The data of Blatt and Adt (Reference 35) for the forced convection transition boiling of Freon-11 in tubes containing twisted tapes support this assertion. These investigators observed that the

twisted tapes caused a substantial increase of the transition boiling heat transfer coefficient.

These four considerations resulted in the following equation:

$$\frac{\left(\frac{h_{TB}}{h_v} - 1\right)}{(1 + a_R)^a} = B \left(\frac{1-x}{x}\right)^b \left(\frac{1}{\Delta T}\right)^c \qquad (5)$$

The exponent c was determined by plotting the left side of Equation (5) versus $1/\Delta T$, using the non-insert data for which $a_R = 0$. The parameter $(1-x)/x$ did not vary significantly for the non-insert data used in the determination of c. The result is shown in Figure 27, from which it is seen that an exponent of c = 2 fits the data quite well.

The exponents a and b together with the coefficient multiplier B were determined by plotting all of the data as $(\frac{h_{TB}}{h_v} - 1)/(1 + a_R)^a$ versus $(\frac{1-x}{x})^b \frac{1}{\Delta T^2}$, and adjusting a and b until the best fit straight line was obtained. The vapor phase heat transfer coefficient h_v was computed assuming all-vapor flow at the total mass velocity for each data point. The Colburn equation (Reference 47) was employed to calculate h_v for the non-insert data. A modified form of the Colburn equation derived in Appendix D using Greene's data for liquid water in helical flow (Reference 33) was employed to calculate h_v for the transition boiling data obtained in tubes containing helical inserts. Values of the acceleration group exponent, a, equal to 1/4 to 1/5 were considered in the empirical fitting of the experimental data. The 1/4 power dependence is suggested by the critical heat flux results, while the theoretical analysis of Reference 48 for individual droplets suggests a 1/5 power dependence. A value of a = 1/5 and b = 0.7 with c = 2 gave the best agreement with the data.

Equation (6) resulted from the fitting of the potassium transition boiling heat transfer coefficient data as described above.

$$\frac{\left(\frac{h_{TB}}{h_v} - 1\right)}{(1 + a_R)^{1/5}} = \frac{2.55 \times 10^5 \left(\frac{1-x}{x}\right)^{0.7}}{(\Delta T)^2} \qquad (6)$$

The values upon which the equation is based are tabulated in Appendix B and cover the following range of test variables:

Saturation Temperature	1512 to 1704°F
Mass Velocity	16 to 101 lb/(ft^2 sec)
Tube Wall to Potassium ΔT	58 to 244°F
Quality	44 to 93%
Radial Acceleration	0 to 140 g's
Tube Internal Diameter	0.67 to 0.92 inches

The transition boiling heat transfer data are compared to the empirical correlating equation on Figure 28. Equation (6) agrees with the experimental data from the two-fluid facility within a probable error of 20%. Also plotted in Figure 28 are some of the forced convection potassium transition boiling heat transfer coefficient data obtained by Bond (Reference 60) at 2100°F in a controlled heat flux facility. These data were plotted after the correlation was established from the lower temperature two-fluid data. Agreement of the data from the constant heat flux facility with the data from the two-fluid facility and with the correlation is fairly good.

Superheated Vapor Heat Transfer Coefficients

The superheated vapor heat transfer coefficients calculated from the boiling data runs with exit superheat are summarized in Table II. A complete tabulation of the superheated vapor data obtained is given in Table XVII. Also

listed in Table II are values calculated using Equation (7) following, which is a correlation of water heat transfer coefficients obtained for tubes containing helical inserts. Equation (7) is derived in Appendix D, based upon the data of Greene (Reference 33).

$$\frac{h_v D_e}{k} = 0.359 \left(\frac{D_e V_H}{\nu}\right)^{0.563} (N_{Pr})^{1/3} \qquad (7)$$

The deviation between the experimental and predicted superheated vapor heat transfer coefficients is large, as can be seen in the tabulation. The experimental values range from one-third to as high as three times the predicted values. There are several possible reasons why the experimental data could be either higher or lower than the prediction, as discussed following.

1. Equation (7), from which the "predicted values" are calculated, is an empirical expression derived in Appendix D from liquid water heat transfer data obtained in tubes containing helical inserts. Gambill (Reference 33) points out that vortex generator inserts will have a different effect on the heat transfer of liquids than of gases due to differencesin natural circulation caused by the radial acceleration developed by the inserts. The radial acceleration produces a density gradient in gases which opposes the natural circulation effects in heating, whereas no such density gradient is created in liquids due to their incompressibility. Heat transfer data with gases using helical inserts and additional analysis are required to substantiate this effect.

2. There is at present considerable uncertainty in the thermal conductivity and viscosity of potassium vapor. The theoretical vapor thermal conductivity and viscosity curves presented by Weatherford (Reference 49) were employed in this investigation. A single experimental potassium

TABLE II

Summary of Superheated Vapor Results

Date	Time	Tube I.D. inches	Insert P/D	δ_{SH} °F	h_{SH} (Experimental) Btu/(hr-ft^2 - °F)	h_{SH} (From Eq$_2$ 7) Btu/(hr-ft^2 - °F)
05274	0005	0.92	2	54	33.4	56.1
05274	0020	0.92	2	215	200.8	52.4
07014	2120	0.92	2	141	173.9	50.4
10114	0230	0.67	6	55	34.7	74.3
10124	0800	0.67	6	133	49.1	93.8
10124	1220	0.67	6	119	20.9	56.8
10124	1240	0.67	6	150	34.4	76.5
10174	0400	0.67	6	211	57.4	105.3

vapor thermal conductivity point found in the literature (Reference 50) is approximately 25% higher than the predicted value. This agreement is good when the rather complex structure of potassium vapor is considered. The presence of molecular aggregates (dimers, trimers, etc) in potassium vapor make it impossible at present to accurately predict the potassium vapor transport properties theoretically. The theoretical transport properties, in addition, do not take into account the influence of pressure and are therefore only applicable at vapor state points far removed from saturation conditions, where the influence of pressure is small. The generalized transport property predictions of Stiel and Thodos (Reference 51) show the vapor thermal conductivity and viscosity to be affected by pressure near saturation conditions for simple fluids, which suggests a similar effect for potassium vapor. The use of Weatherford's potassium vapor transport predictions near the saturation curve, for the analysis and prediction of potassium superheated vapor heat transfer coefficients, is therefore expected to be uncertain.

3. Heat transferred by thermal radiation might possibly constitute a significant portion of the total heat transferred to superheated potassium vapor at the temperatures associated with the experimental data. This effect would result in experimental superheated vapor heat transfer coefficients which are higher than those predicted for forced convection alone. An analysis of this effect is given in Reference 60.

4. Parker and Grosh (Reference 17), in their study of heat transfer to steam in mist flow in a tube, found with a liquid droplet detection device that entrained liquid droplets persist beyond the point of 100% quality calculated by heat balance and exist in a non-equilibrium state in conjunction with superheated vapor. They explain certain of their data which yield heat transfer coefficients lower than those

predicted for superheated vapor on this basis, arguing that the entrained droplets cool the thermocouple at the exit of the tube below the actual local vapor temperature. This results in measured tube wall-to-potassium temperature differences larger than actually the case for the vapor, which gives indicated experimental heat transfer coefficients that are lower than the actual values.

Such effects may be present in the superheated potassium data presented in Table II. One would expect that the number and size of such droplets entrained in the superheated vapor would diminish both as the residence time of the droplets in the superheat region increases and as the degree of superheat of the vapor increases. Increased residence time allows a greater fraction of the droplets to be vaporized for a given evaporation rate, and increased vapor superheat should increase the evaporation rate. If entrained droplets are a factor in the potassium results, the experimental superheated vapor heat transfer coefficient should increase as the product of the vapor superheat and the residence time increases. Figure 29 is a plot of the ratio of experimental to predicted potassium superheated vapor heat transfer coefficients as a function of the product of the exit vapor superheat (δ_{SH}) and the residence time of the vapor in the superheated vapor region (θ_R). The vapor residence time is the quotient of the superheated vapor length (L_{SH}) and the vapor velocity (V_g) as follows:

$$\theta_R = \frac{L_{SH}}{V_g} = \frac{(L_{SH})\ \rho_g}{G_K} \qquad (8)$$

Figure 29 shows that the experimental superheated vapor heat transfer coefficients obtained increase with the product ($\delta_{SH}\ \theta_R$), which indicates that they might have been affected by the presence of liquid droplets entrained in the superheated vapor.

For the experimental boiling potassium data, the heat flux in the superheat region was estimated by an energy balance, for which it was assumed that the vapor was dry and saturated at the beginning of the region. The energy balance was based on the measured change in temperature of the fluid from the saturated value at the beginning of the superheat region to the measured temperature at the boiler exit. If there were droplets of liquid actually present in the vapor at the beginning of the superheat region, subsequent evaporation of them prior to reaching the exit thermocouple could cause an additional error in the heat balance used for the superheat region. In general, this particular heat balance error would result in indicated values of the experimental superheat coefficients which are lower than the actual values. This possible error would add to the measurement error which might have been caused by droplets impinging on the exit thermocouple probe.

The factors discussed above and the limited potassium experimental data both indicate that there is a great deal of uncertainty in the prediction of potassium superheated vapor heat transfer coefficients by means of Equation (7). Two data points deviate from the prediction by more than 100%, and deviations of 75% seem probable. Further analysis of superheated vapor heat transfer and several additional heat transfer coefficient data for superheated potassium vapor at high temperatures are given by Bond in Reference 60.

Nucleate Boiling Heat Transfer Coefficients

As discussed previously, nucleate boiling heat transfer coefficients cannot be calculated with accuracy from data obtained in the two-fluid boiling tests, since the large heat transfer coefficients characteristic of nucleate boiling represent a small fraction of the overall thermal resistance of a two-fluid boiler. A controlled heat flux facility is more appropriate for the determination of these large coefficients, since there is no primary fluid thermal resistance to be accounted for under controlled heat flux conditions. Typical forced

convection potassium nucleate boiling data obtained by Bond (Reference 60) are presented in Figure 30 to show the magnitude of the nucleate boiling heat transfer coefficient. The values plotted were obtained in a controlled heat flux facility at a saturation temperature of 1990°F in a 0.77-inch ID boiler tube containing no insert. It can be seen from the Figure that the local nucleate boiling heat transfer coefficient is generally above 10,000 Btu/(hr-ft^2-°F) and increases with increasing heat flux. There is very little effect of quality upon the heat transfer coefficient for the data shown. A large amount of local potassium nucleate boiling heat transfer coefficient data, including data taken with inserts, is given in Reference 60. In general, these data also indicate that at the relative high heat fluxes anticipated in the nucleate boiling region of once-through boiling the nucleate boiling heat transfer coefficient is in the order of 10,000 Btu/hr-ft^2-°F or higher.

Boiling Potassium Pressure Losses

The boiling pressure losses occurring during the tests were determined, after correction for liquid head, from two absolute Taylor slack-diaphragm transducers positioned at the ends of the boiler tube. The frictional component of the boiling pressure loss was calculated by subtraction of the momentum pressure loss, and the two-phase frictional pressure drop multiplier was computed as the ratio of the frictional component to the all-liquid pressure drop as described in Appendix A. Using the square root of the liquid to vapor density ratio as the slip ratio, the momentum component was generally about 20% of the total two-phase pressure loss.

The friction factors required for the computation of the liquid potassium pressure drop necessary in the formulation of the two-phase multipliers were obtained by water pressure drop tests performed on the boiler tubes with their inserts. The results of the water tests are shown in Figure 31. Typical experimental two-phase potassium pressure drop multipliers are presented in Figure 32 for two different test conditions, and are tabulated along with all

of the experimental results in Appendix B. The experimental values are compared to the "Martinelli" and "homogeneous" model predictions obtained for potassium by Converse (Reference 8). The theoretical curves used for comparison to the experimental data are shown in Figures 33 and 34. The theoretical curves were obtained by integration of the local pressure loss multipliers (Figures 2 and 3) with respect to quality, assuming linear variation of quality with length.

The agreement between theory and experiment shown in Figure 32 is typical. The experimental values generally fall between the predictions of the two models and usually show better agreement with the Martinelli prediction. Figure 35 compares all the experimental two-phase potassium frictional pressure drop multipliers obtained with the values predicted by the Martinelli model. The Martinelli model predicts the experimental values within a probable error of 28%.

The above results indicate that the Martinelli technique can be employed to calculate the pressure losses during the forced convection boiling of potassium in tubes containing helical inserts, providing that the corresponding all-liquid pressure losses are known. The single phase friction factors of Figure 31, together with similar data from Reference 33, were analyzed and correlated to provide a means for the prediction of single phase pressure losses in geometries other than those tested. This effort is described in Appendix D and resulted in the following equations for the calculation of single phase pressure drop in tubes containing helical inserts.

$$\Delta P_f = f_e \frac{L_H}{D_e} \frac{G_H^2}{2g_c \rho_f} \tag{9}$$

where

$$f_e = \frac{0.316}{\left(\frac{D_e G_H}{\mu_f}\right)^{\frac{1}{4}}} \tag{10}$$

$$\frac{G_H}{G} = \frac{L_H}{L} = \sqrt{1 + \left(\frac{\pi D}{P}\right)^2} \qquad (11)$$

$$D_e/D_i = \frac{1 - \left(\frac{D_{cb}}{D_i}\right)^2}{1 + \frac{D_{cb}}{D_i} + \frac{1}{\pi}\left(1 - \frac{D_{cb}}{D_i}\right)} \qquad (12)$$

The boiling pressure drop data obtained at constant power with the 0.67-inch ID boiler tube are plotted in Figure 36 as pressure drop versus mass velocity. Data for two different boiling temperatures, two insert geometries and several power levels are shown.

Under the test plan employed for the data of Figure 36, both the total power and the potassium exit temperature were held approximately constant while the potassium flow rate was varied. For all of the data points for which the exit quality was less than 100%, this corresponded to holding the boiler exit pressure constant also, due to the relationship between fluid pressure and temperature at saturation. However, for the four data points taken with the insert with superheated vapor conditions at the boiler exit, the pressure was lower (exit temperature constant). Lowering the pressure for the superheated vapor data points, as was required to maintain fixed exit temperature, reduced the effective density of the fluid in the boiler. This reduction in density, in turn, caused some of the increase in measured pressure loss with reduced mass velocity shown for the superheated vapor data points.

Before the "Martinelli" and "homogeneous" potassium pressure loss predictions of Reference 8 became available, early adiabatic two-phase potassium

pressure loss data obtained in the test facility were correlated by an alternate technique (Reference 4). This alternate technique assumed the two-phase pressure loss to be proportional to the pressure loss calculated for the vapor fraction of the flow alone, and yielded the following correlating equations.

$$\frac{\Delta P_{TPF}}{\Delta P_g} = 3.0 \tag{13}$$

where

$$\Delta P_g = \frac{f\ L/D\ \rho_g\ V_g^2}{2g_c} \tag{14}$$

$$V_g = \frac{xG}{\rho_g} \tag{15}$$

Equations (13-15) are not employed in this report for correlation or prediction of the experimental pressure loss data as they have several disadvantages with respect to the more general "Martinelli" and "Homogeneous" predictions as follows:

(1) Equation (13) is empirically derived from experimental data, whereas both the "Martinelli" and "Homogeneous" techniques quantitatively predict two-phase potassium pressure loss without recourse to experimental potassium data.

(2) Equations (13-15) predict the pressure loss to be three times the vapor pressure loss at 100% quality, where the flow is all vapor. This is incorrect. Both the "Martinelli" and the "Homogeneous" techniques predict the proper pressure loss at 100% quality.

(3) Equations (13-15) predict the pressure loss to be zero when the quality is zero. This is also incorrect as the pressure loss at zero quality is in

actuality the pressure loss for all liquid flow. Both the "Martinelli" and "Homogeneous" techniques predict the proper pressure loss at zero quality.

The two-phase pressure loss correlation technique described by equations (13-15) is attractive because of its simplicity and it does correlate experimental adiabatic two-phase potassium pressure loss data fairly well at intermediate qualities (Reference 4). Because of the deficiencies cited above, however, the technique is not recommended. The more general "Martinelli" and "Homogeneous" techniques are preferable. As discussed earlier in this section of the report the "Martinelli" prediction yields the best agreement with the experimental boiling potassium data.

The boiling pressure loss results presented in Figures 32, 35 and 36 were measured using the Taylor pressure gages located at the boiler inlet and exit. For data runs in which helical inserts were employed, the local potassium temperature profile, including the potassium temperatures at the initiation of boiling and at the potassium exit, was directly measured by thermocouples positioned inside the insert centerbody. These data were also employed to compute the boiling pressure losses by assuming that the local static pressure is the saturation pressure corresponding to the local temperature measured with the insert thermocouples. Figure 37 shows a comparison for all the insert data of the pressure drop determined from the thermocouples (ΔP_T) against the pressure drop determined from the Taylor pressure gages (ΔP_G). The comparison is quite good, the average arithmetic deviation being only 0.06 psi and the average absolute deviation being 0.8 psi, which is within the estimated error range of the pressure gages themselves. Within the accuracy of the pressure gages, this agreement indicates that the local temperatures measured in the two-phase potassium stream are very nearly, if not exactly, the same as the saturation temperatures corresponding to the local static pressure.

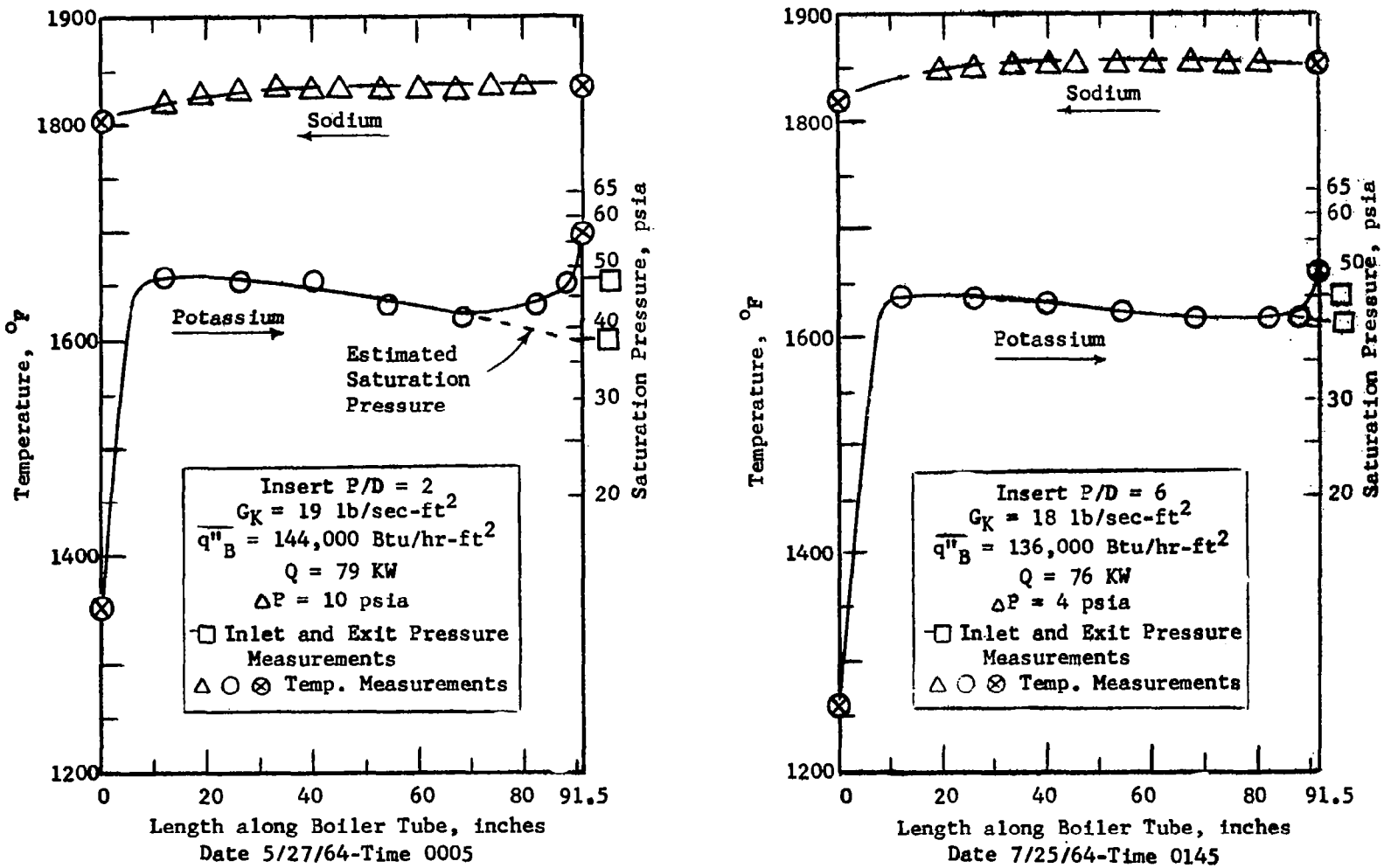

Figure 15. Fluid Temperature and Pressures Measured For Once-Through Boiling of Potassium With Helical Inserts In a 0.92-inch ID Tube

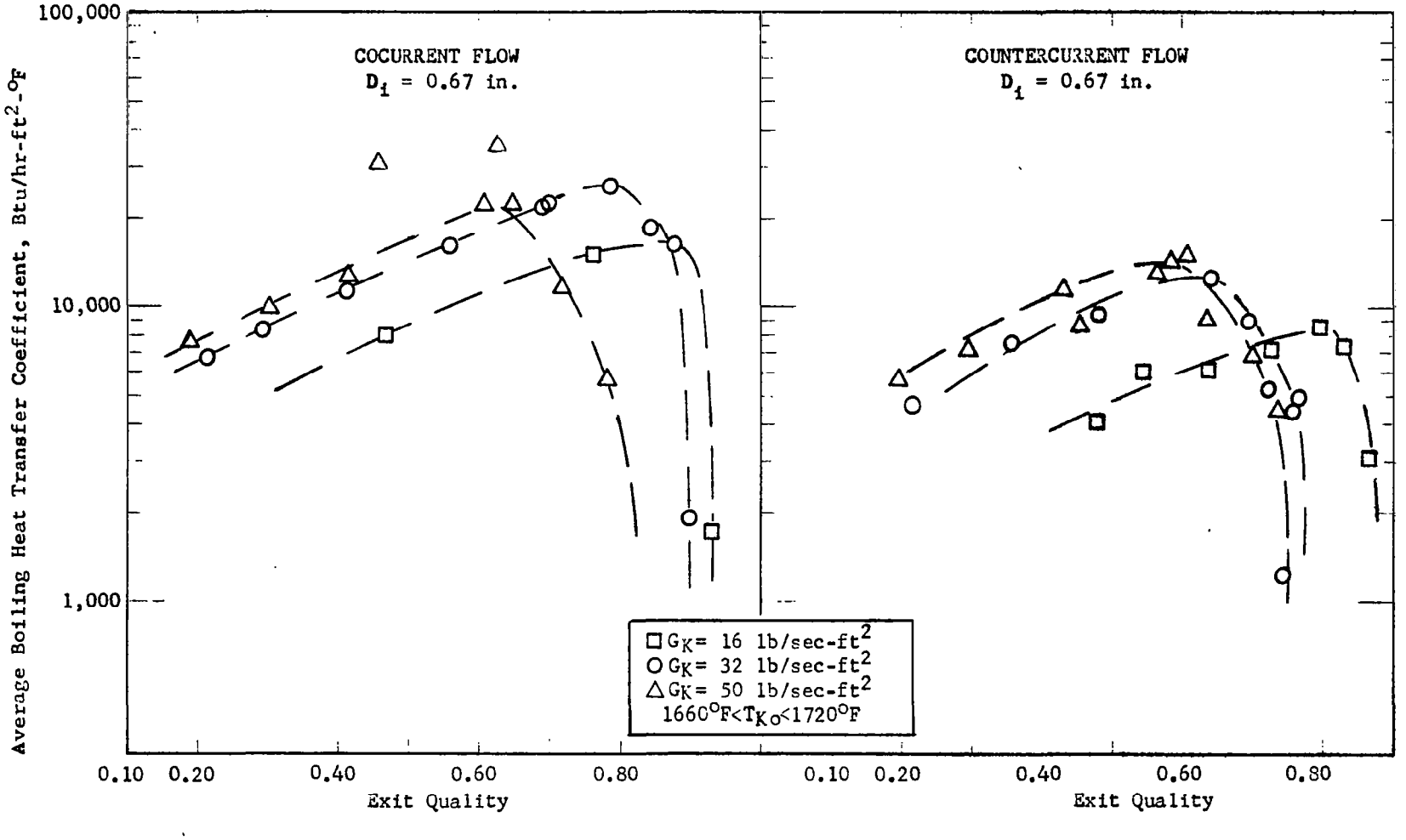

Figure 16. Average Boiling Heat Transfer Coefficients with No Insert Versus Quality; Mass Velocity Parameter

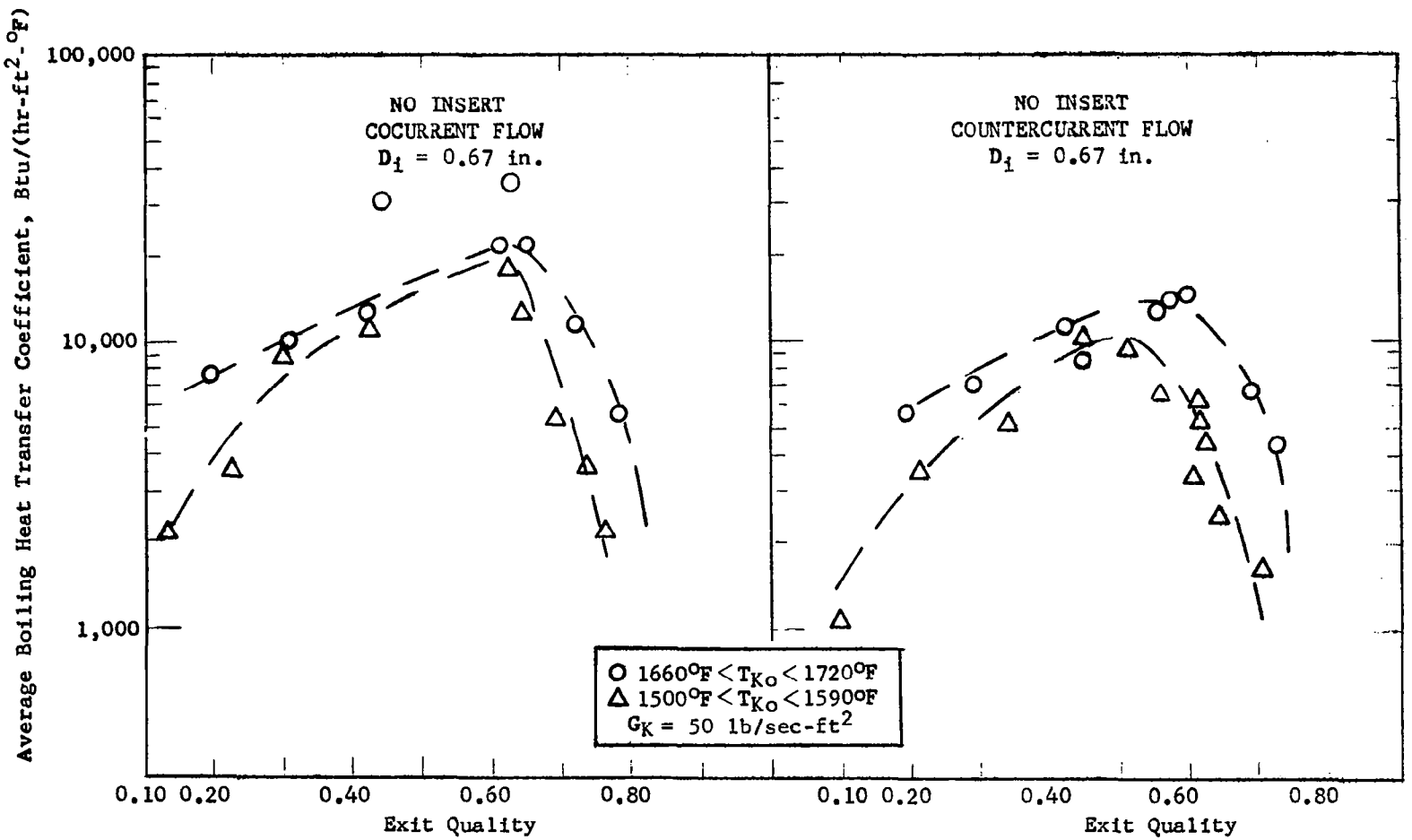

Figure 17. Average Boiling Potassium Heat Transfer Coefficients with No Insert Versus Quality; Boiler Exit Temperature Parameter

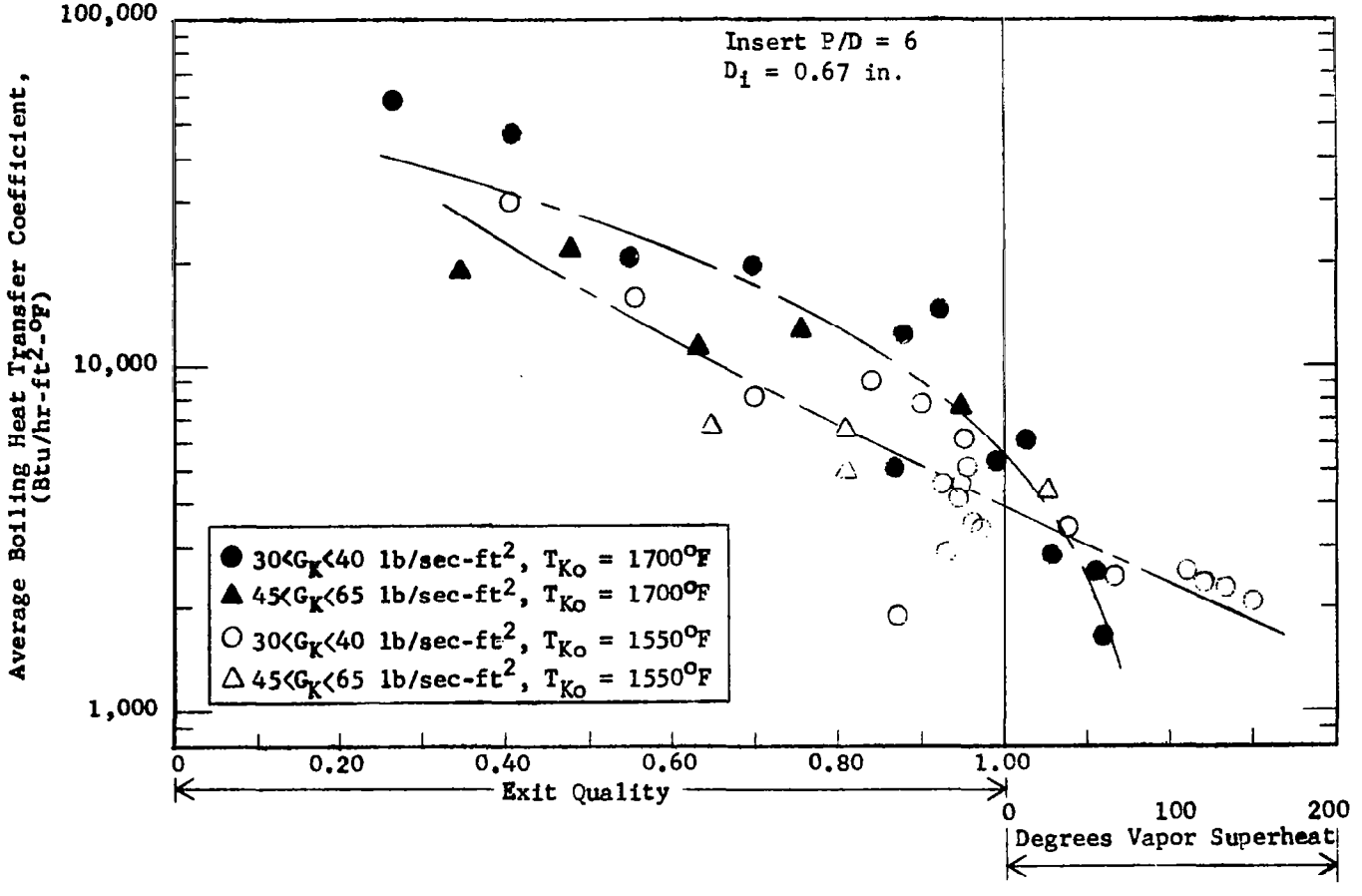

Figure 18. Average Boiling Potassium Heat Transfer Coefficients with Insert Versus Quality; Mass Velocity and Temperature Parameters

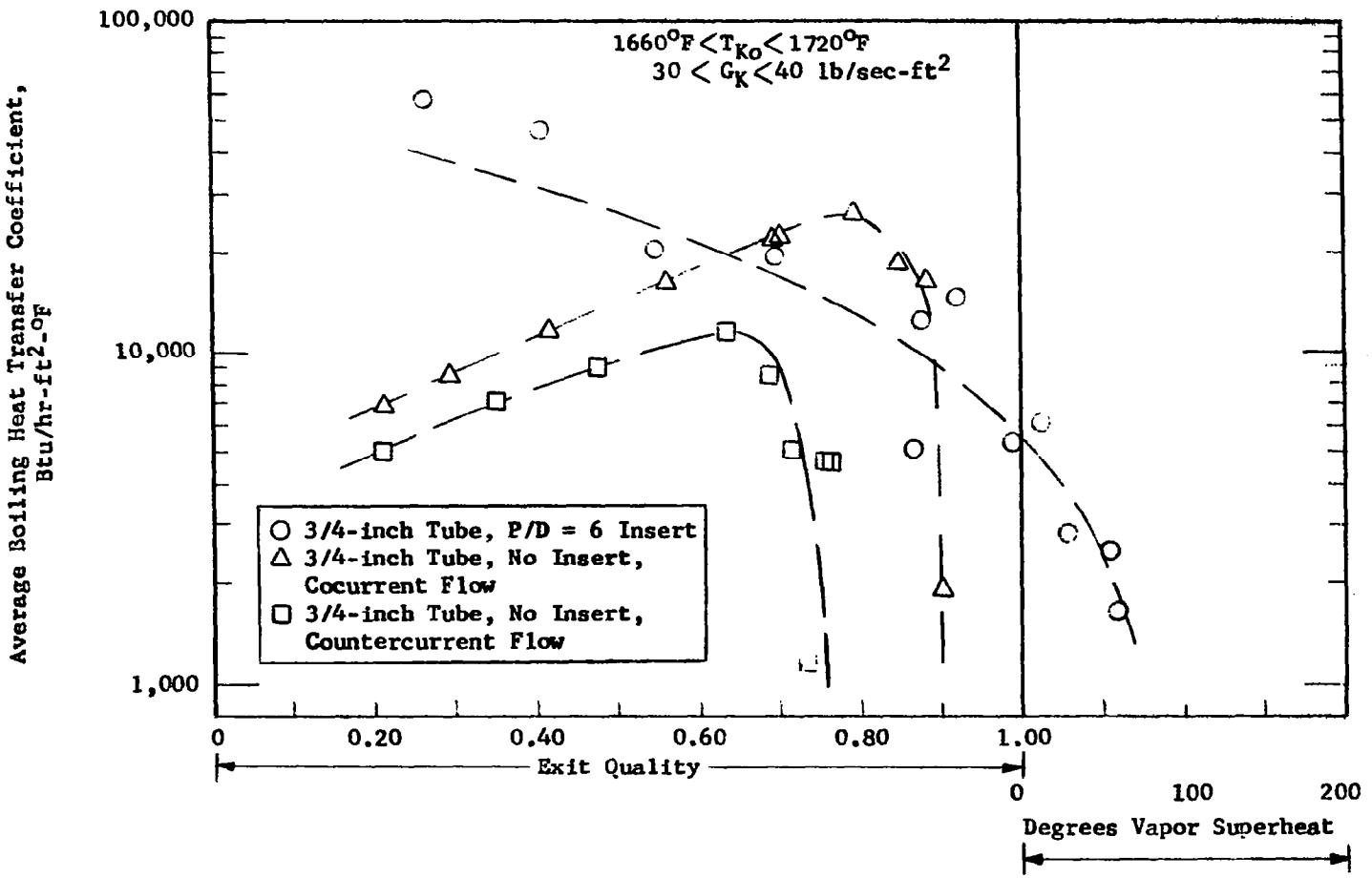

Figure 19. Comparison of Average Boiling Potassium Heat Transfer Coefficients With and Without Inserts, With Countercurrent and Cocurrent Sodium Flow for the Non-Insert Case

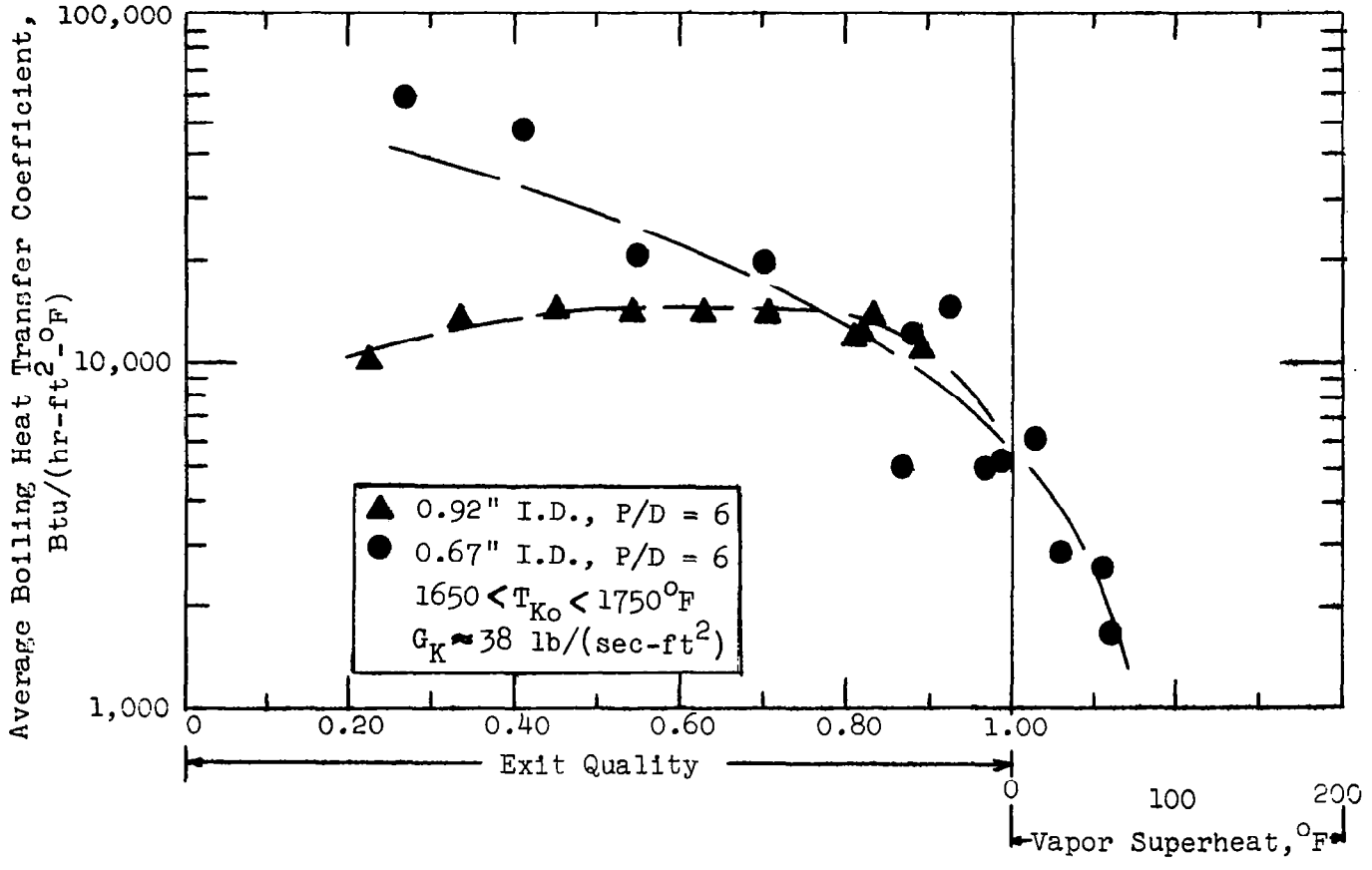

Figure 20. Average Boiling Heat Transfer Coefficients Versus Quality With Tube Diameter As A Parameter

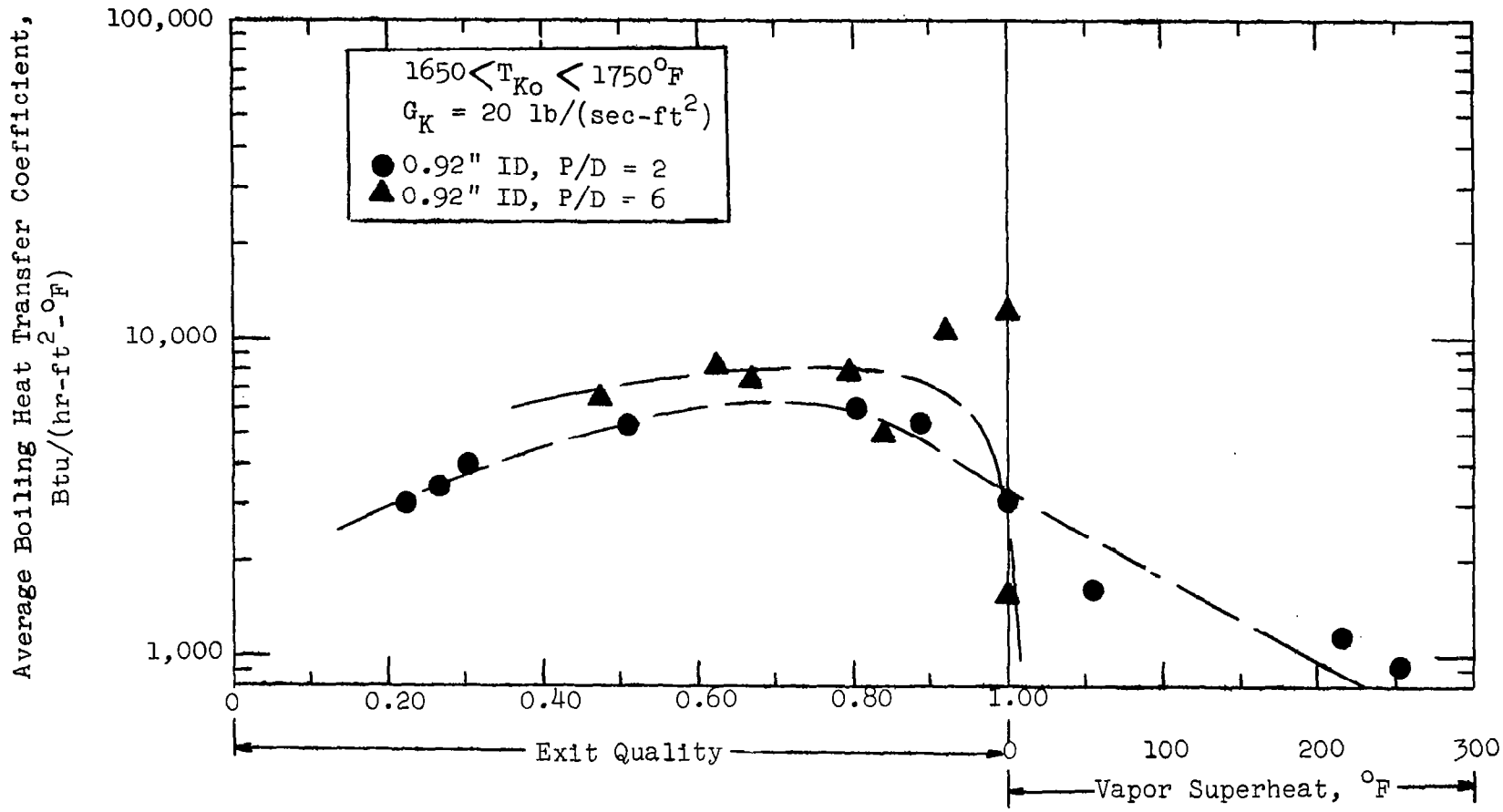

Figure 21. Average Boiling Potassium Heat Transfer Coefficients From 0.92" ID Boiler Tube Versus Quality With Insert Twist Ratio As A Parameter

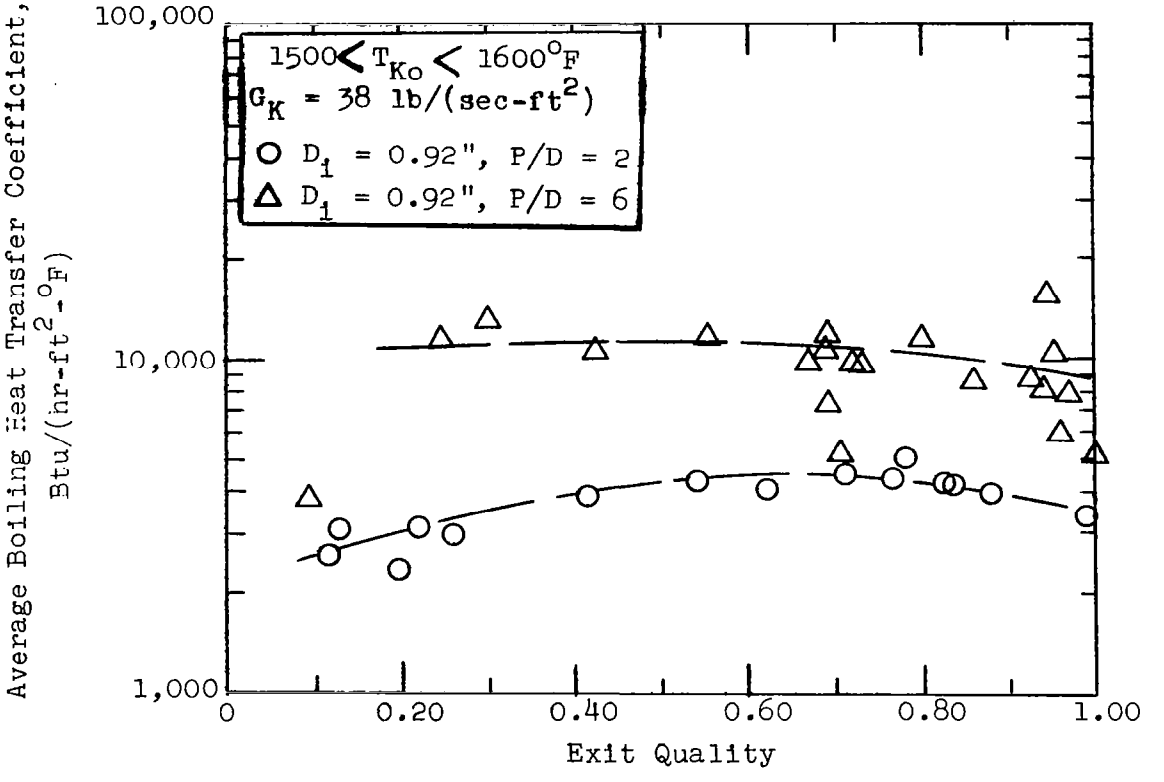

Figure 22. Average Boiling Potassium Heat Transfer Coefficients From 0.92" ID Boiler Tube Versus Quality With Insert Twist Ratio As A Parameter

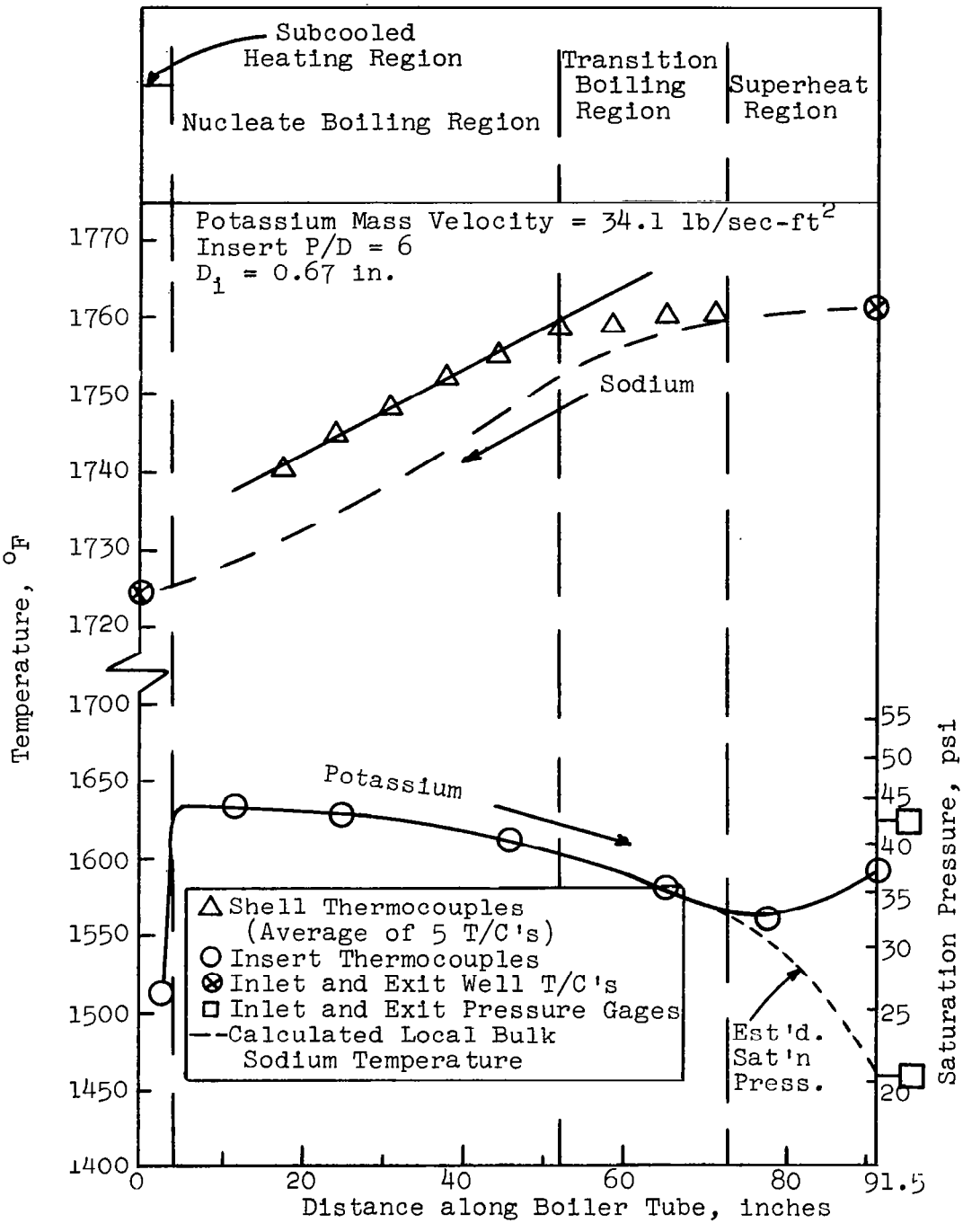

Figure 23. Measured Fluid Temperature Profiles for a Superheat Run (Data Run Obtained at 0800 hours, 10/12/64)

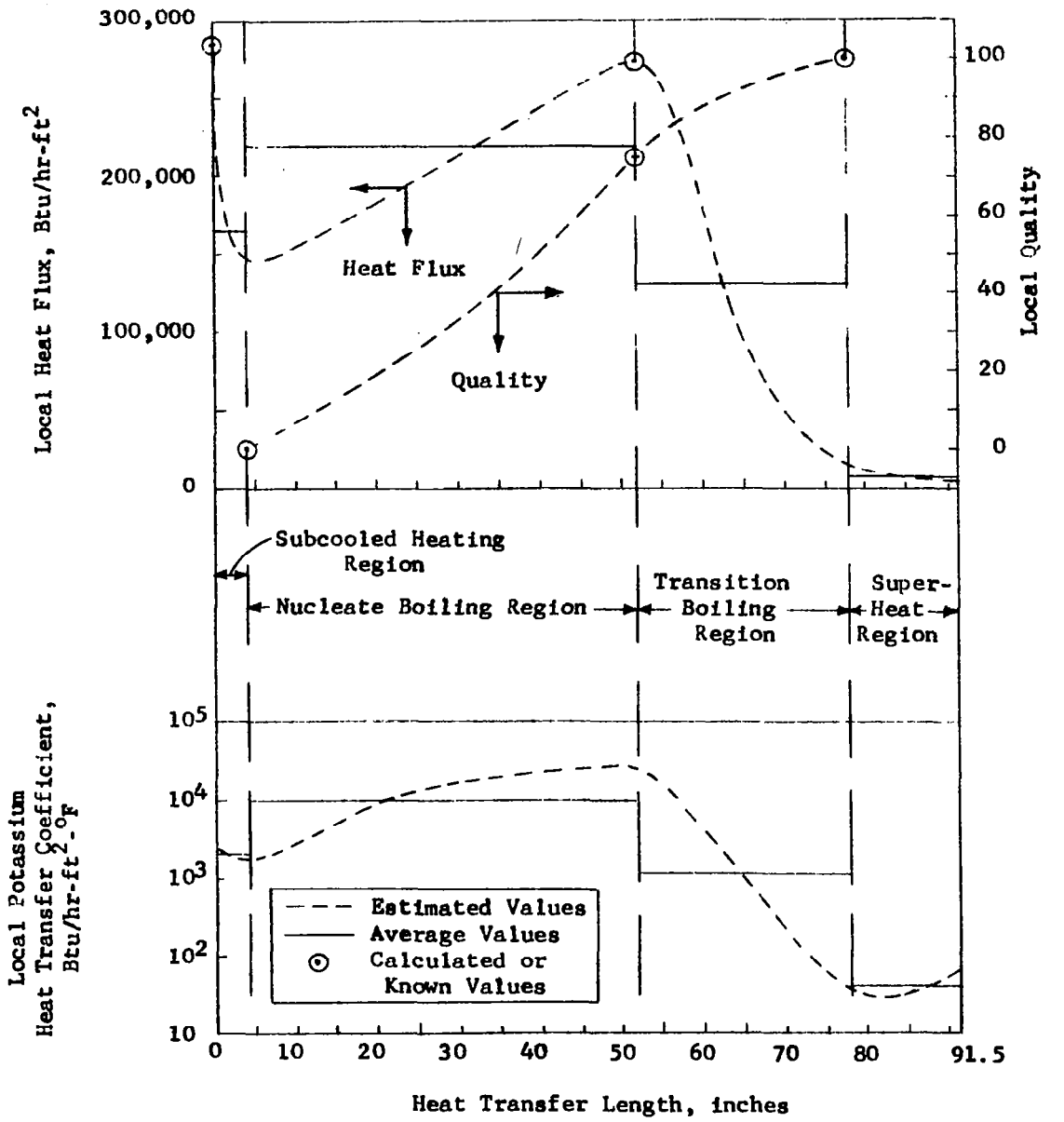

Figure 24. Local Results for a Once-Through Boiling Run With P/D = 6 Insert, (Data Run Obtained at 0800 hours, 10/12/64)

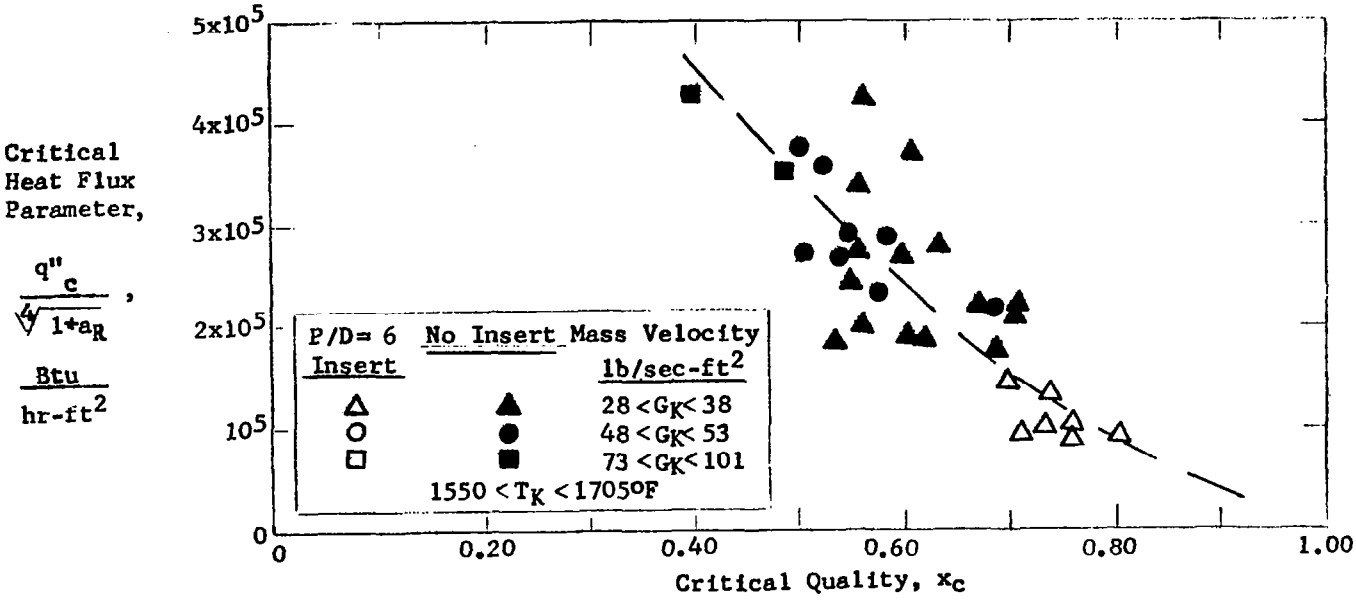

(a) Effect of Mass Velocity

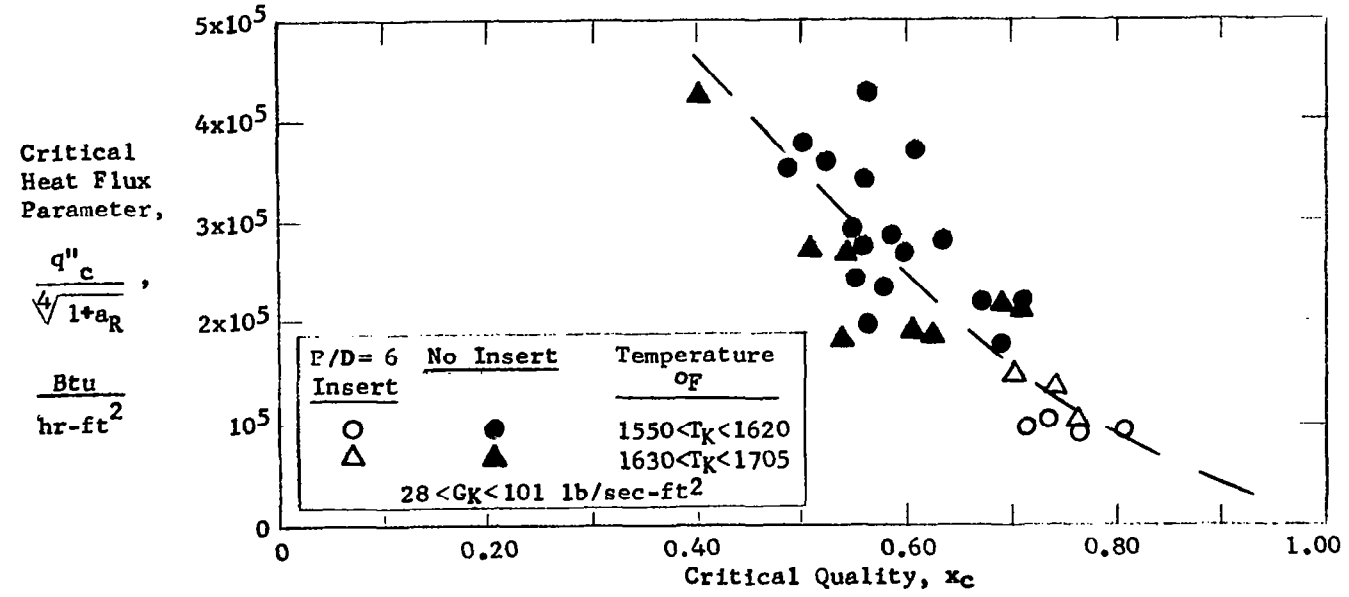

(b) Effect of Temperature

Figure 25. Critical Heat Flux Results Obtained With a 0.67-inch I.D. Boiler Tube

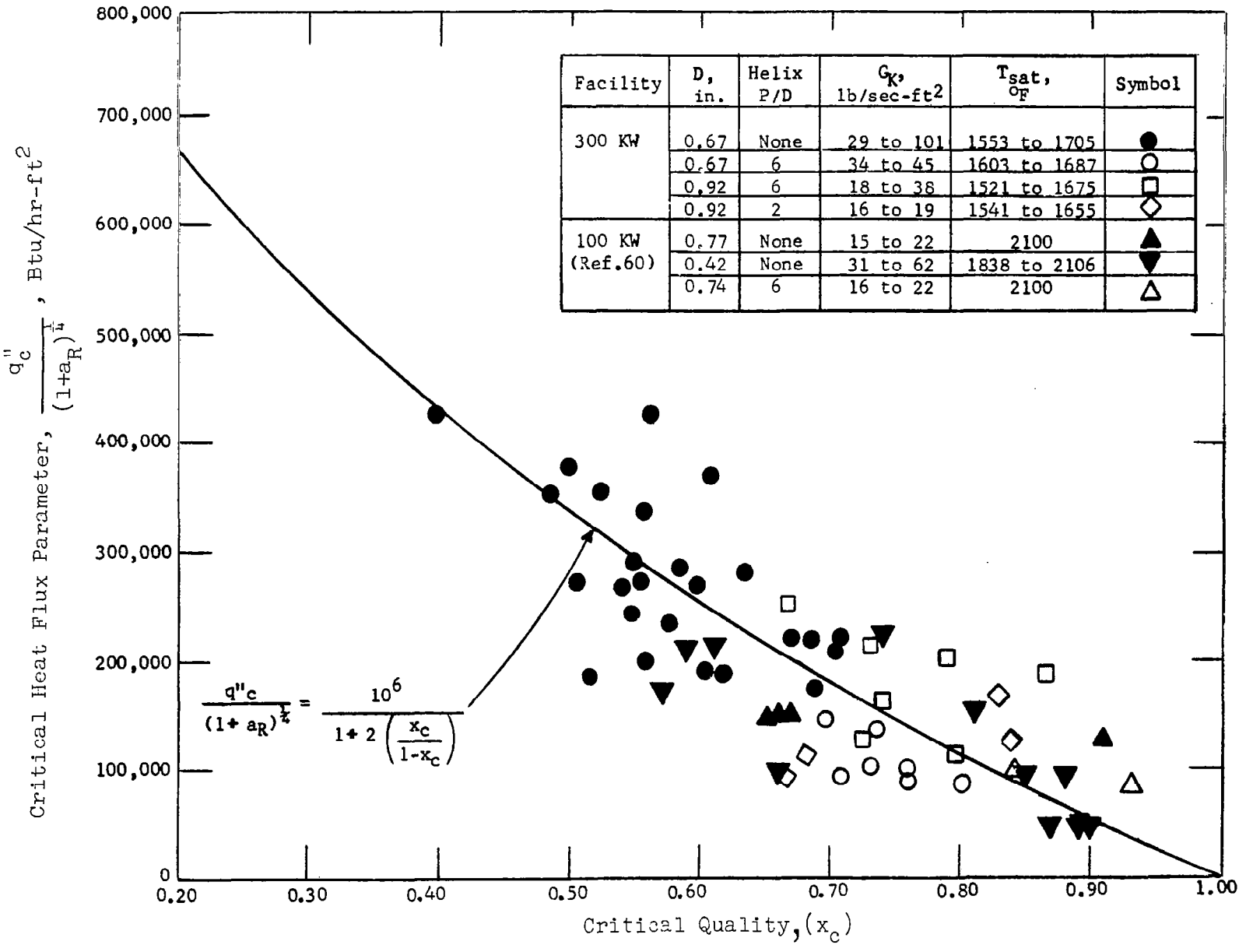

Figure 26. Potassium Critical Heat Flux Data and Correlation

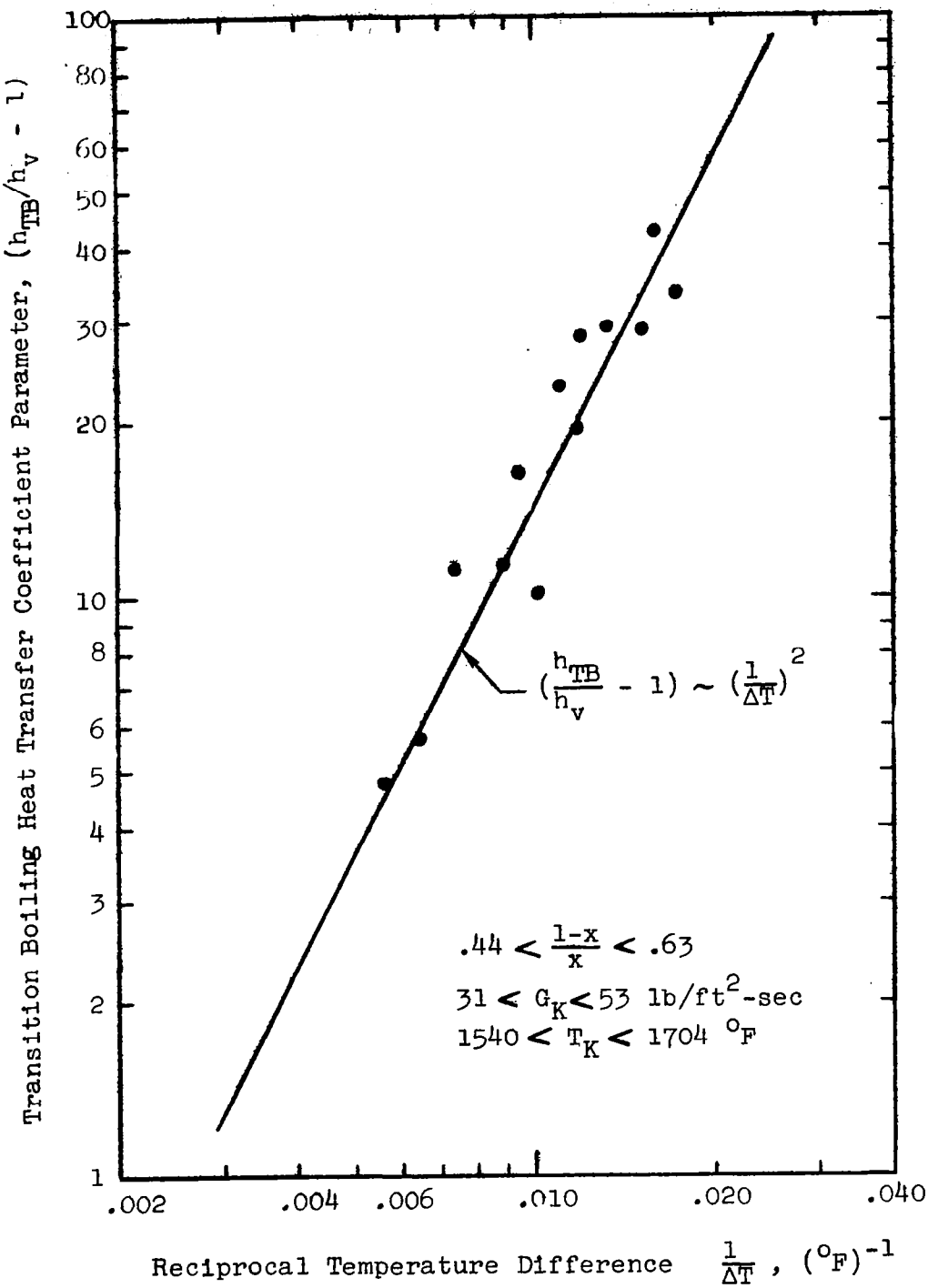

Figure 27. Effect of Tube Wall to Potassium Temperature Difference, Transition Boiling Data from 0.67-inch I.D. Tube with No Insert

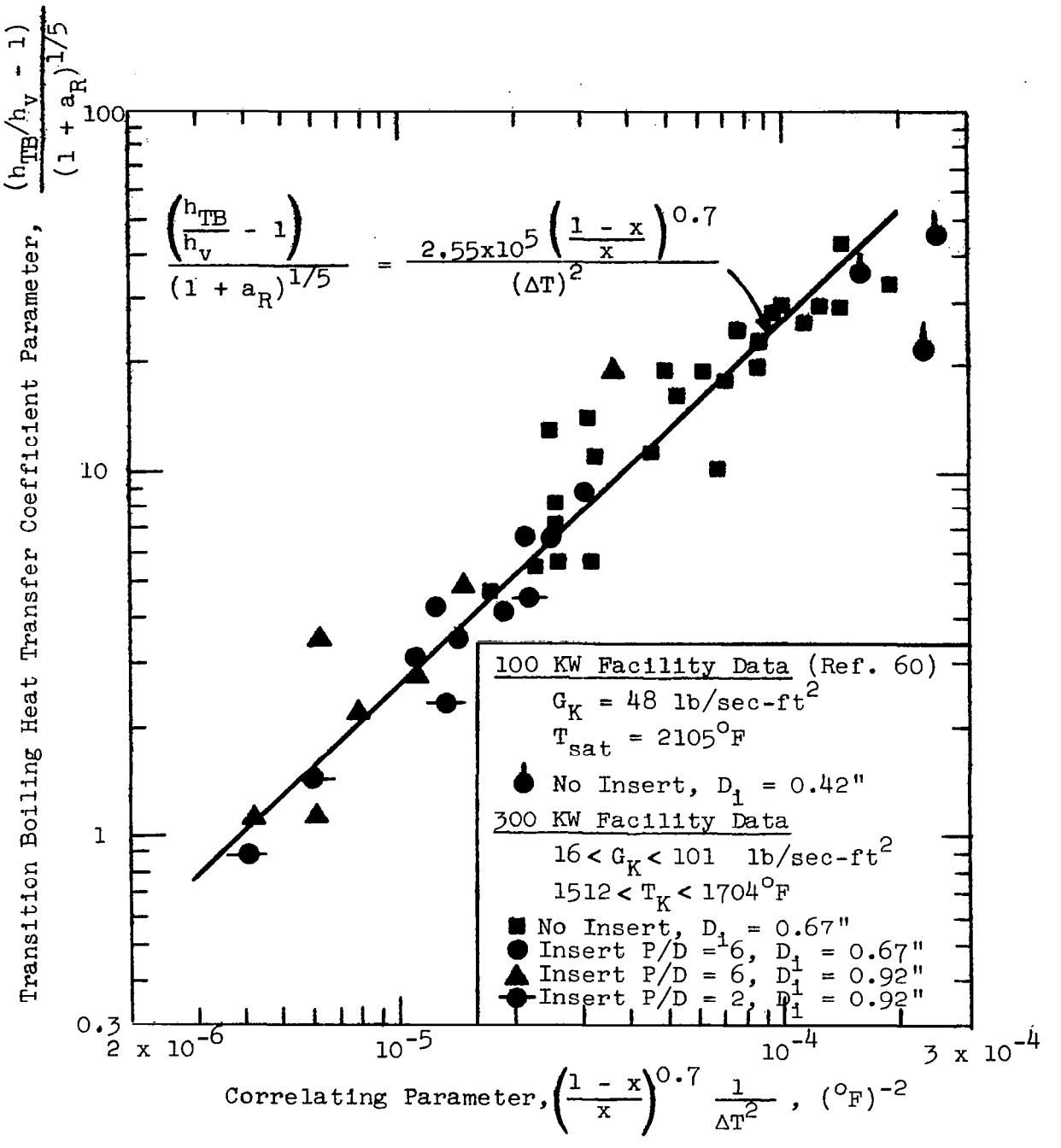

Figure 28. Potassium Transition Boiling Data and Correlation

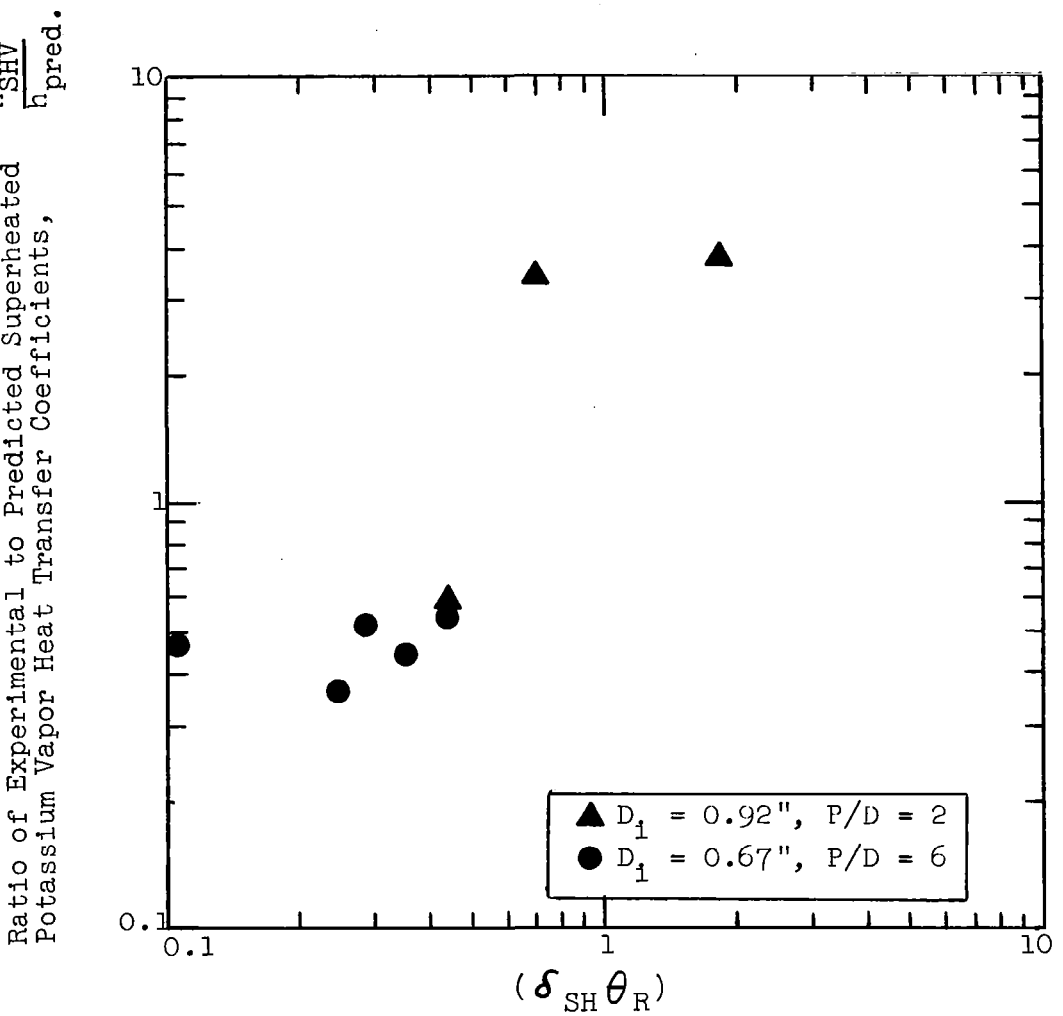

Figure 29. Relation of the Ratio of Experimental and Predicted Superheated Vapor Heat Transfer Coefficients to the Product of Vapor Residence Time and Boiler Exit Bulk Superheat

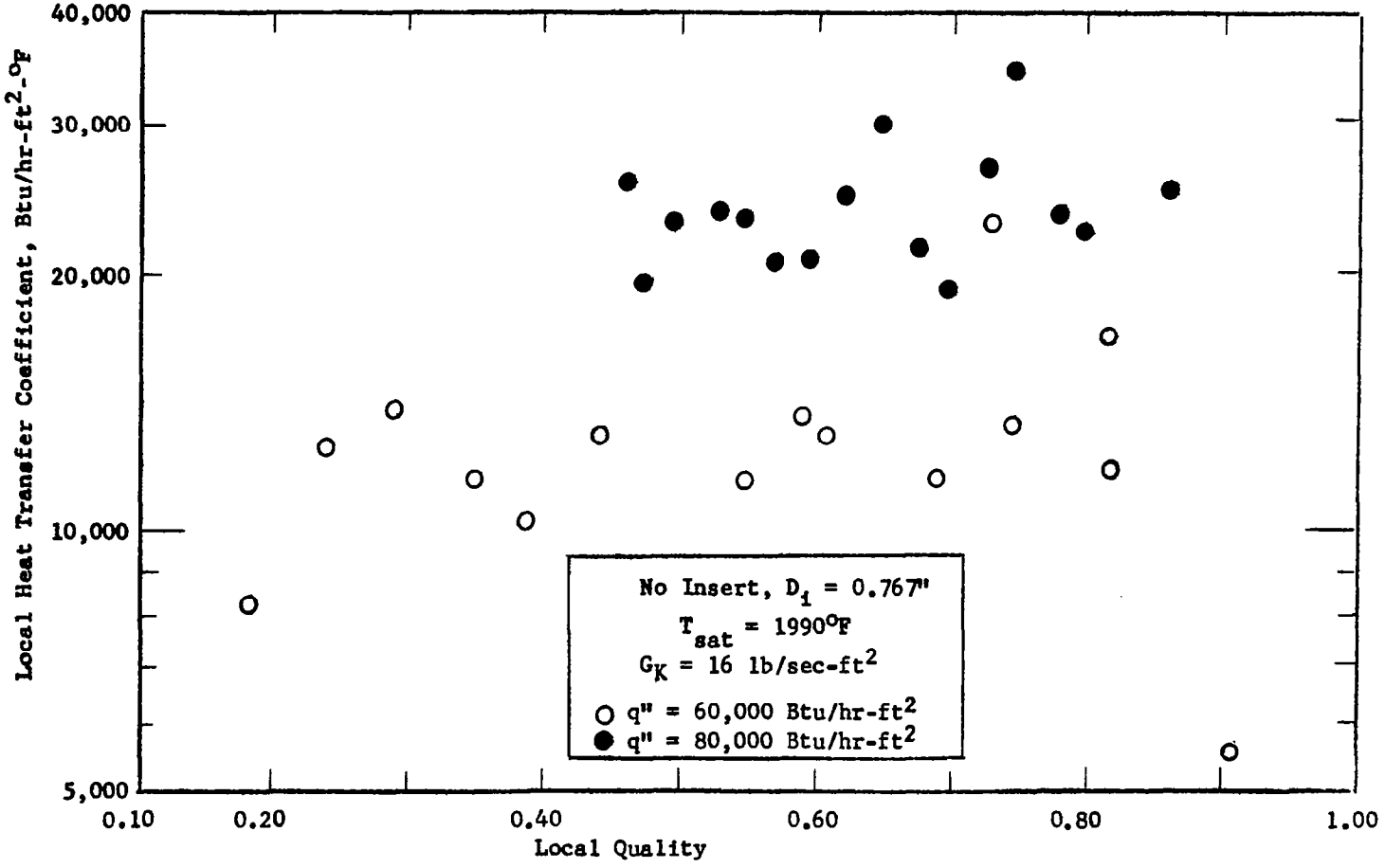

Figure 30. Potassium Nucleate Boiling Data (Reference 60)

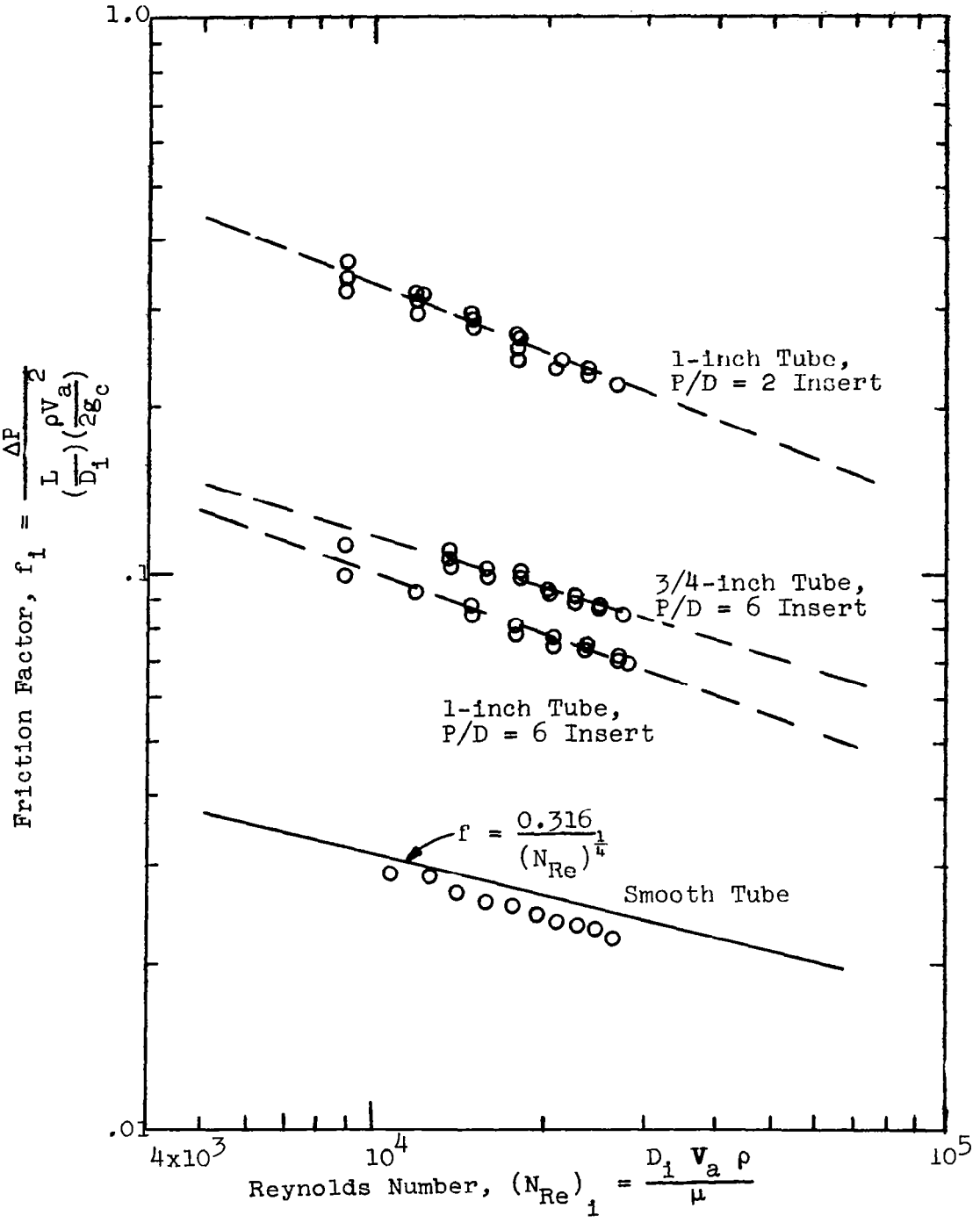

Figure 31. Water Pressure Loss Friction Factors

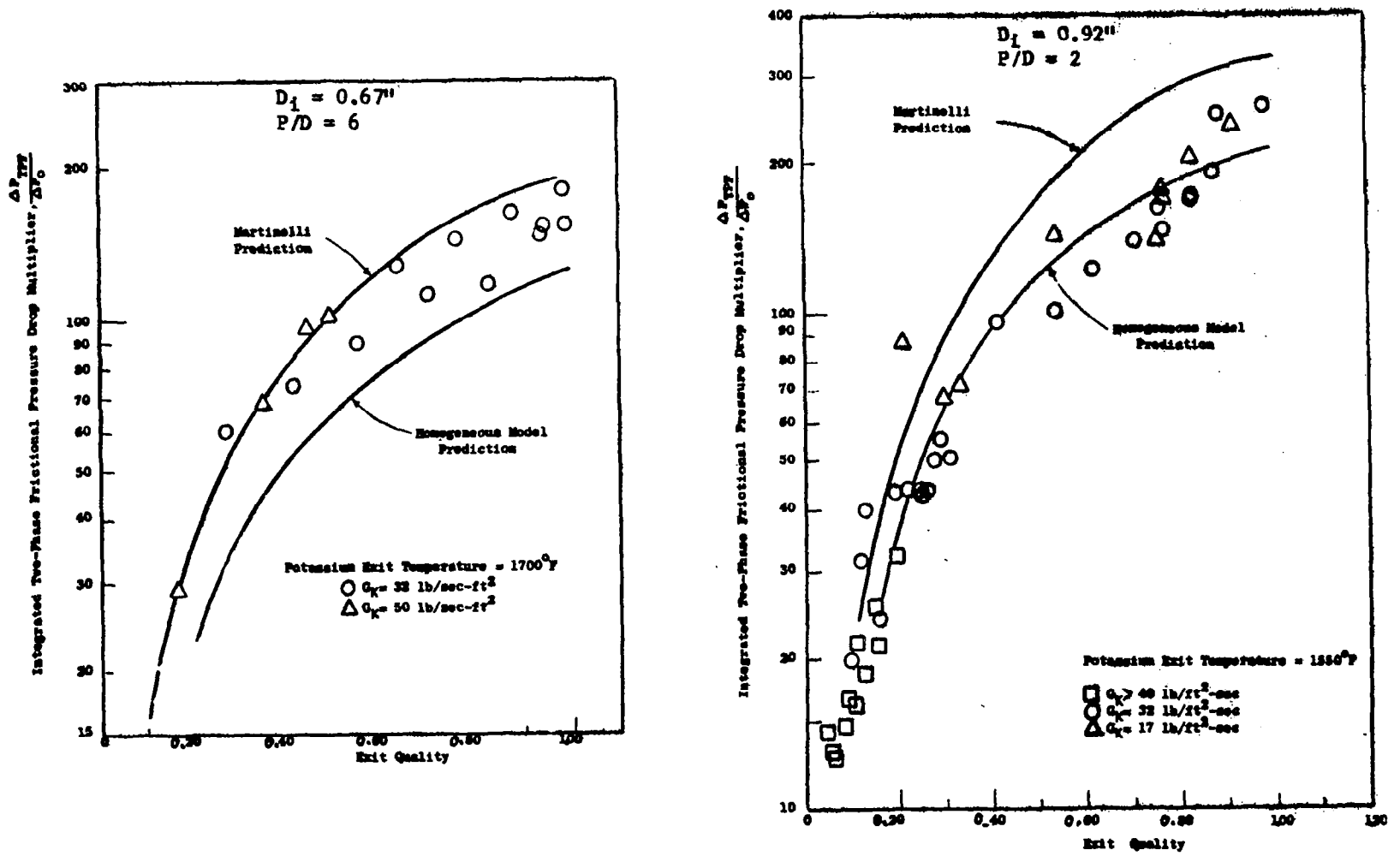

Figure 32. Typical Two-Phase Frictional Pressure Drop Multipliers

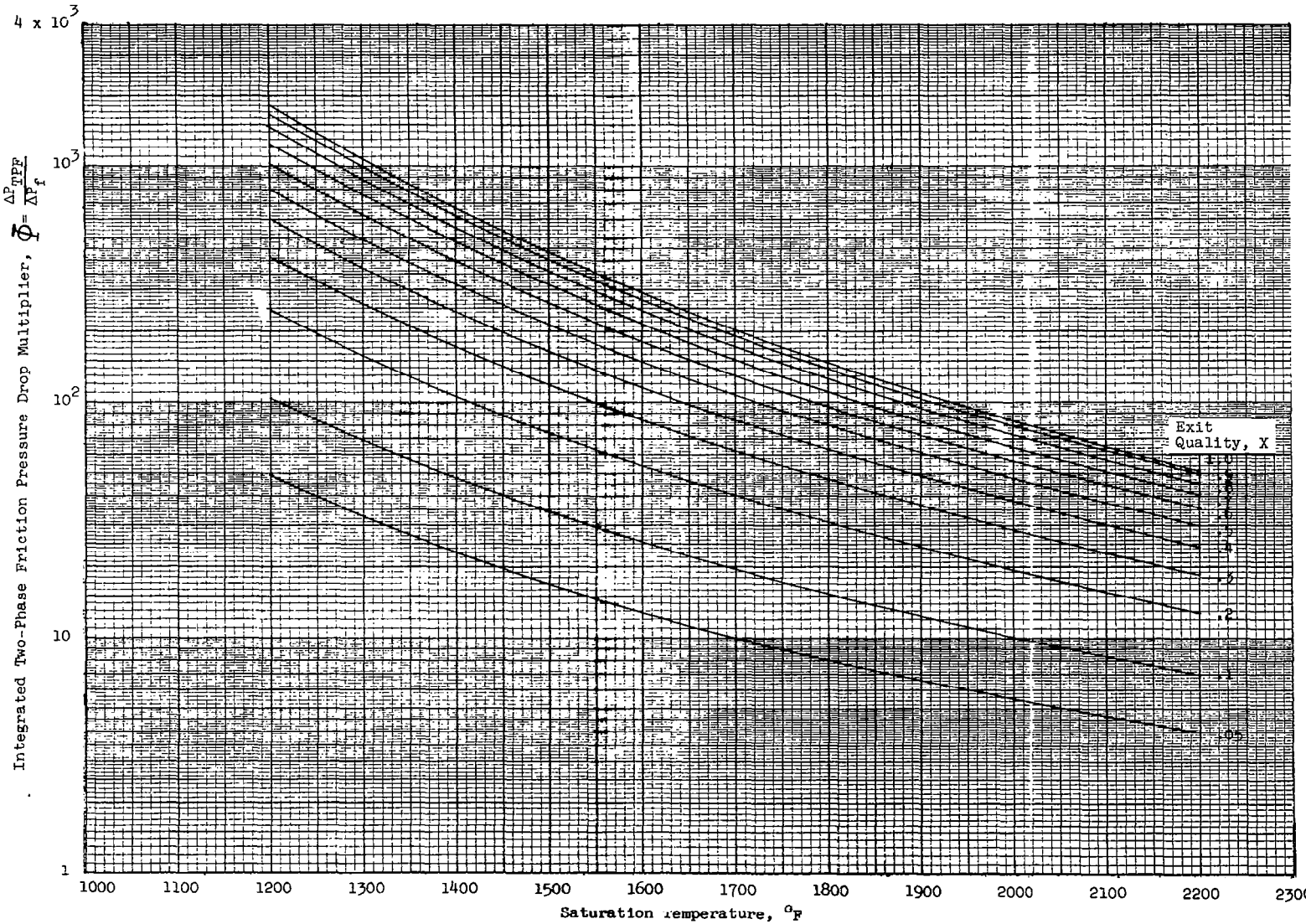

Figure 33. Integrated Two-Phase Friction Pressure Drop Multipliers For Potassium From Modified Martinelli Model of Reference 8

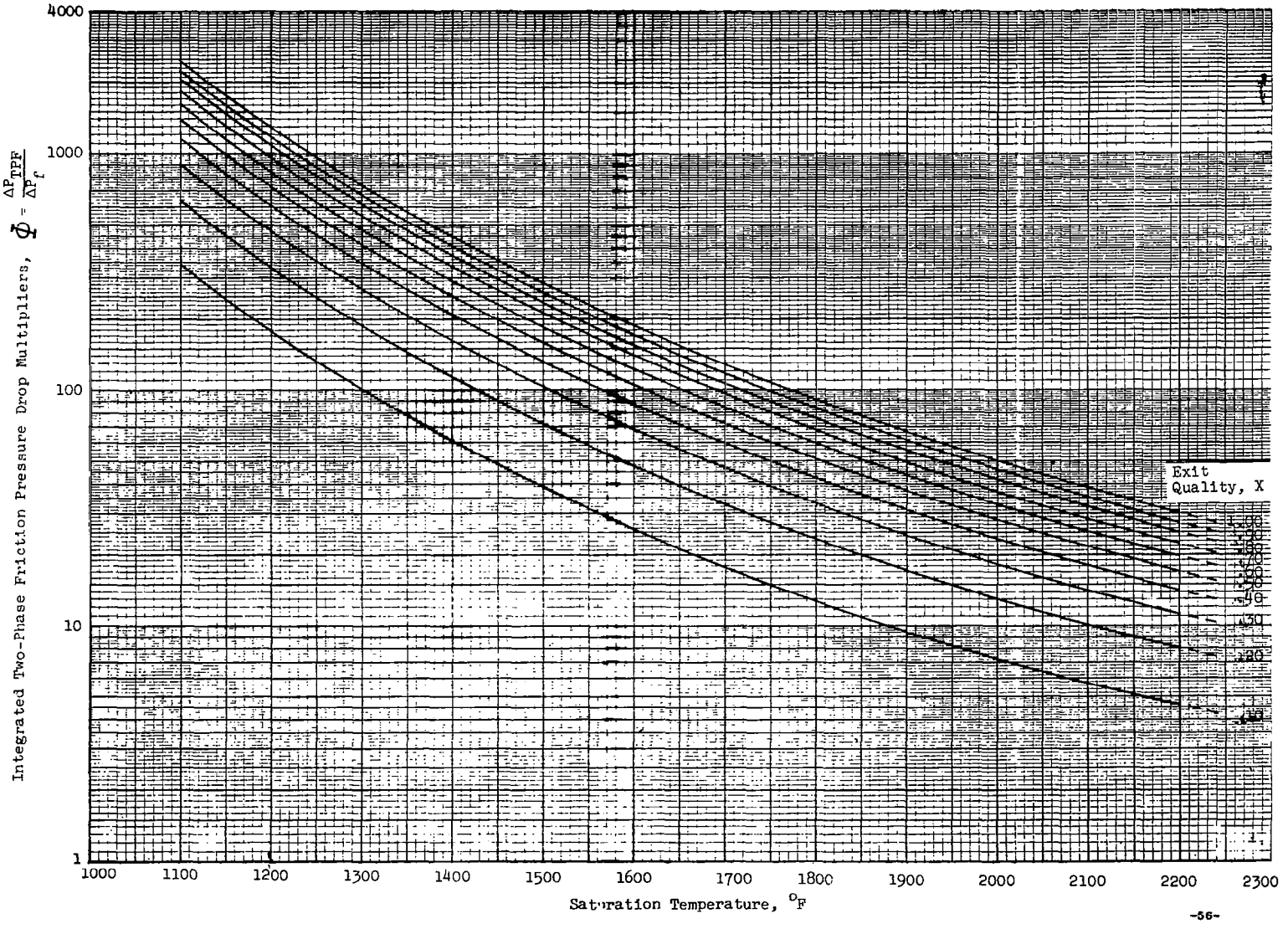

Figure 34. Integrated Two-Phase Friction Pressure Drop Multipliers For Potassium From Homogeneous Flow Model of Reference 8

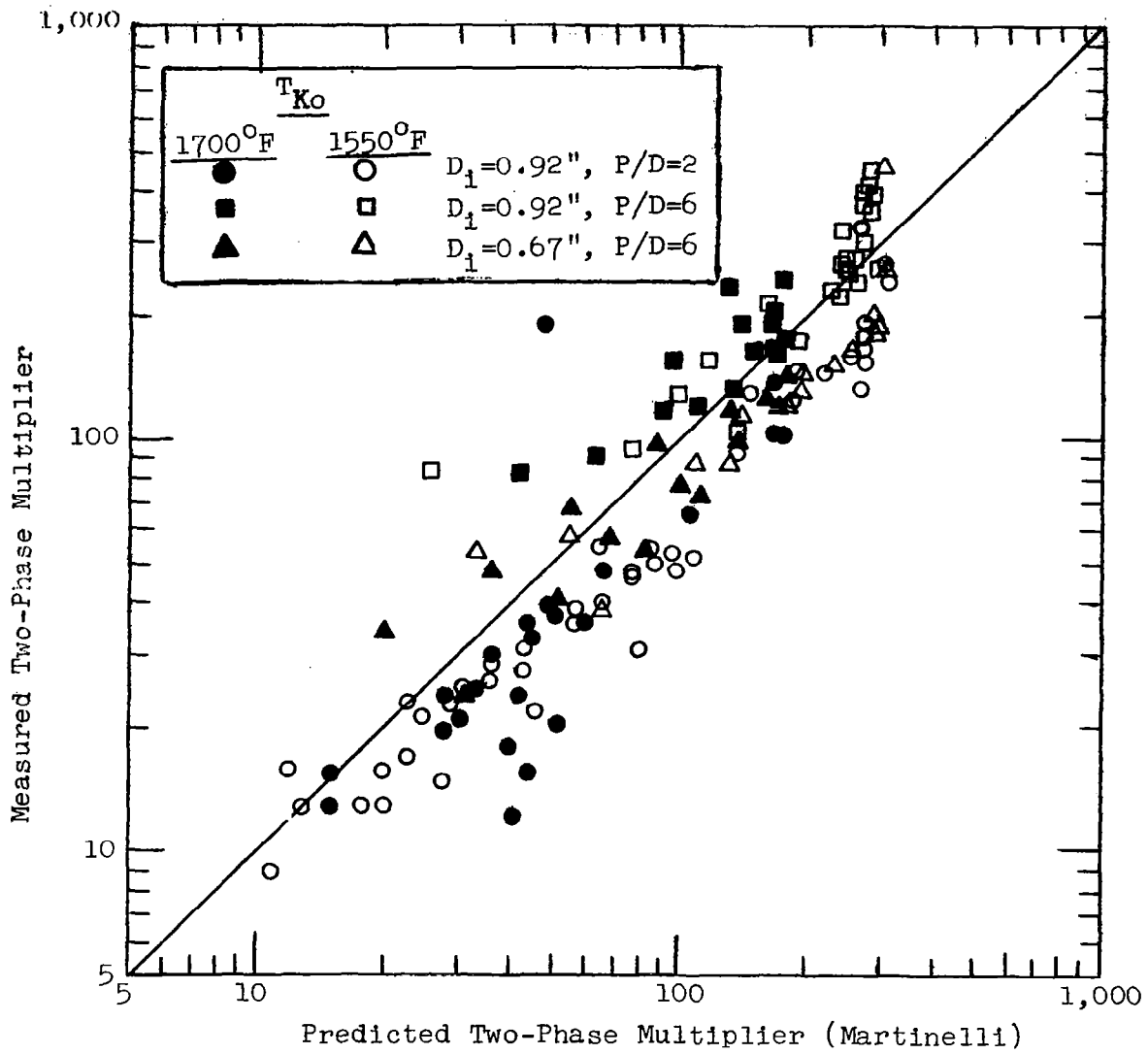

Figure 35. Comparison of Experimental and Predicted Two-Phase Multipliers For Potassium. (Martinelli Predictions are taken from Figure 33)

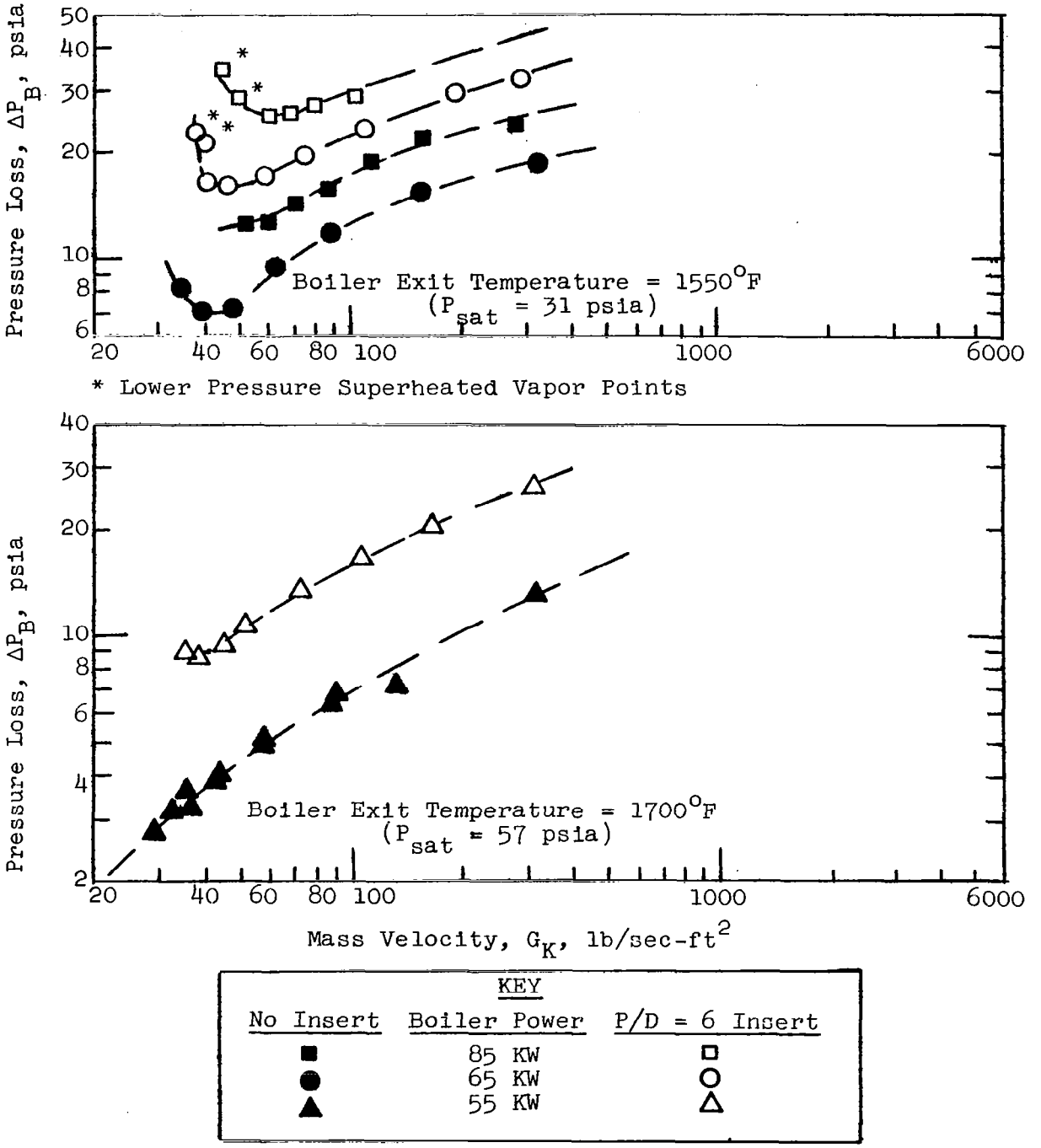

Figure 36. Boiling Pressure Loss Versus Mass Velocity at Various Constant Power Levels and Exit Temperatures for a 0.67-inch I.D. Tube

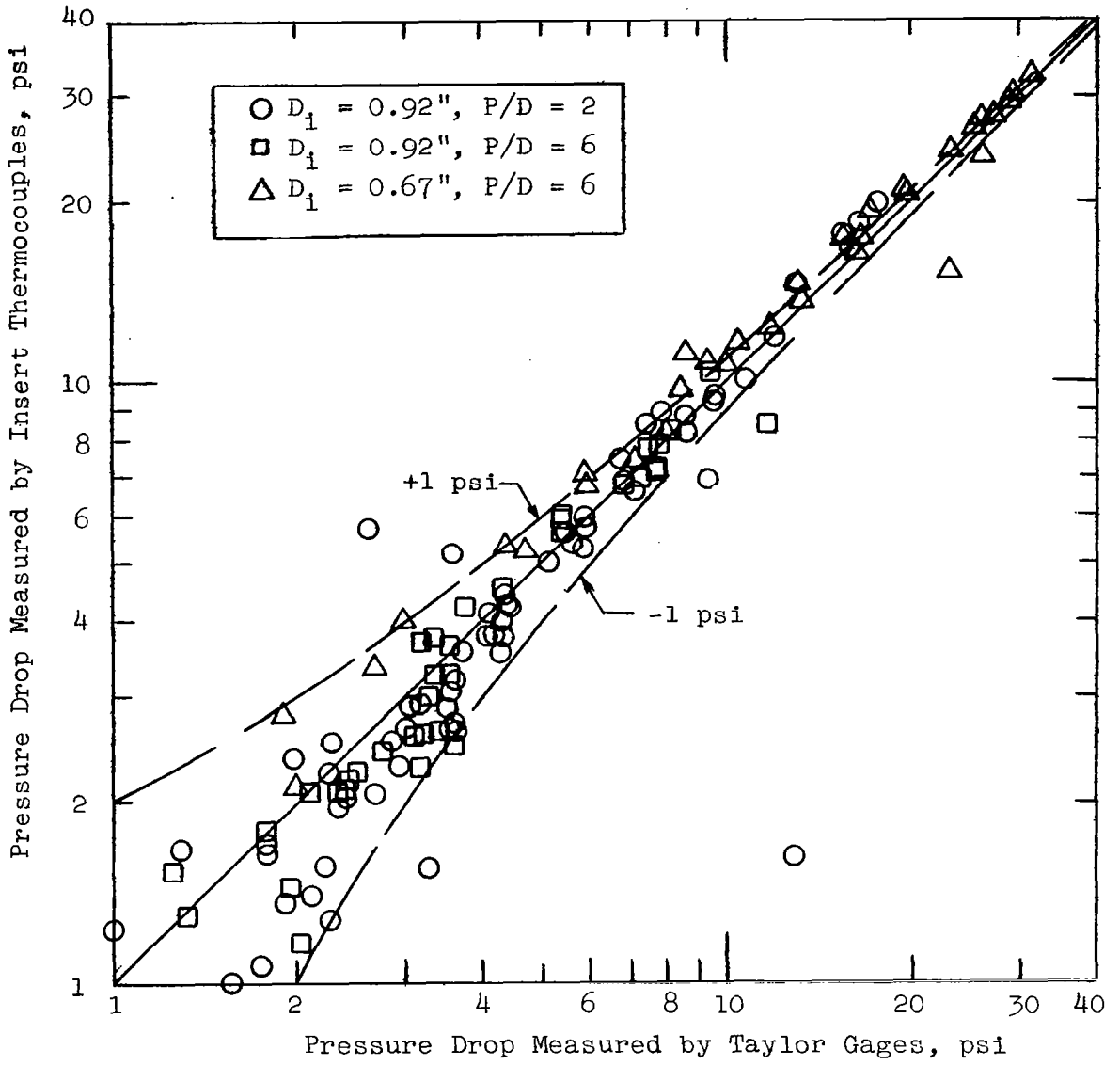

Figure 37. Comparison of Pressure Drop Measured by Insert Thermocouples to Pressure Drop Measured by Gages

VI DISCUSSION OF EXPERIMENTAL RESULTS

The probable error of the experimental boiling potassium frictional pressure loss data with respect to the modified Martinelli model prediction given by Figure 33 is 28%. This indicates that the Martinelli model modified for potassium, as given by Figure 33, when used in conjunction with the single phase liquid pressure drop correlation developed in Appendix D, provides a means for estimating the pressure losses occurring during the forced convection boiling of potassium in tubes containing helical inserts with reasonable accuracy.

The trend of decreasing critical heat flux with increasing vapor quality exhibited by the experimental forced-convection potassium critical heat flux results (Figures 25, 26) agrees with a similar trend shown by high pressure forced convection water data (Reference 25). References 25 and 52 indicate that there is dependence of critical heat flux upon mass velocity for water. The potassium data (Figure 25a) do not evidence a dependence of the critical heat flux upon mass velocity when plotted versus quality. The potassium pool boiling data obtained by Colver (Reference 22) show an increase in the critical heat flux with increasing temperature level, a value of 300,000 Btu/hr-ft^2 being predicted by his correlating line at 800°F and a value of 800,000 Btu/(hr-ft^2) being predicted at 1850°F. This temperature effect also is not observed in the forced convection potassium data (Figure 25b). It is possible that there are mass velocity and temperature effects upon the critical heat flux for the forced convection flow of potassium in tubes, but such effects, if present, are indicated to be less than the scatter of the data obtained in a plot of critical heat flux versus quality.

No theoretical expressions or correlations were found in the literature to which the potassium transition boiling data could be compared. The correlation employed, however, is based upon the potassium droplet experiments of Geoscience (Reference 31), and agrees qualitatively with the droplet

experimental results. In addition, the correlation obtained (Figure 28) predicts the experimental potassium data from the two-fluid facility within a probable error of 20%, which is considered rather good. The form of the correlation obtained predicts that the transition boiling heat transfer coefficient increases without limit as the tube wall-to-potassium temperature difference (ΔT) decreases. The transition boiling heat transfer coefficient, however, cannot exceed the nucleate boiling heat transfer coefficient. For this reason, the transition boiling heat transfer coefficient correlation should only be applied at ΔT's larger than 58°F, which is the smallest ΔT value obtained experimentally.

The agreement of the controlled heat flux, high temperature (to 2100°F) critical heat flux and transition boiling data of Bond (Reference 60) with the lower temperature controlled temperature data from the two-fluid facility is encouraging. The agreement results in an approximate temperature range of applicability of 1550°F to 2100°F for the correlations presented.

The few superheated vapor heat transfer coefficient data obtained from the two-fluid boiling experiments do not agree well with the values predicted with Equation (7). The deviations of the experimental data from the prediction (Figure 29), however, appear to have a trend. Figure 29 shows that the experimental coefficients increase in relation to the predicted values as the degree of vapor superheat increases and as the fluid residence time in the superheat region increases, suggesting an effect due to entrained liquid droplets. There are other factors which also might be significant, however, such as heat transfer by thermal radiation, deficiencies in the prediction of Equation (7) with respect to the effect of helical inserts, uncertainties in potassium vapor transport properties, and errors in the local heat balance required to determine the heat flux in the superheat region for the experimental data. Further analysis of superheated vapor heat transfer and several additional superheated potassium vapor heat transfer coefficient data at high temperatures are given in Reference 60.

Certain of the characteristics exhibited by the average boiling heat transfer coefficients presented can be explained in terms of the local results. The local nucleate boiling data shown in Figure 30 increase with increasing heat flux, but are virtually unaffected by the vapor quality over the rather large range shown. The increase in the average heat transfer coefficients with both mass velocity and exit quality (Figures 16, 17) is therefore indicated to be primarily a heat flux effect since, in the two-fluid facility, heat flux increases in proportion to mass velocity at constant quality and in proportion to exit quality at constant mass velocity. This result suggests that there may be bubble nucleation for potassium in forced convection bulk boiling. A boiling mechanism based upon conduction through the thin liquid film in contact with the boiler tube wall with evaporation from the film surface predicts the heat transfer coefficient to be markedly influenced by quality and to decrease with increasing temperature level (Reference 6). In contrast, the measured average heat transfer coefficients increase with increasing temperature level (Figures 17 and 18) and the measured local nucleate boiling coefficients are virtually independent of quality (Figure 30). Furthermore, the potassium pool boiling data of Bonilla (Reference 1), for which bubble nucleation is presumed to occur, show an increase in heat transfer coefficient with both heat flux and temperature level. The local nucleate boiling data of Reference 60 and the low vapor quality average heat transfer coefficients from the two-fluid facility both suggest that bubble nucleation may be significant in the nucleate boiling region.

The quality beyond which the average heat transfer coefficients decrease with further increase in quality is associated with the critical heat flux and onset of transition boiling. As the boiler exit quality is increased beyond the quality at which the critical heat flux occurs, the fraction of the tube length occupied by the low performance transition boiling region increases, which causes the average heat transfer coefficient to decrease.

Figure 16 shows that the quality corresponding to the maximum average heat

transfer coefficient increases as the mass velocity decreases. This is because at the lower mass velocities the tube power and, consequently, the heat flux are less, which results in higher vapor qualities being attained before onset of the critical heat flux condition (Figure 26).

For similar reasons, the maximum average heat transfer coefficient in cocurrent flow occurs at a higher quality than in countercurrent flow (Figure 19). Under countercurrent flow conditions, the local sodium-to-potassium temperature difference increases in the direction of potassium flow due to the drop in potassium temperature caused by two-phase pressure loss and due to the increase in local sodium temperature. Under cocurrent flow conditions, the sodium temperature decreases in the direction of potassium flow. The local heat flux, which is proportional to the local temperature difference, is therefore higher at the potassium exit under countercurrent conditions than under cocurrent conditions, which results in a lower quality at onset of critical heat flux conditions for countercurrent flow than for cocurrent flow. This result indicates that operation with cocurrent sodium flow can be advantageous for boilers exiting with less than 100% quality. For boilers with superheated vapor at the exit, however, the increased temperature difference obtainable with counterflow in the low performance vapor superheat region can counterbalance the advantage of cocurrent flow in the boiling region. Thus, the proper flow direction for a particular boiler must be determined for the specific operating conditions required.

The trend of decreasing average heat transfer coefficient with decreasing insert twist ratio exhibited by the data obtained with helical inserts in the intermediate and low quality region is not fully understood. The local results obtained show both the critical heat flux and the transition boiling heat transfer coefficient to be increased by inserts, and thus the decrease in the average boiling heat transfer coefficient at low qualities by the inserts must be due to an effect in the nucleate boiling region. This deduction is consistent with

the experiments of Merte and Clark (Reference 53) and Costello and Adams (Reference 44), who studied the effects of acceleration upon the pool boiling of water, and found a decrease in the nucleate boiling heat transfer coefficient with increasing acceleration for heat flux levels above approximately 50,000 Btu/(hr-ft^2). The local forced convection nucleate boiling heat transfer coefficients taken at higher temperatures with and without inserts by Bond (Reference 60) show this same trend of decreased nucleate boiling coefficient with smaller insert twist ratios.

VII APPLICATION TO BOILER DESIGN

In addition to demonstrating the feasibility of high performance once-through boiling of potassium with inserts, other main objectives of this investigation were to provide data and correlations for analysis and design of power boilers and to identify problem areas requiring further development. In this section procedures for application of the overall, average and local results to boiler design are discussed and an example thermal design for a large-scale once-through potassium boiler is given, based upon the local results obtained. The effect upon the tube length in this example design of assumed uncertainties in the various local design parameters is assessed.

The overall boiling data from the tests facility can be used for large scale boiler designs by direct scale-up if the specified design conditions closely approximate the test conditions. For example, a 10,000 KW-thermal power boiler operating at the conditions of the test run with P/D = 2 helical insert shown in Figure 15 would require about 130 0.92-inch ID tubes of 90-inch length (79 KW per tube were obtained in the test run), and would have a shell diameter of less than 20-inches. The boiler would produce potassium at 1700°F with 100°F superheat from liquid potassium entering the boiler at 1350°F. The heating fluid would enter the boiler at 1840°F, flow countercurrent to the potassium and would have a temperature drop of 36°F.

The application of the average and local results for the thermal design of a specific boiler is considerably more complex than the use of the overall results. The specific calculational procedures utilized for a particular design depend upon which design parameters are fixed; for example, whether the boiler size for a specified performance is to be determined or whether the performance of a particular boiler is to be predicted. In general, however, the calculations in the boiling and superheated vapor regions involve a simultaneous iterative solution of the interdependent pressure loss, energy and heat transfer equations for the several coupled heat transfer regions. Boiler thermal design procedures

based upon the average heat transfer and pressure loss data as well as local heat transfer and pressure loss parameters are presented in Appendix E.

In the design procedure based upon average potassium heat transfer coefficients, the 0 to 100% vapor quality region of the boiler is treated as one increment, which results in relatively simple calculational procedures. The average design procedure, however, cannot be employed with confidence for general parametric studies or for thermal designs beyond the range of the test data, since the heat transfer coefficients employed are averaged over both the nucleate and transition boiling regions, which are affected differently by the various test parameters. The average design procedure is useful for designs within the range of test data and for quickly obtaining approximate designs for preliminary studies.

The thermal design procedure based upon local parameters is more general and exact, but also more complex, since each heat transfer region is solved individually on an incremental basis, employing the correlations appropriate to each region. The local design procedure is recommended for general parametric design studies and for calculation of thermal design points which are beyond the range of temperatures, tube diameters and heat flux levels of the test data.

Example Space Power Boiler Design

In order to illustrate the boiler thermal design procedure and to provide a reference point for determination of the significance of the various design parameters, an example space power boiler thermal design was prepared, employing the local design procedure described in Appendix E. The thermal design is for a 8300 KW thermal power boiler which would produce potassium vapor with 150°F superheat at 2150°F from potassium liquid at 1200°F. Lithium is employed as the primary fluid, entering the boiler at 2200°F and exiting at 2050°F in counterflow to the potassium. A summary of the results of this thermal design analysis is given in Table III. The calculated active tube length for the specified

conditions is 68 inches, and the shell diameter for the 254 0.69-inch ID tubes required is approximately 18 inches. Allowing additional length for the tube headers and inlet and exit plenums, the overall length of the boiler is approximately 90 inches, resulting in an overall length-to-shell diameter ratio of five.

To show directly the beneficial effects of the helical inserts employed in the boiler tubes, a second thermal design was prepared for a boiler having identical thermal specifications, number of tubes and tube diameter, but not utilizing helical inserts. Table IV is a comparison of the results calculated for the two cases. A calculated tube length of 256 inches is required without inserts compared to the 68-inch length calculated for the design employing helical inserts.

The saving in required tube length obtained with inserts is a function of insert twist ratio. The heat transfer performance is improved as the insert twist ratio becomes tighter, but the pressure loss and corresponding potassium saturation temperature drop become greater. Therefore, for fixed potassium exit pressure the available lithium to potassium temperature difference decreases in the low quality region of the boiler as the insert twist ratio is reduced, requiring a corresponding increase in tube length to transfer a specified amount of heat. The insert twist ratio for specified design conditions will therefore have an optimum value, which can be determined by performing the thermal design calculations for several twist ratios. In Figure 38 are plotted the two design points calculated, along with the estimated twist ratio at which the pressure drop is sufficient to cause the potassium and lithium temperatures to approach each other. An estimated curve giving the required tube length as a function of insert twist ratio, which approximates that which would be obtained by further design calculations for several twist ratios is also shown. The insert twist ratio of 1.0 utilized in the example design is seen to be close to the estimated optimum value for the boiler studied.

TABLE III

EXAMPLE THERMAL DESIGN

8300 KW POWER BOILER

Tube Material	Cb-1%Zr
Tube O.D.	0.75-inch
Tube Wall Thickness	0.030-inch
Number of Tubes	254
Tube Length	68-inches
Tube Spacing (Center to Center)	0.975-inch
Shell Internal Diameter	18-inches
Helical Insert P/D	1.0
Equivalent Tube Wall Heat Transfer Coefficient	13,900 Btu/(hr-ft^2-°F)

Lithium

Inlet Temperature	2200°F
Exit Temperature	2050°F
Mass Flow Rate	53.6 lb/sec
Mass Velocity	79.5 lb/(ft^2-sec)
Approximate Pressure Drop	5 psi
Heat Transfer Coefficient	9860 Btu/(hr-ft^2-°F)

Potassium

Inlet Temperature	1200°F
Exit Temperature	2150°F
Exit Pressure	152.3 psia
Exit Vapor Superheat	150°F
Mass Velocity	14.2 lb/(ft^2-sec)
Boiling Pressure Loss	10.0 psi
Length of Subcooled Region	3.5-inches
Length of Nucleate Boiling Region	12.4-inches
Length of Transition Boiling Region	13.9-inches
Length of Vapor Superheat Region	37.8-inches
Average Heat Flux	110,000 Btu/(hr-ft^2)

TABLE IV

COMPARISON OF DESIGNS WITH AND WITHOUT INSERTS

8300 KW POWER BOILER

RESULTS	VALUE WITH INSERT	VALUE WITHOUT INSERT
Total Tube Length	68 inches	256 inches
Length of Subcooled Region	3.5 inches	3.1 inches
Length of Nucleate Boiling Region	12.4 inches	6.6 inches
Length of Transition Boiling Region	13.9 inches	130.7 inches
Length of Superheat Region	37.8 inches	115.7 inches
Boiling Pressure Loss	10.0 psi	0.6 psi
Average Heat Flux	110,000 Btu/(hr-ft^2)	30,000 Btu/(hr-ft^2)

The tube diameter and number of tubes used in the example design were selected so as to result in overall boiler dimensions judged reasonable in relation to a compact space power system. In general, tubes of larger diameter would result in a longer boiler of smaller shell diameter with less tubes, whereas tubes of smaller diameter would result in a shorter boiler of greater shell diameter with more tubes. In a more detailed design analysis directed towards a minimum weight boiler, mechanical design aspects, fabrication difficulties and reliability assurance as well as overall boiler weight and shape considerations would influence the choice of tube diameter. It is not certain that smaller tubes than those selected would yield a performance or weight advantage. The correlations of the superheated vapor and transition boiling heat transfer coefficients employed in the design calculations predict higher coefficients for smaller tube diameters, but the potassium pressure drop is also predicted to increase with decreasing tube diameter. Increased values of these coefficients can also be obtained at the expense of increased pressure drop in large diameter tubes by the use of tighter insert twist ratios. A complete optimization of tube diameter is complex, and requires a more extensive design study than employed for the reference design presented herein.

The lithium and potassium inlet and outlet temperatures and the potassium vapor superheat employed in the example design were selected as being representative of values anticipated to be typical for large space power systems. Design of such systems should include a study of the effect of these and other variables upon component size and weight. In illustration of this, the effects of two of these variables upon the tube length required for the example boiler design were calculated.

Calculated boiler tube lengths as a function of lithium temperature change for fixed lithium inlet temperature and fixed potassium exit temperature and pressure are shown in Figure 39. The boiler tube length (and thus the boiler weight) necessary to satisfy the specified conditions is seen to increase as the lithium temperature change is increased. In an actual system, however,

the lithium pressure drop in both the boiler and the reactor would decrease as the lithium temperature change is increased, due to the corresponding reduction in lithium flow rate. There is, therefore, an optimum value of the lithium temperature change, which results in a minimum system weight with respect to this variable.

Figure 40 shows the effect of exit potassium vapor superheat upon the boiler tube length required for the example design, computed for fixed potassium pressure at the boiler exit and fixed lithium inlet and outlet temperatures. Large values of vapor superheat are advantageous to the turbine of a space power system, in terms of increased output and minimization of blade erosion caused by liquid droplets. An optimum potassium superheat is also indicated for the system, since payment for vapor superheat is made in terms of increased boiler tube length and weight, as indicated by Figure 40. As shown in the Figure, the tube length required in the boiler increases very rapidly as the superheat approaches 200°F, at which point the potassium and lithium temperatures become equal.

Magnitude and Significance of Uncertainties in the Thermal Design Parameters

Uncertainties in the various heat transfer and pressure loss data and correlations employed in the calculations for the example boiler thermal design affect the design to different degrees. The change in calculated boiler tube length resulting from a given uncertainty in the nucleate boiling heat transfer coefficient, for example, is different from the effect of a similar uncertainty in the critical heat flux. Knowledge of the significance of the various design parameters is desirable, since such knowledge allows the important design parameters to be identified and emphasized in any future experimental or analytical work.

The uncertainties in calculated tube length resulting from the corresponding uncertainties in each of the major design variables were determined as follows:

The partial derivative of tube length (L) with respect to a particular design variable (Ψ), for fixed values of the other variables, was calculated from the design equations. This partial derivative, when multiplied by Ψ/L, is called the "design sensitivity", as illustrated by the following equation:

$$\text{Design Sensitivity} = \frac{\partial L}{\partial \Psi} \quad \frac{\Psi}{L} \qquad (16)$$

Design sensitivity values at the conditions of the example boiler design were calculated by numerical differentiation of the design equations (Appendix E), and are listed in Table V for the major design variables. As can be seen from the defining equation, the design sensitivity is the ratio of fractional change in tube length to the corresponding fractional change in the design variable.

The design sensitivity values are valid only for the example design presented, as they are dependent upon the boiler performance specifications. For example, the design significance of the superheated vapor coefficient would be zero for a boiler producing potassium vapor with no superheat, since the superheated vapor heat transfer coefficient would not affect the thermal design. The design significance of the transition boiling heat transfer coefficient would be larger for such a boiler than obtained for the example design, since the transition region would be a greater portion of the total tube length in a boiler producing no superheat.

Also presented in Table V are the probable errors which have been estimated for each design variable. These errors are discussed in the following paragraphs. The probable errors in tube length corresponding to these probable errors in the individual design variables are similarly listed in Table V. Each probable error in tube length is the product of the corresponding design sensitivity and probable error in the design variable.

Lithium Heat Transfer Coefficient

The prediction of Dwyer and Tu (Reference 54) for the parallel flow of

TABLE V

EFFECT OF UNCERTAINTIES IN THE DESIGN VARIABLES

UPON THE EXAMPLE POWER BOILER TUBE LENGTH

Design Parameter	Design Sensitivity*	Probable Error of Design Parameter	Probable Error in Tube Length
Lithium Heat Transfer Coefficient	0.11	35%	4%
Potassium Boiling Pressure Loss	0.46	35%	16%
Potassium Liquid Heat Transfer Coefficient	0.06	100%	6%
Nucleate Boiling Heat Transfer Coefficient	0.14	50%	7%
Critical Heat Flux Correlation	0.30	26%	8%
Transition Boiling Heat Transfer Coefficient Correlation	0.32	30%	10%
Superheated Vapor Heat Transfer Coefficient	0.85	75%	64%

* Equation (16)

liquid metals in tube bundles was employed to estimate the lithium heat transfer coefficient for the example design. Data obtained from multiple tube test boilers for mercury (Reference 55) are approximately 20% lower than the prediction, and similar data for sodium flowing parallel to tube banks (Reference 56) are about 25% lower than the predicted values at the Peclet number employed in the example design. Allowing additional uncertainty due to unknown effects of tube spacers shell-side baffles likely to be employed in an actual boiler, the probable error in the lithium heat transfer coefficient employed in the example design is estimated to be 35%. As can be seen from Table V, this error in the lithium heat transfer coefficient has little effect upon the tube length calculated for the example design.

Subcooled Potassium Heat Transfer Coefficient

No theoretical or empirical expressions are available for the prediction of liquid potassium heat transfer coefficients for tubes containing helical inserts. The prediction of Rohsenow (Reference 57), which is applicable to tubes without inserts, was employed to calculate the liquid potassium heat transfer coefficient for the example design. Due to the undetermined effect of the insert in the subcooled region, the error in the predicted liquid heat transfer coefficient is estimated to be 100%. Table V shows that this large error has very little effect upon the example design.

Boiling Potassium Pressure Loss

The modified Martinelli model, given by Figure 33, was employed to predict the frictional component of the boiling pressure loss for the example boiler design and a slip ratio equal to the square root of the liquid-to-vapor density ratio was used to predict the momentum component of the boiling pressure loss. These same procedures resulted in a correlation of the experimental boiling potassium pressure losses with a probable error of 28%. The error in the pressure drop calculated for the example design is expected to be larger than that obtained for the experimental since the boiling temperature employed in the example design is higher than the range of boiling temperatures tested, and

since the twist ratio employed also is outside the range tested. Taking these factors into account, the probable error in the calculated pressure loss for the example design is estimated to be 35%.

Nucleate Boiling Heat Transfer Coefficient

A value of 10,000 Btu/(hr-ft^2-°F) was assumed for the nucleate boiling heat transfer coefficient in the example boiler design. The local nucleate boiling data of Figure 30 for a 0.77-inch ID tube without insert were obtained at a mass velocity of 16 lb/(ft^2-sec) and a boiling temperature of 1990°F (Reference 60), which are very close to the mass velocity of 14.2 lb/(ft^2-sec) and boiling temperature of approximately 2015°F employed in the example design. Figure 30 shows the nucleate boiling heat transfer coefficient to be about 20,000 Btu/(hr-ft^2-°F) at a heat flux of 80,000 Btu/(hr-ft^2) and to increase with increasing heat flux. The nucleate boiling heat transfer coefficient employed in the example design, therefore, is indicated to be conservative, since the average heat flux in the nucleate boiling region of the example design is 330,000 Btu/(hr-ft^2). The data of Figure 30, however, are for a plain tube without insert. The average heat transfer coefficient data of Figures 21 and 22 indicate that there is a decrease in heat transfer coefficient with inserts as the insert twist ratio is decreased. For this reason, the apparently conservative value of 10,000 Btu/(hr-ft^2-°F) was assumed for the nucleate boiling heat transfer coefficient, since a tight twist ratio insert is employed in the example design. The probable error of the value assumed is estimated to be 50%.

Critical Heat Flux

The correlation derived in this report (Equation 4) was employed to estimate the critical heat flux for the example boiler design. The probable error of the experimental data with respect to the correlating equation is 26%. The potassium critical heat flux data upon which the correlation is based include values obtained in a controlled heat flux facility at potassium temperatures up to 2100°F (Reference 60) as well as the values from the two fluid boiling experiments.

Since the potassium temperature in the example design (2000°F) is in the range of experimental data, the probable error in the critical heat flux predicted for the example design is assumed also to be 26%.

Transition Boiling Heat Transfer Coefficient

The correlation developed in this report (Equation 6) was employed to estimate the transition boiling heat transfer coefficient for the example boiler design. The probable error of the experimental transition boiling data with respect to the correlating equation is 20%. The experimental transition boiling heat transfer coefficients have additional systematic error due to uncertainties in the equivalent sodium and boiler tube wall heat transfer coefficients required in the data reduction procedure. Furthermore, the experimental data employed to derive the correlation were obtained at potassium temperatures lower than that for the example design, which also introduces additional error into the predicted transition boiling heat transfer coefficient. Taking these factors into account, the probable error in the transition boiling heat transfer coefficient employed in the example design is estimated to be 30%.

Superheated Vapor Heat Transfer Coefficient

The superheated vapor heat transfer coefficient employed for the example boiler design was calculated from Equation (7) of this report, which is a correlation of the water heat transfer data of Greene (Reference 33) for a tube containing helical inserts. The few potassium superheated vapor heat transfer coefficient data obtained from the two-fluid boiling experiments, however, deviate considerably from the prediction of Equation (7). As discussed previously, the experimental data suggest that effects not included in the correlation, such as thermal radiation and entrained liquid droplets, may be significant. Considering these undetermined uncertainties and the large deviations of the experimental data from the calculated values (Figure 29), the probable error in the superheated vapor heat transfer coefficient employed in the example design is estimated to be 75%.

Combination of Errors

If the uncertainties in boiler tube length for the example design due to the various design parameters are assumed independent, the combined probable error in tube length caused by the variables can be determined according to the methods of Beers (Reference 46). Beers recommends that independent errors be combined as the square root of the sum of the squares of the individual errors. The combined probable error in the tube length for the example design calculated in this manner is 68%. Most of this rather large uncertainty in the example design is due to the uncertainty in the superheated vapor heat transfer coefficient. If the error in the superheated vapor heat transfer coefficient were assumed zero, for example, the probable error calculated for the reference design is only 23%. This latter value should not be equated to the probable error of a boiler producing no superheat, since the effects of errors in the other design variables are dependent upon the specified boiler operating conditions. It does illustrate, however, the reduction in uncertainty in the example design which would be expected if the superheated vapor heat transfer coefficient were known more accurately.

These results show that the effects upon boiler design of uncertainties in design parameters, other than the superheated vapor heat transfer coefficient, are relatively minor. Sufficient potassium forced convection boiling data have been obtained, therefore, to permit the thermal design of large scale once-through potassium boilers to proceed on a reasonable technical basis, provided that the specified exit vapor superheat is small (on the order of 50°F). Further experimental and analytical effort is indicated, however, before boilers producing larger exit superheat can be designed with equal confidence.

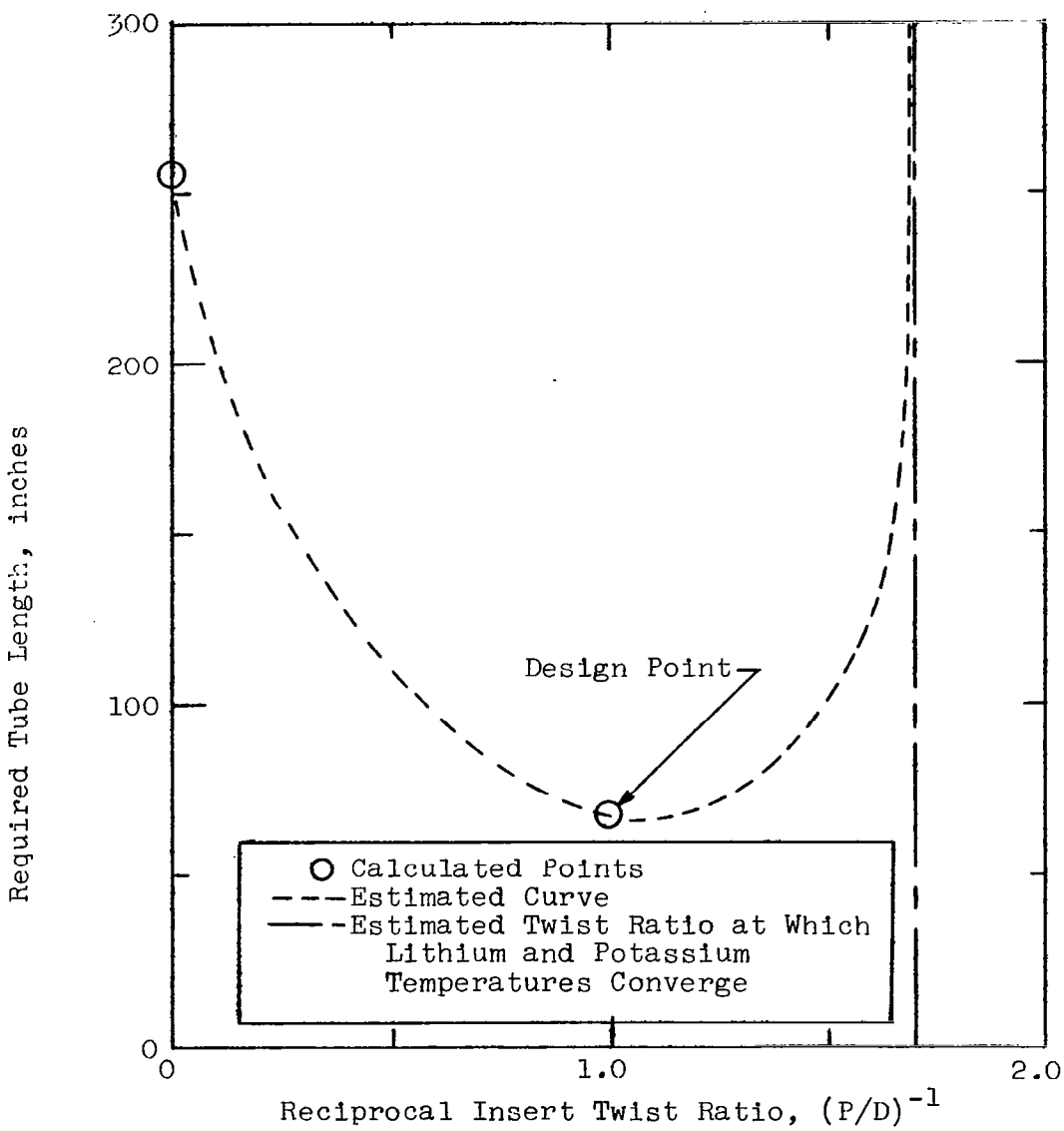

Figure 38. Variation of Calculated Tube Length With Insert Twist Ratio At Constant Potassium Exit Pressure And Temperature For The 8300 KW Example Boiler Design

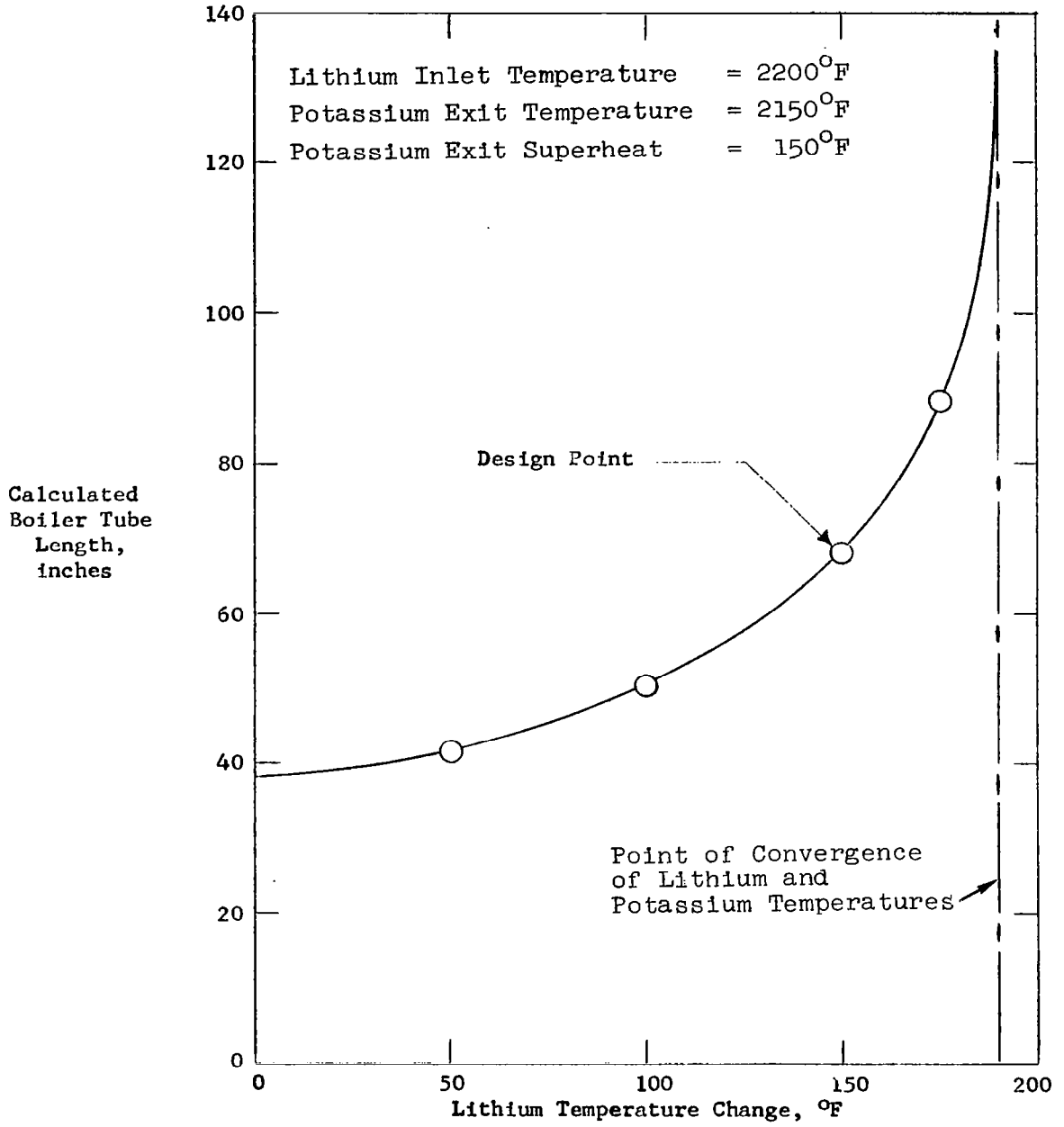

Figure 39. Variation of Calculated Tube Length With Lithium Temperature Change At Constant Potassium Exit Pressure And Temperature for the 8300 KW Example Boiler Design

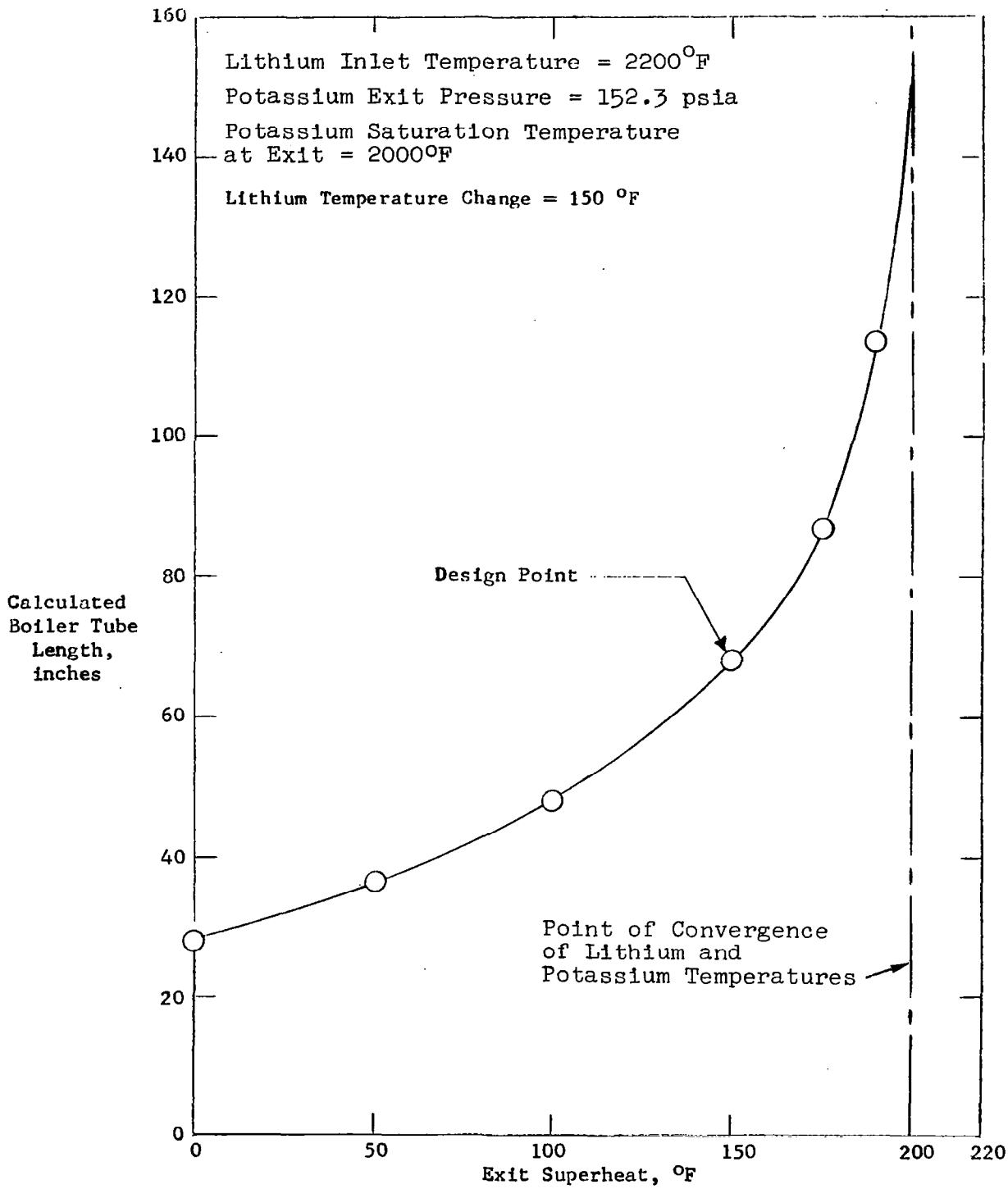

Figure 40. Variation of Calculated Tube Length with Potassium Exit Superheat At Constant Potassium Exit Pressure and Lithium Inlet Temperature for the 8300 KW Example Boiler Design

VIII CONCLUDING REMARKS

A considerable body of experimental and analytical information on forced convection boiling of potassium in a two-fluid boiler has resulted from this investigation. Both average and local boiling potassium heat transfer coefficients have been determined and correlations of the critical heat flux and transition boiling heat transfer coefficient have been obtained. The pressure losses occurring during the forced convection boiling of potassium have also been measured and correlated. The general conclusions derived from these results are listed following:

1. The feasibility of high performance once-through potassium boiling for space power application has been shown. Potassium exit conditions of up to 200°F vapor superheat have been obtained at average heat fluxes in excess of 125,000 Btu/hr-ft^2 (37 KW/ft^2) in single-tube two-fluid boiling tests using vortex generator helical inserts. Heat fluxes up to 200,000 Btu/hr-ft^2 (59 KW/ft^2) were obtained for saturated vapor potassium exit conditions.

2. The boiling heat transfer and pressure loss data and correlations obtained provide a reasonable basis for the thermal design of two-fluid once-through potassium boilers in either cocurrent or countercurrent flow. An illustration of this, design procedures based upon the experimental results and an example thermal design for a large multiple tube boiler producing potassium vapor at 2150°F with 150°F of superheat have been prepared. This boiler design employing helical inserts has an average heat flux of 110,000 Btu/hr-ft^2 (32 KW-ft^2), which is almost four times the heat flux calculated for a similar boiler that does not employ inserts (Table IV). The example design analysis indicates that large two-fluid potassium boilers become larger and more massive as the potassium exit superheat increases and as the temperature change in the primary fluid increases (Figures 39, 40).

3. Analysis of the example boiler design shows the superheated vapor heat transfer coefficient to be a major source of uncertainty in the design of large potassium boilers (Table V). The uncertainty caused by the vapor coefficient is larger than that caused by all the other design variables for boilers producing substantial superheat (150°F), due to the paucity of data available for superheated potassium vapor heat transfer.

In addition to the general conclusions cited above, the following more specific trends are shown by the experimental data or predicted by correlations derived from the data.

The radial acceleration developed by the helical inserts employed in the experiments was found to be a significant parameter affecting boiling potassium heat transfer. In particular:

(a) The critical heat flux was found to increase approximately in proportion to the 1/4 power of the acceleration (Figure 25).

(b) The local transition boiling heat transfer coefficient was found to increase approximately in proportion to the 1/5 power of the acceleration (Figure 28).

(c) The potassium nucleate boiling heat transfer coefficient was found to be lower for tubes containing helical inserts than in tubes without inserts (Figure 22).

Besides the effects of acceleration, the following trends were observed in the critical heat flux and in the transition boiling heat transfer coefficients

(a) The critical heat flux decreased with increasing local vapor quality (Figure 26).

(b) When the critical heat flux data were plotted versus exit quality, no effects of mass velocity or temperature were evident within the range of experimental data.

(c) The local transition boiling heat transfer coefficient was found to be proportional to the single-phase vapor heat transfer coefficient (Figure 28).

(d) The local transition boiling heat transfer coefficient was found to be strongly dependent upon the difference between tube wall and potassium temperature, increasing with decreasing temperature difference squared (Figure 28).

(e) The local transition boiling heat transfer coefficient was found to increase with decreasing vapor quality (Figure 28).

In addition to the effects listed regarding the potassium heat transfer results, the following trends were observed in the boiling potassium pressure loss results:

(a) The boiling pressure loss was found to be proportional to the single-phase liquid pressure loss in tubes containing helical inserts (Figure 32).

(b) The two-phase pressure drop multiplier (ratio of two-phase to single-phase pressure loss) was found to increase with increasing quality (Figure 32).

(c) The two-phase pressure drop multiplier was found to increase with decreasing saturation temperature (Figure 32).

APPENDIX A

Instrument Calibrations and Calculational Procedures

The potassium thermodynamic properties employed in the reduction and analysis of the experimental data were obtained from Reference 41. The potassium vapor and liquid transport properties and the sodium thermodynamic properties employed were taken from Reference 49. The symbols utilized in the equations presented are defined in the Nomenclature.

Instrument Calibrations

Electromagnetic Flowmeters: The relationship between output signal and liquid metal flow rate for the permanent magnet flowmeters used in each loop of the facility was obtained by theoretical calculation, using the methods of Reference 58. Measured values of the field strengths of the magnets, which were maintained at low temperatures, were used in the calculations. The effects of changes in liquid metal and duct resistivities with temperature level were corrected for in the data reduction procedure by use of the temperatures measured by thermocouples located on the flowmeter ducts.

An indication of the resulting accuracy in the measured flows was obtained through intercalibration between the sodium and potassium loop flowmeters by heat balance around the test section, using liquid-liquid runs. The disagreement obtained was 2%, which is assumed to be also representative of the probable error in the individual flow measurements.

Taylor Pressure Gages: Two Taylor slack-diaphragm absolute pressure gages were employed to determine the boiling pressure losses in the test section. These gages were calibrated before and after the experiments with each test section by inert gas pressurization of the secondary loop. The calibration of the Taylor gages was found in shake-down operation to be dependent upon the

diaphragm temperature, thus the transducers were maintained at constant temperature by the use of auxiliary heating wire. The pressure gage calibrations shifted a total of only 2 psi over the time period in which the data reported were obtained. The reproducibility of the calibrations made before and after the experiments with a single test section generally agreed to within 1 psi, thus the probable error in an individual pressure measurement is judged to be about $\pm$ 3/4 psi.

Sodium and Potassium Well Thermocouples: The three thermocouples located in each of the four thermocouple wells at the boiler inlet and exit of the sodium and potassium streams were calibrated periodically in a melting point apparatus. The calibration temperatures utilized spanned the temperature range of test operation. The thermocouple corrections obtained in this manner were less than 10°F, and thus the well thermocouples are judged to have a probable error after correction of less than $\pm$ 2°F.

Sodium Well Thermocouples - Relative Calibration: As described subsequently, the amount of heat transferred in each data run is determined from the temperature change across the boiler in the sodium stream. For this reason, special runs were performed in the facility to provide data for the calibration of these thermocouples relative to each other with higher accuracy than obtained with the absolute melting point calibrations. The requisite calibration data consist of runs at two sodium flow rates with no potassium in the secondary loop, so that the temperature change in the sodium stream is due to thermocouple error and test section heat loss only. The data at each of the two sodium flow rates are obtained at the same average sodium temperature, so that the test section heat losses and the thermocouple corrections, which are assumed a function only of temperature, are identical for the two cases.

At each of the two sodium flow rates W_{Na1} and W_{Na2}, the heat losses (Q_L) can be expressed as follows:

$$Q_L = W_{Na1}\, C_{Na} \left[(T_{Nai})_{1R} - T_{1mj} - E_j \right] \qquad \text{(A1)}*$$

$$Q_L = W_{Na2}\, C_{Na} \left[(T_{Nai})_{2R} - T_{2mj} - E_j \right] \qquad \text{(A2)}$$

where:

$(T_{Nai})_R$ is the measured temperature of the sodium inlet thermocouple selected as the reference for the relative calibration.

T_{mj} is the temperature measured by the j^{th} thermocouple whose calibration relative to the reference thermocouple is to be determined.

E_j is the error of the j^{th} thermocouple relative to the reference inlet thermocouple, defined in terms of the corrected reading of the j^{th} thermocouple (T_j) as follows:

$$T_j = T_{mj} + E_j \qquad \text{(A3)}$$

Equations (A1) and (A2) are two simultaneous equations in two unknowns and can be solved for the values of Q_L and E_j. These calibrations were performed for all of the sodium well thermocouples at a minimum of two sodium temperatures (generally three) for each test section. An equation expressing the error as a linear function of sodium temperature was obtained for each thermocouple from these data and was employed to correct the thermocouple readings for the experimental data runs. These relative corrections are about 3°F. The probable error in sodium temperature difference obtained from the well thermocouples calibrated in this manner is judged to be about $\pm$ 1°F.

*Equations are numbered consecutively in each Appendix

The heat losses determined by the above procedure were essentially the same for all of the test sections used in the experiments. The test section heat losses varied from 0.8 KW at a sodium temperature of 1200°F to 3 KW at a sodium temperature of 1800°F.

Boiler Shell Thermocouples: The sodium well thermocouples, calibrated as described above, were used as standards for the calibration of the boiler shell thermocouples. The calibration runs obtained with no potassium in the secondary loop were employed for this purpose. The procedure followed was to plot all of the shell thermocouple readings obtained in the high sodium flow calibration run versus boiler length and correct these readings to a straight line drawn between the readings plotted for the previously-calibrated sodium inlet and exit well thermocouple readings. The total change in sodium temperature for the high flow calibration runs was less than 1°F.

This calibration procedure was employed at the several temperatures for which calibration data were obtained. Equations were derived expressing the error in each shell thermocouple for each test section as a function of average sodium temperature. These equations were employed to make the thermocouple corrections in the boiling runs. The probable error in the corrected shell thermocouple temperature readings is judged to be $\pm$ 2°F.

Insert Thermocouples: The thermocouples positioned inside the insert centerbody for those data runs with helical inserts were calibrated relative to the previously calibrated potassium boiler exit well thermocouples. Boiling runs were used for this calibration, which was accomplished by comparing the insert thermocouple readings to the boiler exit well thermocouple readings. The boiling runs employed were those in which the two-phase pressure drop was small, for which the expected temperature change between the insert thermocouple and exit well thermocouple was also small.

Calculational Procedures

The calculational procedures employed to derive the various test results presented in Appendix B are listed in this section of the report. The nomenclature used in the equations following is conformal to the data column headings of Appendix B and is listed elsewhere in this report. The various temperatures employed in the calculations are defined and illustrated by sketches (a & b) which show typical sodium and potassium temperature profiles as obtained in boiling runs for which all four heat transfer regions were present. In runs with exit qualities less than 100% the superheated vapor region is not present. The transition boiling region also is generally not present in runs with exit qualities less than 50%.

The subscripts (i) and (o) in sketch (a) refer to boiler inlet and exit temperatures. The subscript (IB) refers to the point of boiling initiation and the subscript (c) refers to the point of critical heat flux. The subscript (IS) refers to the point where vapor superheating commences.

Overall and Average Results

The potassium mass velocity (G_K) is the quotient of the potassium mass flow rate (W_K) and the flow area A_F as follows:

$$G_K = \frac{W_K}{A_F} \tag{A4}$$

For boiler tubes without inserts, $A_F = \frac{\pi D_i^2}{576}$ (A5)

For boiler tubes containing helical inserts, A_F is given in terms of the insert centerbody diameter D_{cb} and the insert tape thickness Δ_T as follows:

$$A_F = \frac{\pi(D_i^2 - D_{cb}^2)}{576} - \frac{(D_i - D_{cb})\,\Delta_T}{288} \tag{A6}$$

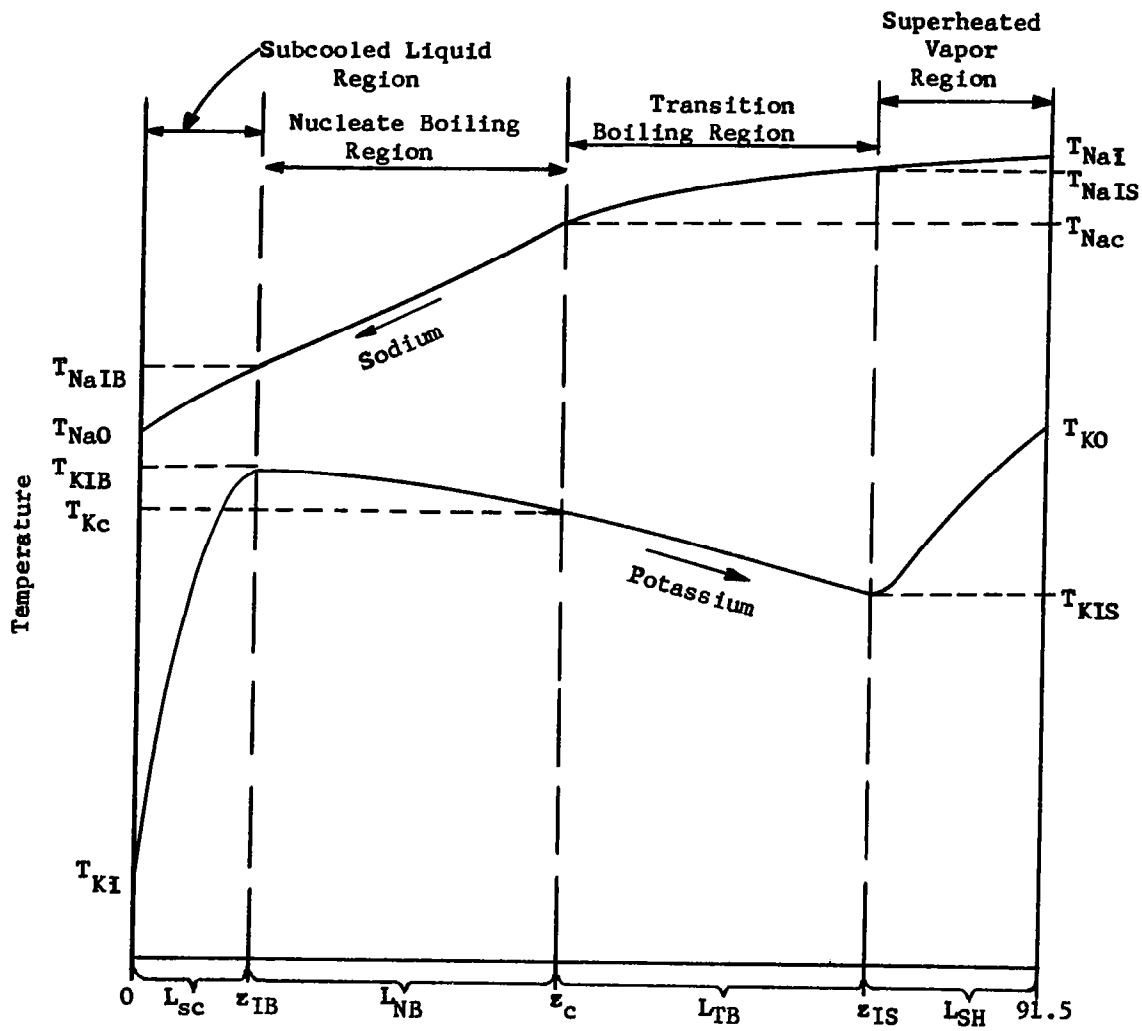

Sketch (a)

Typical Boiler Temperature Profiles - Countercurrent Flow

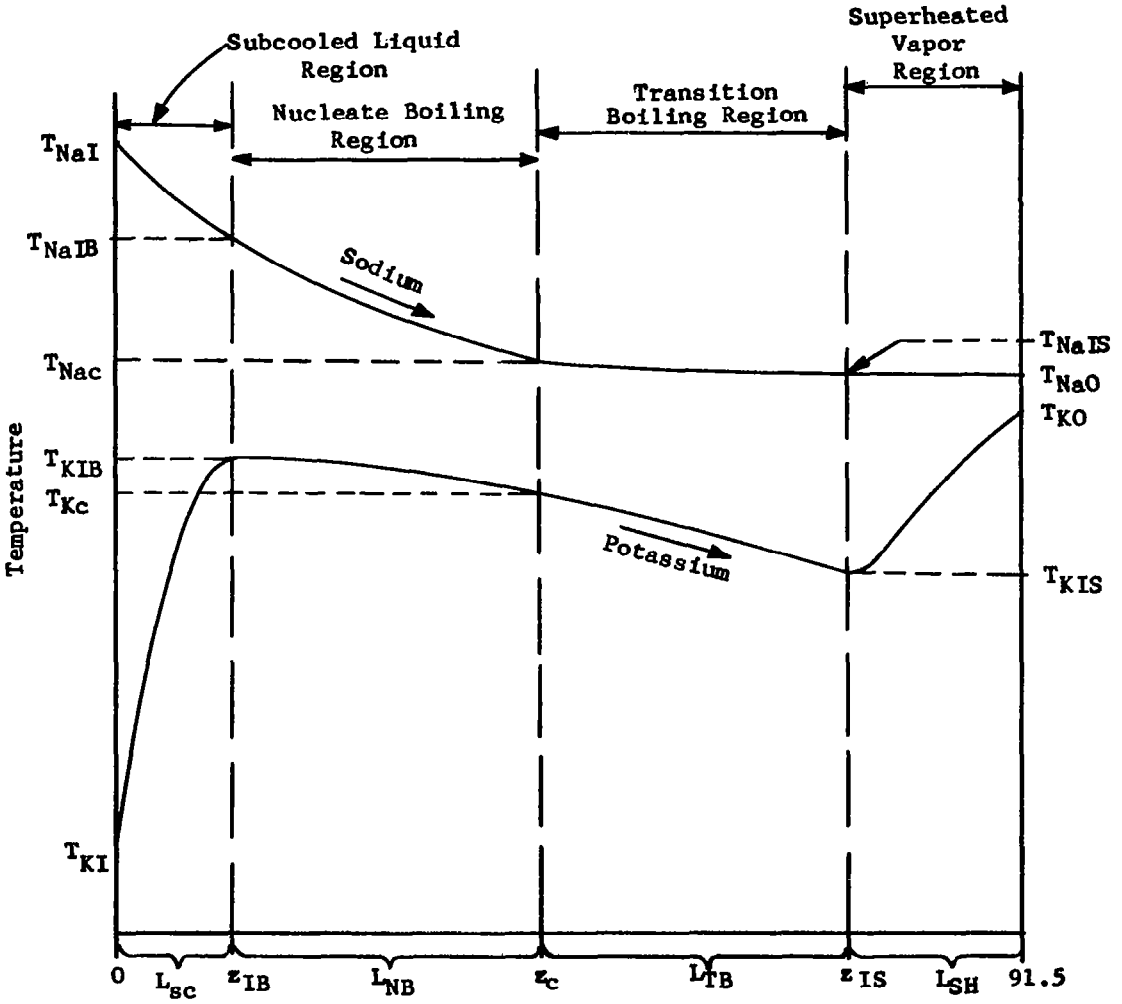

Sketch (b)

Typical Boiler Temperature Profiles - Cocurrent Flow

The net rate of heat transfer in the boiler tube is given by equation (A7), where the test section heat losses (Q_L) are obtained at the average sodium temperature from the calibration results described previously.

$$Q_T = W_{Na}\, C_{Na}\, (T_{Nai} - T_{Nao}) - Q_L \qquad \text{(A7)}$$

The length of the subcooled heating region (L_{sc}), which is numerically equal to the distance from the start of the heated length to the point of boiling initiation (z_{IB}), is obtained directly from the potassium temperature profile determined from the insert thermocouples for those runs in tubes containing inserts. For the no insert runs, L_{sc} was obtained from a single-phase heat transfer calculation as follows:

$$L_{sc} = \frac{Q_{sc}\,(3600)(144)}{U_{Osc}\;\pi D_i\;\overline{\Delta T}_{Osc}} \qquad \text{(A8)}$$

The heat transferred in the subcooled heating region (Q_{sc}) is given by equation A9.

$$Q_{sc} = W_K\, C_K\, (T_{KIB} - T_{Ki}) \qquad \text{(A9)}$$

The potassium temperature at boiling initiation (T_{KIB}) is obtained directly from the measured potassium temperature profile in runs with inserts. In runs without inserts, T_{KIB} is assumed equal to the saturation temperature corresponding to the local pressure (P_{KIB}), determined from the measured inlet pressure P_{Ki} by correction for liquid head, as follows. The liquid density ρ_{Kf} is obtained at the average potassium temperature in the subcooled heating region.

$$P_{KIB} = P_{Ki} - \frac{\rho_{Kf}\, L_{sc}}{1728} \qquad \text{(A10)}$$

The sodium temperature at boiling initiation (T_{NaIB}) is calculated by heat balance from equation A11.

$$T_{NaIB} = T_{Nao} + \frac{Q_{sc}}{W_{Na}\ C_{Na}} \qquad \text{(A11)}$$

The average overall sodium-to-potassium temperature difference in the subcooled heating region ($\overline{\Delta T}_{Osc}$) is calculated as follows:

$$\overline{\Delta T}_{Osc} = \frac{\Delta T_{OKi} - \Delta T_{OIB}}{\log_e \left(\frac{\Delta T_{OKi}}{\Delta T_{OIB}}\right)} \qquad \text{(A12)}$$

where

$$\Delta T_{OKi} = T_{Nao} - T_{Ki} \quad \text{for countercurrent operation (A13)}$$

$$\Delta T_{OKi} = T_{Nai} - T_{Ki} \quad \text{for cocurrent operation (A13a)}$$

$$\Delta T_{OIB} = T_{NaIB} - T_{KIB} \qquad \text{(A14)}$$

The overall heat transfer coefficient in the subcooled heating region (U_{Osc}) is calculated from the individual sodium tube wall and liquid potassium heat transfer coefficients as follows:

$$U_{sc} = \left\{ \frac{1}{\frac{D_o}{D_i}\ h_{Na}} + \frac{D_i \log_e \left(\frac{D_o}{D_i}\right)}{2k_w} + \frac{1}{h_{Kf}} \right\}^{-1} \qquad \text{(A15)}$$

The sodium heat transfer coefficient is calculated from Lyon's equation (Reference 42) for an annulus as follows:

$$h_{Na} = \frac{(0.75)(12)\ k_{Na}}{(D_{si} - D_o)} \left(\frac{D_{si}}{D_o}\right)^{0.3} \left[7 + 0.025\ (N_{Pe})_{Na}^{0.8} \right] \qquad \text{(A16)}$$

where

$$(N_{Pe})_{Na} = \frac{(300)(576)\ W_{Na}\ C_{Na}}{\pi(D_{si} + D_o)\ K_{Na}} \tag{A17}$$

The boiler tube wall thermal conductivity (k_w) for Haynes-25 was obtained from Reference 43.

The prediction recommended by Rohsenow (Reference 57), given following, is employed to calculate the potassium liquid heat transfer coefficient (h_{Kf}).

$$h_{Kf} = \frac{12\ k_{Kf}}{D_i}\left[6.7 + 0.0041\ (N_{Pe})_K^{0.793}\ e^{41.8(N_{Pr})_K}\right] \tag{A18}$$

where

$$(N_{Pe})_K = \frac{300\ D_i\ G_K\ C_{Kf}}{k_{Kf}} \tag{A19}$$

$$(N_{Pr})_K = \frac{C_{Kf}\ \mu_{Kf}}{k_{Kf}} \tag{A20}$$

Equations A8 through A14 are solved by iteration in the data reduction computer program, since the value of L_{sc} provided by equation A8 is also required directly or indirectly in the other equations.

The average boiling heat flux ($\bar{q}''_B$) is calculated as follows:

$$\bar{q}''_B = \frac{(3600)(144)(Q_T - Q_{sc})}{\pi D_i\ (91.5 - L_{sc})} \tag{A21}$$

The vapor quality at the test section exit (x_o) is obtained from equation A22.

$$x_o = \frac{Q_T}{W_K h_{fgo}} - \frac{(H_{Kfo} - H_{Kfi})}{h_{fgo}} - \frac{V_{Hgo}^2}{2Jg_c h_{fgo}} \qquad \text{(A22)}$$

The term V_{Hgo} appearing in equation A22 is the helical vapor velocity at the test section exit, which is calculated as follows:

$$V_{Hgo} = \frac{x_o G_K}{\rho_g} \frac{V_H}{V_a} \qquad \text{(A23)}$$

The ratio of helical to average velocities, V_H/V_a, is derived in Appendix C and is given as follows in terms of the insert twist ratio P/D.

$$\frac{V_H}{V_a} = \sqrt{1 + \left(\frac{\pi}{P/D}\right)^2} \qquad \text{(A24)}$$

The average boiling potassium heat transfer coefficient $\bar{h}_B$ is computed as follows:

$$\bar{h}_B = \left[\frac{1}{U_{OB}} - \frac{D_i \log_e \left(\frac{D_o}{D_i}\right)}{2k_w} - \frac{1}{\frac{D_o}{D_i} h_{Na}} \right]^{-1} \qquad \text{(A25)}$$

$$U_B = \frac{\bar{q}''_B}{\overline{\Delta T}_{OB}} \qquad \text{(A26)}$$

$$\overline{\Delta T}_{OB} = \frac{\Delta T_{OK_o} - \Delta T_{OIB}}{\log_e \frac{\Delta T_{OK_o}}{\Delta T_{OIB}}} \qquad \text{(A27)}$$

$$\Delta T_{OK_o} = T_{Nai} - T_{Ko} \text{ for countercurrent operation} \qquad \text{(A28)}$$

$$\Delta T_{OK_o} = T_{Nao} - T_{Ko} \text{ for cocurrent operation} \qquad \text{(A28a)}$$

The boiling pressure loss is computed in twc ways. One value $(\Delta P_B)_G$ is obtained from the Taylor gages using equation A29,

$$(\Delta P_B)_G = P_{KIB} - P_{Ko} \tag{A29}$$

For the data runs with inserts, a second value of the boiling pressure loss $(\Delta P_B)_T$ is computed from the measured temperatures at the point of boiling initiation and at the boiler exit, using the saturation curve of potassium to obtain the pressures corresponding to the measured temperatures.

The boiling frictional pressure loss (ΔP_{TPF}) is obtained from the total pressure loss by subtraction of the momentum pressure loss,

$$\Delta P_{TPF} = (\Delta P_B)_G - \Delta P_M \tag{A30}$$

The momentum pressure loss is calculated as follows (Reference 6).

$$\Delta P_M = \frac{(G_K \frac{V_H}{V_a})^2}{144\, g_c} \left[\frac{1}{\hat{\rho}_o} - \frac{1}{\rho_{fIB}} \right] \tag{A31}$$

where

$$1/\hat{\rho}_o = \frac{1}{\rho_g} \left[(1 - x) \frac{\rho_g}{\rho_f} + \frac{x}{K} \right] \left[1 + x\,(K - 1) \right] \tag{A32}$$

The slip ratio K in the above equation is the ratio of average vapor velocity to average liquid velocity and is assumed equal to the square root of the liquid-to-vapor density ratio.

The two-phase frictional pressure drop multiplier, Φ, is computed as follows:

$$\Phi = \frac{\Delta P_{TPF}}{\Delta P_f} \tag{A33}$$

The all-liquid pressure drop ΔP_f is computed from the measured friction factors for the boiler tubes and their inserts as follows, where f_i is the measured friction factor for the tube with insert, obtained from Figure 31.

$$\Delta P_f = f_i \frac{(91.5 - L_{sc})}{D_i} \frac{G_K^2}{288 \rho_{kf} g_c} \qquad \text{(A34)}$$

Results for the Individual Heat Transfer Regions:

In this section are described the procedures employed to obtain the transition boiling and superheated vapor heat transfer coefficient data and the critical heat flux values tabulated in Appendix B. Sketch (a) of the preceeding section illustrates some of the nomenclature employed. Figure 23 shows the temperature measurements made in an actual data run from which the local information was extracted and Figure 24 presents the local results calculated for this same run.

The heat flux in the nucleate boiling region is obtained from the temperature gradient in this region measured by the boiler shell thermocouples. It is assumed that the temperature gradient along the shell is equal to the sodium temperature gradient. The average shell temperature gradient is obtained by drawing a straight line through the temperatures provided by the shell thermocouples as shown in Figure 23. The nucleate boiling heat flux $\overline{q''_{NB}}$ is obtained from the shell temperature gradient dT_s/dz as follows:

$$\overline{q''_{NB}} = \frac{(144)(3600)\ W_{Na}\ C_{Na}}{\pi D_i} \frac{dT_s}{dz} - q''_L \qquad \text{(A35)}$$

The heat flux due to heat losses (q''_L) is given by equation A36:

$$q''_L = \frac{(144)(3600)\ Q_L}{\pi D_i\ (91.5)} \qquad \text{(A36)}$$

The point of boiling initiation (z_{IB}) and the subcooled heating length (L_{sc})

are obtained as described previously. It is assumed that the break in shell temperature gradient illustrated in Figure 23 demarks the axial position(z_c) at which the critical heat flux occurs. The axial position at which vapor superheating commences (z_{IS}) is assumed to be the point at which the potassium temperature begins to rise as shown in sketch (a) and Figure 23.

The length of the vapor superheating region (L_{SH}), of the transition boiling region (L_{TB}) and of the nucleate boiling region (L_{NB}) are given by equations A37 - A39 following.

$$L_{SH} = 91.5 - z_{IS} \tag{A37}$$

$$L_{TB} = z_{IS} - z_c \tag{A38}$$

$$L_{NB} = z_c - z_{IB} \tag{A39}$$

The amount of heat transferred in the nucleate boiling region (Q_{NB}) is calculated from equation (A40).

$$Q_{NB} = \frac{\pi D_i \, L_{NB} \, \overline{q''_{NB}}}{(144)(3600)} \tag{A40}$$

The amount of the heat transferred in the vapor superheat region (Q_{SH}) can be determined from the potassium temperature rise in this region as follows:

$$Q_{SH} = W_K \, C_{Kg} \left[T_{Ko} - T_{KIS} \right] \tag{A41}$$

The potassium temperature at the point where superheating commences (T_{KIS}) is provided by the potassium temperature profile as measured by the insert thermocouples.

The heat transferred in the transition boiling region (Q_{TB}) is obtained by subtraction as follows:

$$Q_{TB} = Q_T - Q_{NB} - Q_{SH} - Q_{sc} \tag{A42}$$

The heat flux levels in the transition boiling and vapor superheating regions ($\overline{q''_{TB}}$ and $\overline{q''_{SH}}$) are calculated as follows:

$$\overline{q''_{TB}} = \frac{(3600)(144)\ Q_{TB}}{\pi D_i\ L_{TB}} \tag{A43}$$

$$\overline{q''_{SH}} = \frac{(3600)(144)\ Q_{SH}}{\pi D_i\ L_{SH}}$$

The sodium temperature at the point where vapor superheating commences and at the critical heat flux point are calculated by heat balance from the measured sodium inlet temperature.

$$T_{NaIS} = T_{Nai} - \frac{Q_{SH}}{W_{Na}\ C_{Na}} \tag{A44}$$

$$T_{Nac} = T_{NaIS} - \frac{Q_{TB}}{W_{Na}\ C_{Na}} \tag{A45}$$

The average overall sodium-to-potassium temperature differences in the nucleate boiling, transition boiling and vapor superheating regions are computed as follows:

$$\overline{\Delta T}_{ONB} = \frac{(T_{Nac}-T_{Kc}) - (T_{NaIB}-T_{KIB})}{\log_e\left(\frac{T_{Nac}-T_{Kc}}{T_{NaIB}-T_{KIB}}\right)} \tag{A46}$$

$$\overline{\Delta T}_{OTB} = \frac{(T_{NaIS}-T_{KIS}) - (T_{Nac}-T_{Kc})}{\log_e\left(\frac{T_{NaIS}-T_{KIS}}{T_{Nac}-T_{Kc}}\right)} \tag{A47}$$

$$\overline{\Delta T}_{OSH} = \frac{(T_{Nai}-T_{Ko}) - (T_{NaIS}-T_{KIS})}{\log_e \left(\frac{T_{Nai}-T_{Ko}}{T_{NaIS}-T_{KIS}}\right)} \tag{A48}$$

The overall heat transfer coefficients for the various regions are calculated from the overall temperature difference values.

$$U_{NB} = \frac{\bar{q}''_{NB}}{\overline{\Delta T}_{ONB}} \tag{A49}$$

$$U_{TB} = \frac{\bar{q}''_{TB}}{\overline{\Delta T}_{OTB}} \tag{A50}$$

$$U_{SH} = \frac{q''_{SH}}{\overline{\Delta T}_{OSH}} \tag{A51}$$

The transition boiling and superheated vapor heat transfer coefficients are calculated by subtracting the sodium and boiler tube wall thermal resistances from the overall thermal resistance as follows. The sodium heat transfer coefficient h_{Na} is calculated from equation A16.

$$h_{TB} = \left[\frac{1}{U_{TB}} - \frac{D_i \log_e \left(\frac{D_o}{D_i}\right)}{2k_w} - \frac{1}{\frac{D_o}{D_i} h_{Na}}\right]^{-1} \tag{A52}$$

$$h_{SHV} = \left[\frac{1}{U_{SH}} - \frac{D_i \log_e \left(\frac{D_o}{D_i}\right)}{2k_w} - \frac{1}{\frac{D_o}{D_i} h_{Na}}\right]^{-1} \tag{A53}$$

The potassium nucleate boiling heat transfer coefficient is large and is a small fraction of the overall nucleate boiling thermal resistance. For this reason, the overall heat transfer coefficient in the nucleate boiling region is nearly constant. The average overall nucleate boiling heat transfer coefficient can be employed, therefore, to calculate with good accuracy values of the local heat flux. In particular, the critical heat flux (q''_c) is calculated as the product of the overall nucleate boiling coefficient and the measured sodium-to-potassium temperature difference at the critical point.

$$q''_c = U_{NB} \, (T_{Nac} - T_{Kc}) \tag{A54}$$

The local quality at the critical heat flux point (x_c) is calculated by energy balance as follows:

$$x_c = x_o \, \frac{h_{fgo}}{h_{fgc}} - \frac{Q_{TB}}{W_K \, h_{fgc}} - \frac{C_{Kf}}{h_{fgc}} \, (T_{Kc} - T_{Ko}) + \frac{V_{Ho}^2 - V_{Hc}^2}{2Jg_c \, h_{fgc}} \tag{A55}$$

For runs with exit qualities less than 100%, x_o in equation A55 is the exit quality. For runs with superheated vapor exit conditions, x_o is the quality at the initiation of bulk superheat which is assumed to be 100%. All the property and temperature subscripts in equation (A55) are changed from (o) to (IS) when it is applied to superheated vapor runs.

The arithmetic average quality in the transition region is associated with the transition boiling heat transfer coefficient as follows:

$$x_{TB} = \frac{x_c + x_o}{2.0} \tag{A56}$$

The temperature associated with the transition boiling heat transfer coefficient and the superheated vapor heat transfer coefficient are the arithmetic average potassium temperatures in the respective heat transfer regions.

The local potassium temperatures T_{KIB}, T_{Kc} and T_{KIS} required in the above calculations are determined from the temperature profile measured by insert thermocouples in those data runs with helix inserts. No exit qualities higher than 90% were obtained in runs without inserts, thus the temperature T_{KIS} is not required. The temperature at boiling initiation for the no-insert runs is calculated from the measured inlet pressure as described previously. The local pressure at the critical heat flux point, from which T_{Kc} is determined by use of the potassium saturation curve, is computed by two-phase pressure drop calculation as follows for the no-insert runs.

$$P_{Kc} = P_{KIB} - \left[\!\!\left[\Phi\right]\!\!\right] f_i \frac{L_{NB}}{D_i} \frac{G_K^2}{288\, \rho_{Kf}\, g_c} - \Delta P_M \qquad \text{(A57)}$$

$\left[\!\!\left[\Phi\right]\!\!\right]$ is the two-phase pressure drop multiplier integrated from 0 to x_c, and f_i is the single-phase friction factor for smooth tubes. The momentum pressure loss ΔP_M is obtained from equation A31.

APPENDIX B

Tabulation of Experimental Results

The numerical experimental results obtained from the two-fluid boiling experiments are presented in this appendix. The overall and average results, consisting of the overall boiler performance, average boiling potassium heat transfer coefficients and frictional pressure loss multipliers, are listed in Tables VII through XIV. The critical heat flux results, transition boiling heat transfer coefficients and superheated vapor heat transfer coefficients are presented in Tables XV through XVII. The symbols employed for data column headings in the various tabulations are defined in Table VI.

All of the data presented are grouped according to the test section with which they were obtained. The overall and average results are further differentiated with respect to the test procedure by which they were acquired. A majority of the data (Tables VII through XI) were obtained according to a test plan whereby the boiler exit quality was varied by changing the test section power while the potassium mass velocity and boiler exit temperature were held constant. Data were obtained in this manner for several mass velocities at the two nominal boiler exit temperatures of 1550°F and 1700°F. This test plan is designated Test Plan A in the data tables.

Additional data (Tables XII through XIV) were obtained according to a second test plan, designated Test Plan B. In Test Plan B, the boiler exit quality was varied by changing the potassium mass velocity while the boiler power and potassium boiler exit temperature were held constant. Data were obtained with this procedure at the two nominal boiler exit temperatures of 1550°F and 1700°F.

The original measured temperatures, flow rates and pressures from which the various quantities listed in the data tables are derived have been

reported in Quarterly Progress Reports (References 2-13). The source of the original data for each test case is given in the following listing. The test case numbers utilized to define the test conditions for each data tabulation are also identified. The boiler tube length was 91.5-inches, the shell inside diameter was 2.07-inches and the potassium was in vertical upflow for all test cases.

Test Case	Test Conditions	Source Of Original Data
I	0.92-inch ID Boiler Tube With P/D = 2.2 Helix Insert, Countercurrent Sodium Flow	Reference 9
II	0.92-inch ID Boiler Tube With P/D = 6 Helix Insert, Countercurrent Sodium Flow	Reference 10
III	0.67-inch ID Boiler Tube With P/D = 6 Helix Insert, Countercurrent Sodium Flow	Reference 10
IV_a	0.67-inch ID Boiler Tube With No Insert, Countercurrent Sodium Flow	Reference 11
IV_b	0.67-inch ID Boiler Tube With No Insert, Cocurrent Sodium Flow	Reference 11

Each data run in the various data tabulations is identified according to the date and military time at which it was obtained. This is conformal with the data run identification employed in References 9, 10 and 11.

TABLE VI

Data Table Nomenclature

a_{Rc}	Radial acceleration developed by the insert at the point of critical heat flux	g's
a_{RTB}	Radial acceleration developed by the insert in the transition boiling region	g's
G_K	Potassium mass velocity	lb/(ft^2-sec)
$\bar{h}_B$	Potassium heat transfer coefficient averaged from the point of boiling inception to the boiler tube exit	Btu/(hr-ft^2-°F)
h_{SH}	Potassium heat transfer coefficient in the superheated vapor region	Btu/(hr-ft^2-°F)
h_{TB}	Potassium heat transfer coefficient in the transition boiling region	Btu/(hr-ft^2-°F)
L_{SH}	Boiler tube length in the superheated vapor region	inches
P_{Ko}	Potassium pressure at the potassium boiler exit	psia
$(\Delta P_B)_G$	Potassium pressure loss after boiling inception, computed from the pressure gages	psi
$(\Delta P_B)_T$	Potassium pressure loss after boiling inception, computed from the insert thermocouples	psi
$\bar{q}''_B$	Average heat flux after boiling inception	Btu(hr-ft^2)
q''_c	Critical heat flux	Btu(hr-ft^2)
q''_{SH}	Average heat flux in the superheated vapor region	Btu(hr-ft^2)
Q_T	Net heat transferred in boiler tube	Btu/sec
T_{Kc}	Potassium temperature at the critical heat flux point	°F
T_{KSH}	Average potassium temperature in the superheated vapor region	°F
T_{KTB}	Average potassium temperature in the transition boiling region	°F
ΔT_{TB}	Average tube wall-to-potassium temperature difference in the transition boiling region	°F
δ_{SH}	Degrees of vapor superheat at the potassium boiler exit	°F

TABLE VI (Cont'd)

T_{Nai}	Sodium temperature at the sodium boiler inlet	°F
T_{Nao}	Sodium temperature at the sodium boiler outlet	°F
T_{Ki}	Potassium temperature at the potassium boiler inlet	°F
T_{Ko}	Potassium temperature at the potassium boiler exit	°F
$\int \phi$	Integrated boiling potassium frictional pressure loss multiplier	dimensionless
x_c	Potassium quality at the critical heat flux point	dimensionless
x_{TB}	Average potassium quality in the transition boiling region	dimensionless
x_o	Potassium quality at the boiler exit	dimensionless
Date	Calendar date on which data run was obtained, e.g., 05224 = 5/22/64	
Time	Military time at which data run was obtained, e.g., 2300 = 11:00 P.M.	

TABLE VII

Overall and Average Results
0.92-inch ID Boiler Tube With P/D = 2.2 Helix Insert
Countercurrent Sodium Flow, Test Plan A

Test Case I

G_K	P_{Ko}	T_{Ko}	x_o	$(\Delta P_B)_G$	$(\Delta P_B)_T$	Φ	$\bar{h}_B$	$\bar{q}''_B$	Q_T	T_{Nai}	T_{Nao}	T_{Ki}	Date	Time
$1650 < T_{Ko} < 1750^{\circ}F$														
20.45	59.29	1711.9	0.226	0.88	0.09	32.9	3,060	33,580	20.60	1741.2	1730.3	1054.9	05224	1100
21.37	50.81	1671.0	1.145	8.90	7.69	270.7	3,150	167,480	85.93	1844.8	1803.7	1387.5	05264	2345
18.79	38.22	1654.1	54*	9.80		374.2	1,650	143,820	75.26	1839.9	1803.7	1352.4	05274	0005
16.43	30.43	1762.3	216*	12.44		599.5	1,150	136,010	71.51	1841.0	1806.4	1323.4	05274	0020
14.86	25.87	1762.6	252*	13.18		751.0	950	130,190	68.59	1842.5	1809.3	1301.0	05274	0025
22.82	53.47	1686.1	0.266	0.70	0.35	20.4	3,470	44,420	25.87	1723.2	1709.9	1384.5	05274	0745
20.86	53.82	1687.9	0.304	1.03	0.37	35.8	4,130	46,080	26.40	1724.0	1710.5	1379.6	05274	0900
21.79	56.70	1700.5	0.509	2.11	1.39	65.7	5,410	79,510	42.60	1759.5	1738.2	1366.0	05274	1130
19.35	59.55	1713.1	0.806	2.93	2.30	103.4	6,150	109,200	56.88	1793.4	1764.9	1355.0	05274	1400
20.28	58.42	1707.8	0.888	3.28	1.55	103.1	5,500	125,800	65.23	1798.9	1767.1	1341.9	05274	1500
39.60	60.38	1716.2	0.202	1.00	1.24	12.3	3,390	61,660	33.72	1768.8	1751.8	1496.8	05224	0100
39.77	59.17	1711.5	0.110	0.65	0.55	8.8	2,330	34,470	20.91	1745.6	1734.6	1521.2	05224	0650
37.81	47.66	1657.0	0.334	3.52	2.88	47.6	4,310	94,740	48.58	1735.5	1711.5	1450.4	05254	2230
37.15	57.85	1705.7	0.127	0.65	0.31	9.5	2,430	36,790	22.12	1740.6	1729.1	1500.2	05264	0630
38.67	47.15	1706.3	0.252	12.89	1.64	190.5	3,490	73,550	38.81	1768.7	1749.1	1501.5	05264	0930
38.10	54.83	1691.7	0.262	2.70	2.09	37.3	2,900	74,450	39.48	1760.6	1740.8	1488.1	05264	1100
36.68	55.55	1691.0	0.702	9.61	9.40	128.5	5,700	185,110	90.87	1842.0	1798.6	1495.7	05264	1800
31.99	56.96	1698.4	0.828	8.59	8.28	138.2	6,120	188,940	93.57	1846.1	1801.6	1457.8	05264	1930
27.41	56.99	1699.5	0.978	6.87	7.60	131.9	5,770	188,730	94.31	1847.3	1802.3	1430.6	05264	2130
25.35	54.94	1689.9	1.028	8.24	7.17	186.7	4,550	181,810	91.73	1841.4	1797.8	1407.9	05264	2230
25.31	54.08	1688.9	1.033	8.06	7.60	182.3	4,710	182,910	92.25	1841.0	1797.1	1399.7	05264	2300
55.99	56.75	1699.5	0.162	3.07	2.87	25.05	3,290	72,320	37.64	1765.8	1747.0	1540.5	05214	2100
49.33	56.52	1698.8	0.197	1.98	2.35	18.23	3,490	75,660	39.32	1764.1	1744.7	1524.9	05214	2200
45.64	56.87	1703.3	0.209	2.25	2.26	23.94	3,480	73,970	39.09	1767.1	1747.8	1504.7	05214	2300
40.60	60.15	1716.9	0.223	1.29	1.68	15.35	3,620	69,460	37.24	1775.0	1756.2	1496.9	05214	2400
41.72	62.71	1728.1	0.128	0.52	0.62	6.01	2,690	42,280	25.06	1766.6	1753.6	1515.6	05224	0338
162.0	71.41	1761.0	0.048	4.19	3.81	8.71	4,150	78,260	34.40	1824.8	1807.3	1695.1	05204	2200
75.6	60.53	1717.0	0.248	7.86	8.96	39.51	5,270	149,400	69.63	1840.6	1806.4	1591.0	05214	0528
79.0	64.38	1733.9	0.223	7.60	7.86	36.11	4,760	140,190	65.61	1850.0	1817.9	1613.5	05214	0700
75.7	60.70	1717.1	0.183	5.85	5.30	29.99	3,960	110,720	53.37	1812.9	1786.5	1593.6	05214	0930
75.5	63.43	1729.4	0.119	3.66	2.63	19.66	3,130	74,140	37.55	1796.5	1777.6	1604.7	05214	1300
75.4	63.20	1730.1	0.068	2.25	1.28	13.03	2,250	44,680	25.30	1775.5	1762.4	1600.5	05214	1730
65.2	55.78	1694.8	0.134	3.61	2.73	23.90	3,040	70,650	36.49	1760.9	1742.7	1557.9	05214	1900
60.5	56.38	1695.8	0.147	3.01	2.68	22.00	3,100	71,630	37.41	1762.1	1743.4	1540.0	05214	2000
65.8	46.23	1647.6	0.072	2.22	1.58	15.70	2,530	40,490	23.03	1688.8	1676.9	1518.3	05224	1400
$1500 < T_{Ko} < 1600^{\circ}F$														
18.93	27.96	1533.4	0.213	1.30	0.18	55.0	3,460	30,120	18.94	1558.8	1549.0	1205.1	05254	1300
23.93	31.85	1558.3	0.303	1.93	1.36	53.5	2,960	53,560	30.21	1610.4	1595.3	1276.6	07014	1130
21.00	34.42	1576.4	0.337	1.56	1.01	52.2	3,470	51,970	29.57	1623.0	1608.0	1255.7	07014	1400
20.88	28.24	1535.6	0.544	4.32	3.55	143.8	3,040	82,220	44.23	1620.7	1599.1	1215.0	07014	1730
19.87	27.69	1527.5	0.922	7.19	6.84	238.9	4,100	131,270	67.98	1658.6	1625.9	1190.4	07014	1930
18.91	25.56	1509.2	1.101	9.45	9.00	332.6	3,190	147,930	76.30	1674.8	1638.2	1190.2	07014	2100
24.14	25.53	1507.2	0.893	10.81	10.08	266.3	3,700	156,390	80.11	1677.1	1638.6	1200.3	07014	2225
20.95	36.01	1585.1	0.758	4.35	4.45	133.4	4,570	113,820	59.37	1685.7	1656.8	1248.1	07024	0330
21.36	30.40	1547.4	0.770	5.59	5.38	167.5	4,090	118,510	61.54	1663.4	1630.2	1227.2	07024	0630
21.39	29.50	1540.4	0.773	5.92	5.82	177.9	3,990	119,250	61.62	1663.9	1626.6	1239.2	07024	0730
20.41	29.38	1538.7	0.835	-3.61	6.12	-182.0	3,910	122,510	63.26	1672.3	1628.0	1225.9	07024	0830
20.39	26.30	1512.7	0.748	9.33	6.94	326.2	2,080	109,540	57.14	1687.5	1615.1	1217.2	07024	0930
16.06	19.56	1601.8	151*	10.28		487.7	1,380	125,200	66.01	1687.6	1655.7	1181.7	07014	2120

* Degrees of vapor superheat at potassium exit

TABLE VII (Cont'd)

G_K	P_{Ko}	T_{Ko}	x_o	$(\Delta P_B)_G$	$(\Delta P_B)_T$	Φ	$\bar{h}_B$	$\bar{q}''_B$	Q_T	T_{Nai}	T_{Nao}	T_{Ki}	Date	Time
37.65	31.69	1562.4	0.222	2.85	2.53	40.8	3,210	64,470	34.97	1625.7	1608.1	1351.7	05254	0530
38.75	31.29	1556.9	0.116	1.75	1.07	25.6	2,640	35,840	21.34	1593.7	1582.6	1372.3	05254	0830
30.78	29.50	1543.4	0.127	1.38	0.70	28.8	3,150	30,830	19.10	1572.3	1562.4	1321.2	05254	1100
26.93	35.26	1575.7	0.780	7.39	8.54	154.0	5,150	154,180	79.54	1716.4	1679.3	1194.2	05274	0130
38.31	30.83	1550.5	0.415	7.14	6.65	92.9	3,890	118,830	59.76	1669.3	1640.3	1371.8	06304	1130
37.81	31.01	1548.3	0.540	9.60	9.53	123.0	4,420	151,950	75.23	1699.0	1662.5	1367.7	06304	1430
38.22	29.60	1537.0	0.622	11.93	11.98	145.8	4,110	176,320	87.09	1718.9	1677.3	1355.1	06304	1600
36.74	30.00	1536.9	0.710	12.89	14.66	164.1	4,560	193,170	94.82	1737.6	1692.4	1355.4	06304	1800
37.67	29.66	1532.9	0.764	15.79	16.78	193.8	4,470	213,220	104.40	1758.4	1707.9	1349.1	06304	1930
36.22	31.29	1539.8	0.833	15.31	17.61	193.3	4,270	221,860	109.10	1775.9	1722.7	1346.1	06304	2045
37.74	30.30	1531.8	0.827	16.54	18.64	194.8	4,280	230,090	112.60	1777.9	1724.3	1358.5	06304	2130
36.72	30.24	1527.6	0.878	17.61	19.95	214.6	4,020	236,900	116.30	1787.6	1731.8	1347.9	06304	2200
34.72	28.27	1521.6	0.987	21.33	21.84	285.1	3,420	249,480	123.40	1809.7	1750.0	1334.6	06304	2300
34.93	31.85	1557.1	0.196	2.40	2.02	38.6	2,380	52,020	28.82	1614.9	1600.4	1370.3	07014	1000
28.92	31.23	1551.9	0.259	1.79	1.70	36.2	2,970	56,090	30.88	1607.5	1591.9	1327.0	07014	1030
54.41	36.21	1588.9	0.152	3.19	2.93	27.0	3,050	66,240	34.89	1654.9	1637.1	1436.1	05244	1630
51.87	34.39	1572.6	0.197	4.06	4.15	35.6	3,080	79,870	40.99	1655.2	1634.7	1427.5	05244	1800
44.75	33.26	1567.3	0.246	4.44	4.28	48.2	3,380	85,020	43.87	1652.6	1631.1	1393.9	05244	1930
44.68	35.09	1581.3	0.250	4.31	4.01	47.3	3,650	86,900	45.19	1664.2	1642.0	1382.9	05244	1930
38.31	34.34	1577.1	0.278	3.71	3.57	50.3	3,540	81,140	42.41	1655.3	1634.1	1377.2	05254	0030
40.72	30.83	1552.3	0.097	1.07	0.94	14.4	2,690	32,140	19.56	1584.9	1574.6	1375.8	05254	0930
41.29	31.60	1558.0	0.159	1.81	1.64	22.3	2,810	51,280	28.12	1609.1	1594.9	1390.3	06304	0430
40.22	30.58	1551.2	0.288	4.38	3.80	54.2	3,770	88,540	45.45	1635.8	1613.4	1372.5	06304	0830
74.00	30.74	1549.4	0.154	6.03	6.03	31.6	3,210	93,380	46.05	1648.7	1626.3	1432.6	05224	2130
71.10	32.22	1562.4	0.127	4.39	4.29	25.7	3,140	75,130	38.08	1640.6	1621.5	1439.4	05224	2400
74.30	28.58	1537.6	0.102	4.08	3.78	23.2	2,870	63,850	32.90	1607.6	1591.1	1424.0	05234	0300
71.50	30.61	1553.5	0.094	3.55	3.10	21.4	2,800	56,820	29.84	1614.6	1599.5	1437.6	05234	0430
78.60	33.17	1568.3	0.056	2.69	2.09	14.7	2,290	37,860	20.71	1612.2	1601.5	1481.8	05234	1130
90.30	35.98	1585.5	0.044	2.60	5.76	16.3	3,600	40,650	21.71	1638.9	1628.0	1477.7	05234	1353
65.30	36.12	1586.2	0.083	2.28	2.52	15.6	2,080	45,220	25.58	1639.8	1627.0	1456.9	05234	1430
143.10	31.01	1551.8	0.084	8.57	8.81	22.0	4,730	117,330	49.52	1665.9	1641.6	1478.0	05234	2300
152.30	33.83	1567.3	0.069	6.73	7.53	16.1	5,420	105,900	43.68	1665.4	1643.7	1504.5	05244	0030
150.00	35.01	1578.3	0.043	5.14	5.02	13.5	4,110	66,570	29.15	1644.8	1630.2	1522.6	05244	0830
147.80	30.83	1550.3	0.024	3.50	3.19	10.7	2,570	36,880	18.70	1595.5	1585.6	1496.4	05244	1200
118.60	29.69	1543.0	0.031	3.56	2.66	12.8	2,380	35,490	19.04	1586.8	1576.7	1477.7	05244	1300
61.30	25.34	1511.4	0.109	3.65	3.20	26.7	2,360	53,870	28.73	1576.6	1562.1	1397.1	05244	1400

TABLE VIII

Overall and Average Results
0.92-inch ID Boiler Tube With P/D = 6 Helix Insert
Countercurrent Sodium Flow, Test Plan A

Test Case II

G_K	P_{Ko}	T_{Ko}	x_o	$(\Delta P_B)_G$	$(\Delta P_B)_T$	Φ	$\bar{h}_B$	$\bar{q}''_B$	Q_T	T_{Na1}	T_{Nao}	T_{K1}	Date	Time
$1650 < T_{Ko} < 1750^\circ F$														
19.26	57.73	1706.0	0.473	1.32	1.30	156.8	6,470	65,350	36.18	1753.1	1734.9	1320.3	07244	1030
19.23	57.27	1703.2	0.624	2.03	1.17	235.9	8,380	85,450	45.81	1760.2	1737.6	1305.5	07244	1500
23.25	58.80	1711.4	0.671	2.39	2.10	191.1	7,480	111,600	58.09	1788.4	1760.2	1354.4	07244	1900
22.25	59.29	1712.5	0.794	2.44	2.19	195.4	8,010	125,300	64.66	1797.5	1766.2	1348.8	07244	2100
22.67	55.51	1695.3	0.842	3.12	2.58	243.6	5,220	134,770	69.71	1796.6	1762.8	1331.9	07244	2300
19.12	47.72	1656.4	1.101	3.93	3.88	394.5	1,640	143,410	75.90	1841.6	1804.4	1272.8	07254	0100
19.11	47.72	1654.6	1.102	3.94	4.16	396.6	1,600	143,400	76.02	1846.1	1809.0	1268.9	07254	0120
24.37	66.54	1742.9	0.921	3.50	3.02	241.6	10,930	158,850	80.24	1844.9	1806.2	1391.7	07264	1645
20.35	65.50	1739.6	1.201	3.24	2.59	270.6	12,380	170,060	86.17	1846.1	1804.5	1351.2	07264	1745
39.60	60.12	1715.7	0.223	1.97	1.44	82.7	10,190	70,190	36.83	1761.5	1743.0	1481.4	07254	1200
39.52	55.97	1696.1	0.449	3.35	3.26	117.6	14,140	134,820	66.10	1782.0	1750.1	1468.1	07254	1900
39.49	55.43	1694.1	0.540	3.78	4.20	122.3	13,860	159,860	77.78	1797.3	1759.9	1468.5	07254	2230
39.45	57.79	1705.6	0.630	4.31	4.53	132.7	13,960	184,600	89.62	1823.5	1780.4	1465.8	07264	0030
37.45	57.44	1703.0	0.813	5.44	5.98	166.8	12,580	221,680	107.70	1847.8	1796.5	1462.3	07264	0300
37.97	57.47	1711.4	0.829	5.44	5.87	160.0	13,610	229,080	111.00	1858.2	1805.5	1467.9	07264	0430
35.37	57.82	1704.7	0.890	5.43	5.98	176.1	11,150	227,360	111.10	1855.2	1802.2	1447.1	07264	0600
31.52	66.37	1742.9	0.704	3.53	3.28	164.3	13,880	161,460	80.03	1843.5	1804.8	1451.4	07264	1335
27.42	65.94	1741.1	0.806	3.53	3.65	204.8	12,070	158,470	79.40	1843.0	1804.5	1419.0	07264	1530
40.67	59.52	1712.9	0.332	2.51	2.21	90.8	13,450	104,780	52.12	1778.7	1753.4	1487.9	07254	1630
$1500 < T_{Ko} < 1600^\circ F$														
15.25	36.22	1585.3	1.283	4.16	4.78	604.5	810	131,540	69.92	1860.4	1826.2	1252.9	07254	0200
18.96	31.38	1548.2	0.362	1.26	1.54	154.0	9,290	50,950	28.55	1587.3	1572.9	1215.1	07284	0900
18.94	32.11	1556.5	0.476	1.79	1.80	212.5	10,770	66,350	36.07	1605.3	1587.3	1203.6	07284	1030
18.96	35.07	1576.9	0.630	2.11	2.07	230.7	16,210	87,240	46.10	1636.2	1613.4	1209.2	07284	1245
18.90	31.96	1554.9	0.778	3.34	3.74	357.3	3,540	105,050	55.69	1655.0	1627.4	1180.6	07284	1430
18.91	33.07	1562.6	0.915	3.32	3.53	319.6	4,660	123,350	64.40	1667.4	1636.3	1187.2	07284	1530
18.91	33.20	1564.2	0.975	3.62	3.87	343.4	4,660	131,260	68.29	1676.0	1643.1	1186.8	07284	1630
19.77	24.63	1508.8	1.109	8.33	7.12	803.0	1,810	154,260	80.95	1706.9	1667.9	1151.0	07284	1740
20.33	31.10	1550.5	0.664	3.18	2.29	318.4	6,380	99,570	55.20	1632.8	1599.0	982.9	08034	2400
18.44	32.15	1559.9	0.773	3.21	2.61	371.5	6,950	104,400	57.26	1654.0	1607.5	958.2	08044	0330
18.48	31.59	1555.5	0.769	2.74	2.43	301.2	6,500	104,720	56.63	1665.5	1597.1	989.7	08044	0530
18.47	29.00	1538.6	0.749	3.34	2.63	398.3	5,930	104,500	55.39	1696.9	1561.6	979.5	08044	0700
18.47	30.95	1551.8	0.808	3.39	2.63	391.2	5,010	111,880	59.18	1723.4	1577.7	979.3	08044	0900
18.98	33.20	1567.0	0.787	3.63	2.48	402.9	9,520	108,520	59.37	1638.1	1617.4	993.4	08044	1530
38.71	32.33	1557.2	0.094	1.75	0.75	83.5	3,880	30,120	18.88	1583.6	1573.8	1357.9	07274	0430
38.63	32.18	1558.0	0.249	2.35	2.10	94.5	11,530	76,980	39.61	1613.2	1593.5	1344.6	07274	0915
38.69	34.34	1570.4	0.311	3.24	3.01	128.6	13,270	95,270	48.03	1638.5	1614.9	1346.3	07274	1215
38.56	34.12	1563.7	0.425	3.20	3.69	103.6	10,730	127,010	63.32	1655.8	1624.9	1323.6	07274	1420
38.71	33.81	1566.4	0.553	5.44	5.68	176.0	11,710	163,020	79.58	1686.6	1648.3	1350.7	07274	1630
37.24	33.38	1564.4	0.668	6.78	6.79	223.1	9,880	186,710	91.24	1706.2	1662.3	1346.5	07274	1800
38.74	33.75	1566.1	0.731	8.09	8.36	241.6	9,710	212,120	103.04	1729.3	1680.0	1355.9	07274	1930
38.68	33.47	1563.1	0.857	9.51	10.36	259.3	8,730	246,610	119.79	1757.6	1700.6	1348.1	07274	2130
38.69	32.39	1558.9	0.924	11.60	12.28	299.8	8,870	272,790	131.92	1776.6	1713.9	1357.0	07274	2300
39.13	30.82	1547.9	0.967	12.48	12.97	322.5	7,950	280,870	136.20	1778.6	1713.6	1344.6	07274	2330
37.06	26.08	1515.2	1.022	14.92	14.66	433.2	5,210	279,060	136.92	1776.7	1710.8	1321.4	07284	0017
36.84	32.02	1558.4	0.689	7.67	7.30	272.3	10,840	196,690	101.07	1694.2	1659.4	1075.3	08044	1930
37.25	31.84	1555.9	0.688	7.57	7.82	263.6	11,910	201,530	102.34	1717.3	1655.7	1063.5	08044	2100
36.79	31.65	1554.8	0.720	7.82	7.94	272.8	9,900	208,350	105.08	1740.4	1656.3	1066.5	08044	2300
37.79	32.02	1556.9	0.691	7.68	7.21	261.2	7,500	207,220	103.65	1772.7	1649.5	1082.9	08054	0200
36.76	30.55	1547.4	0.705	7.27	6.90	255.0	5,180	210,800	103.08	1858.9	1612.6	1061.2	08054	0500
36.42	30.95	1570.8	0.800	11.68	8.62	452.3	11,880	223,570	113.38	1723.1	1683.9	1087.2	08054	1100
38.11	32.58	1561.0	0.952	11.92	12.22	342.9	10,600	270,030	131.14	1755.2	1710.4	1328.9	08054	1700
38.53	31.56	1554.2	0.939	11.97	12.43	336.9	8,280	270,550	131.06	1788.6	1710.3	1322.4	08054	2000
38.47	31.22	1553.5	0.945	12.08	16.37	349.7	15,910	279,430	131.87	1814.3	1709.3	1315.2	08054	2230
37.93	30.48	1523.6	0.959	12.25	15.65	352.8	6,070	274,790	132.04	1860.2	1701.3	1309.4	08064	0100

TABLE IX

Overall and Average Results
0.67-inch ID Boiler Tube With P/D = 6 Helix Insert
Countercurrent Sodium Flow, Test Plan A

Test Case III

G_K	P_{Ko}	T_{Ko}	x_o	(ΔP_{B_G})	(ΔP_{B_T})	Φ	$\bar{h}_B$	$\bar{q}''_B$	Q_T	T_{Nai}	T_{Nao}	T_{Ki}	Date	Time
$1650 < T_{Ko} < 1700^{\circ}F$														
38.28	58.05	1707.4	0.266	1.89	2.79	40.8	59,190	49,280	20.20	1742.7	1729.3	1432.2	10094	1815
39.96	57.39	1706.2	0.409	2.98	4.05	54.6	37,130	78,530	30.49	1761.1	1741.7	1409.9	10104	0230
39.80	53.62	1688.6	0.550	4.40	5.34	75.2	20,610	104,000	39.21	1763.2	1738.8	1402.8	10104	0430
39.11	56.38	1701.6	0.698	5.92	6.83	100.7	19,520	128,260	47.64	1794.2	1764.8	1417.2	10104	0800
39.07	57.50	1707.5	0.832	7.98	8.28	119.8	471,240	161,430	56.09	1817.7	1783.3	1407.7	10104	1200
39.58	49.64	1668.8	0.966	10.69	12.23	163.1	5,070	174,640	64.16	1832.0	1792.8	1479.7	10104	1930
38.15	50.00	1680.4	13*	11.67		196.6	6,140	179,340	66.23	1835.6	1795.4	1417.4	10104	2015
34.56	37.32	1654.5	60*	15.47		341.1	1,670	148,660	55.88	1842.8	1808.4	1489.1	10104	2050
38.56	43.30	1660.0	29*	14.80		260.2	2,840	168,810	62.79	1837.7	1799.4	1481.7	10104	2150
38.54	55.26	1695.8	0.879	8.44	9.83	141.9	12,270	158,080	58.48	1818.6	1782.0	1387.8	10154	0130
35.59	55.43	1697.6	0.990	8.78	8.91	164.5	5,310	160,630	59.92	1837.3	1800.7	1414.7	10154	0330
40.29	57.42	1705.6	0.921	9.34	10.09	143.2	14,710	172,740	63.21	1835.0	1796.4	1434.1	10104	1530
40.48	38.36	1656.3	55*	18.36		299.2	2,570	183,970	68.48	1855.5	1814.0	1469.6	10114	0230
44.78	48.77	1661.8	0.986	13.36	15.47	158.7	5,320	202,830	73.81	1850.8	1806.2	1500.4	10114	0430
48.75	51.51	1679.3	0.947	13.59	15.36	140.4	7,640	214,650	77.55	1861.4	1814.7	1490.8	10114	0700
52.31	57.33	1703.6	0.634	10.44	11.74	117.9	11,210	159,230	58.42	1831.0	1795.3	1422.8	10144	1900
45.18	57.42	1702.0	0.757	9.28	10.89	125.2	12,590	161,470	59.37	1828.8	1792.4	1415.9	10144	2230
44.66	16.96	1632.8	211*	34.51		483.9	2,080	218,860	81.83	1869.7	1803.5	1339.5	10174	0400
309.1	54.11	1684.6	0.089	25.87	23.79	33.7	12,210	196,880	51.99	1853.4	1820.9	1624.1	10144	0500
163.5	54.68	1690.0	0.188	19.78	20.84	48.5	11,670	179,900	56.81	1848.5	1813.6	1576.6	10144	1000
107.5	54.13	1689.5	0.287	16.40	16.60	68.9	8,040	162,540	56.47	1835.9	1801.0	1518.8	10144	1200
71.7	57.22	1702.3	0.441	13.23	13.70	98.6	9,310	157,620	57.14	1836.0	1800.9	1458.5	10144	1500
60.9	61.04	1718.6	0.487	8.57	11.18	78.1	21,590	145,810	52.55	1830.4	1797.9	1484.5	10154	0530
60.8	60.76	1717.7	0.348	5.88	7.06	57.9	18,760	106,070	40.03	1797.8	1772.7	1444.4	10154	0830
69.7	59.46	1711.2	0.157	2.67	3.41	23.6	12,390	57,830	24.60	1755.0	1739.1	1443.2	10154	1130
$1500 < T_{Ko} < 1600^{\circ}F$														
39.27	30.24	1550.5	0.406	4.69	5.27	94.1	29,690	78,470	30.19	1618.4	1599.3	1273.0	10114	1830
38.31	29.84	1548.3	0.557	7.10	7.47	67.8	15,560	103,770	38.93	1643.1	1618.8	1281.3	10114	2130
39.44	30.15	1548.5	0.699	9.97	10.09	30.7	8,180	132,230	48.96	1678.0	1647.4	1309.0	10124	0030
39.47	31.66	1558.8	0.839	11.73	12.57	180.0	9,060	158,350	58.10	1711.7	1675.4	1316.3	10124	0230
34.10	20.32	1592.2	133*	22.17		947.9	2,280	159,870	59.49	1761.1	1724.5	1421.3	10124	0800
34.10	20.32	1568.7	110*	22.16		595.6	2,560	167,560	62.15	1762.8	1724.6	1421.8	10124	0800
39.93	23.39	1516.4	0.972	20.72	19.18	209.9	3,380	181,260	66.68	1754.4	1713.5	1392.1	10124	0900
39.94	25.93	1522.2	0.964	19.80	19.02	250.8	3,440	180,020	66.18	1754.0	1713.5	1390.1	10124	1000
38.06	22.31	1545.6	67*	23.40		428.7	2,430	171,680	63.77	1770.0	1731.4	1406.5	10124	1200
38.04	20.24	1576.6	119*	24.95		458.6	2,370	174,760	64.92	1772.2	1732.9	1403.9	10124	1220
36.98	18.10	1585.4	150*	25.68		492.1	2,080	173,130	64.49	1773.0	1733.7	1392.6	10124	1240
39.69	25.44	1526.0	0.929	21.53	19.68	367.0	2,870	171,740	64.06	1764.0	1725.1	1338.9	10134	1530
37.61	21.84	1543.0	0.871	23.07	15.65	456.6	1,880	150,740	57.25	1764.9	1730.2	1323.4	10134	1630
39.70	30.95	1571.3	0.901	14.98	13.39	235.7	7,610	169,880	62.28	1712.2	1690.4	1333.9	10154	2030
39.48	31.72	1557.0	0.952	15.28	16.40	235.3	6,060	177,430	65.05	1737.3	1705.1	1348.6	10164	0030
39.82	33.17	1569.2	0.954	15.19	15.79	232.7	5,290	179,070	65.58	1769.9	1716.6	1356.5	10164	0230
39.81	31.97	1560.1	0.948	15.48	16.31	236.8	4,510	178,760	65.24	1790.8	1711.8	1356.2	10164	0430
39.78	31.32	1555.9	0.945	15.04	16.51	227.6	4,090	178,710	65.04	1812.6	1707.6	1352.8	10164	0700
40.35	33.95	1574.9	0.222	2.00	2.13	39.4	216,150	44,660	18.91	1607.4	1595.0	1286.7	10114	1600
40.53	31.57	1558.0	0.866	13.10	14.78	191.1	8,780	166,440	59.95	1725.7	1688.2	1423.8	10124	0630
40.03	25.65	1546.5	38*	21.33		347.3	3,430	182,150	67.09	1769.3	1727.8	1402.3	10124	1100
58.60	34.36	1576.2	0.647	17.23	19.58	152.6	6,740	186,040	67.17	1772.3	1730.9	1359.6	10134	0730
45.92	34.14	1576.2	0.810	16.05	17.41	205.5	4,910	177,300	65.54	1769.2	1728.9	1319.8	10134	0850
40.60	32.06	1561.3	0.880	16.56	17.58	261.2	3,510	167,590	62.35	1763.0	1725.2	1331.9	10134	1130
40.05	32.68	1563.5	0.926	13.87	15.25	206.2	4,620	178,090	63.63	1849.9	1693.4	1395.6	10164	1000
50.14	26.11	1538.9	26*	28.80		310.6	4,370	240,250	87.13	1847.6	1777.6	1405.6	10174	0230
290.6	34.00	1564.9	0.116	31.51	32.79	55.5	71,550	304,380	67.29	1808.4	1766.5	1486.2	10124	2400
192.6	33.54	1563.2	0.186	29.24	30.40	57.8	7,070	223,690	67.90	1807.9	1765.7	1473.5	10134	0200
108.1	33.29	1566.5	0.342	23.07	24.64	88.3	6,230	198,170	67.52	1787.7	1745.7	1434.4	10134	0400
75.3	34.09	1573.4	0.510	19.60	21.33	121.4	7,620	195,380	68.80	1777.8	1735.0	1393.5	10134	0544
102.6	34.92	1570.8	0.424	28.92	29.76	115.8	6,210	228,920	77.15	1840.6	1778.4	1467.2	10164	1500
80.8	35.01	1571.7	0.566	27.09	27.78	147.3	6,430	232,800	80.64	1839.6	1774.7	1438.1	10164	1730
69.5	34.14	1566.2	0.708	25.93	27.89	165.4	7,700	246,680	86.01	1842.3	1773.2	1423.2	10164	2030
61.3	33.02	1560.1	0.820	25.44	27.20	188.4	6,480	247,230	87.35	1842.7	1772.3	1418.2	10174	0030

*Degrees of vapor superheat at potassium exit.

TABLE X

Overall and Average Results
0.67-inch ID Boiler Tube With No Insert
Countercurrent Sodium Flow, Test Plan A

Test Case IV_a

G_K	P_{Ko}	T_{Ko}	x_o	$(\Delta P_B)_G$	$\bar{h}_B$	$\bar{q}''_B$	Q_T	T_{Nai}	T_{Nao}	T_{K1}	Date	Time
$1650 < T_{Ko} < 1750^oF$												
16.70	57.96	1710.8	0.470	0.671	3,940	43,340	17.35	1744.1	1732.3	1448.9	11144	0545
15.78	58.17	1709.4	0.860	0.189	2,910	73,600	28.27	1772.7	1754.7	1445.4	11144	0730
17.26	59.72	1717.2	0.534	0.466	5,800	51,630	20.71	1762.8	1735.5	1379.3	11174	1630
17.26	57.07	1703.9	0.624	0.075	5,820	60,170	23.65	1756.7	1726.0	1379.0	11174	1800
17.24	57.76	1708.5	0.736	0.883	6,480	70,630	27.42	1770.5	1735.4	1372.4	11174	1930
17.25	59.17	1715.4	0.786	1.427	8,100	75,430	29.10	1780.5	1743.3	1374.0	11174	2100
17.25	58.80	1713.7	0.826	1.117	6,810	79,040	30.41	1782.7	1744.0	1375.4	11174	2115
32.79	56.15	1700.2	0.213	0.983	4,930	41,710	18.16	1732.0	1719.6	1423.3	10294	0400
33.26	57.19	1704.7	0.350	1.042	7,070	68,360	27.34	1751.6	1734.1	1420.1	10294	0530
32.17	57.81	1708.4	0.474	1.627	8,880	88,130	33.98	1766.8	1745.5	1430.5	10294	0730
32.79	54.68	1690.2	0.634	1.847	11,460	118,900	44.14	1768.4	1740.9	1464.1	10294	0930
31.70	54.15	1687.3	0.762	2.590	4,680	135,430	50.54	1795.0	1763.6	1462.0	10294	1130
33.51	45.62	1650.5	0.735	2.916	1,140	134,520	51.10	1844.4	1812.5	1483.8	10294	1255
36.03	52.85	1681.7	0.715	3.454	5,020	146,770	54.94	1797.1	1763.5	1421.1	10304	1330
33.29	56.06	1700.5	0.688	2.896	8,390	131,840	48.64	1815.4	1754.8	1448.0	11184	0030
33.30	56.73	1702.0	0.758	2.749	4,650	143,190	53.12	1840.4	1774.2	1451.3	11184	0215
58.29	58.22	1709.4	0.428	4.805	10,380	151,090	55.12	1813.4	1779.0	1483.7	10304	1030
44.07	57.59	1704.6	0.579	3.827	12,760	150,100	55.33	1804.0	1770.2	1442.9	10304	1130
51.32	58.02	1708.0	0.195	1.693	5,430	61,720	24.70	1754.7	1738.7	1503.6	10304	1730
51.95	55.26	1694.8	0.293	2.819	6,730	92,390	35.11	1763.1	1741.0	1485.5	10304	1930
50.27	53.70	1687.6	0.449	3.965	8,280	133,540	49.06	1782.9	1752.7	1487.4	10304	2230
49.29	55.78	1698.3	0.602	4.561	13,240	173,870	62.90	1812.9	1774.0	1491.2	10314	0100
50.57	51.82	1680.0	0.693	5.965	6,460	202,210	73.56	1831.2	1786.4	1485.7	10314	0300
47.88	53.24	1687.3	0.726	6.314	4,180	200,850	74.89	1854.1	1808.8	1396.7	11144	1830
50.65	55.32	1695.4	0.617	5.085	8,360	182,670	65.29	1858.1	1778.0	1523.7	11184	0530
88.56	56.90	1701.4	0.298	6.145	11,630	168,130	59.04	1817.6	1781.1	1532.3	10304	0830
315.1	59.43	1712.6	0.071	13.280	-30,750	242,720	59.47	1847.7	1811.5	1619.0	11144	1200
136.6	59.06	1713.4	0.218	10.120	10,740	202,990	68.05	1857.0	1815.9	1572.6	11144	1400
84.5	58.71	1710.9	0.387	8.221	10,930	204,460	71.88	1853.4	1810.0	1520.4	11144	1530
62.0	57.30	1704.9	0.563	7.124	11,630	209,740	75.24	1847.9	1802.5	1473.4	11144	1700
$1500 < T_{Ko} < 1600^oF$												
16.30	32.40	1558.3	0.170	16.612	6,290	184,980	67.76	1752.7	1711.4	1446.6	11014	0545
16.49	33.17	1549.3	0.352	1.344	-25,090	34,050	13.06	1586.0	1577.2	1371.1	11154	0200
15.63	33.17	1570.0	0.721	1.468	3,660	62,990	24.09	1625.2	1609.8	1357.2	11154	0430
16.40	32.25	1561.3	0.794	0.911	4,300	72,860	27.55	1620.6	1603.2	1368.9	11154	0545
16.11	33.26	1570.3	0.391	1.156	2,420	35,990	15.21	1614.7	1594.4	1237.5	11164	1700
16.20	31.11	1554.1	0.686	1.560	3,060	62,900	24.42	1625.9	1594.5	1277.6	11164	1900
16.53	32.31	1565.7	0.760	1.968	3,910	71,090	27.35	1640.8	1606.1	1283.4	11164	2130
16.98	32.71	1569.3	0.806	2.900	6,020	77,830	29.78	1647.4	1609.9	1269.9	11164	2245
32.50	32.40	1559.8	0.160	1.567	1,290	30,720	14.54	1607.2	1597.4	1306.5	10314	1030
32.44	28.33	1535.3	0.249	1.551	1,760	47,710	20.26	1592.1	1579.0	1287.7	10314	1400
32.43	28.67	1538.7	0.421	2.961	6,400	81,300	31.55	1605.0	1585.1	1284.0	10314	1630
32.47	29.01	1541.3	0.564	3.191	10,570	108,570	40.84	1620.6	1595.3	1296.2	10314	1900
32.46	28.15	1534.1	0.713	4.386	12,290	136,610	50.59	1635.1	1604.1	1297.7	10314	2100
31.66	29.04	1543.8	0.820	5.477	5,120	150,710	56.22	1673.2	1638.2	1301.6	11014	0030
32.38	32.71	1554.8	0.068	20.097	12,010	189,180	67.31	1755.0	1713.9	1440.0	11014	0430
37.97	27.96	1534.4	0.743	8.096	1,830	161,330	61.12	1737.6	1700.4	1329.3	11014	1730
32.52	30.83	1555.7	0.727	5.620	2,440	134,880	51.55	1688.1	1669.9	1306.8	11014	2100
31.66	28.76	1540.0	0.808	5.451	2,240	145,970	55.43	1696.1	1668.6	1300.8	11014	2330
32.42	28.06	1535.2	0.794	5.570	2,610	148,430	56.01	1700.8	1655.1	1290.6	11024	0100
32.13	27.90	1532.6	0.795	5.926	2,280	147,240	55.42	1724.4	1657.2	1298.8	11024	0230
32.62	32.71	1566.3	0.753	4.284	4,140	143,440	53.06	1734.5	1647.6	1331.1	11024	1000
31.62	24.54	1506.9	0.753	6.333	860	135,390	51.97	1826.3	1697.9	1287.1	11024	1230
32.64	31.66	1561.0	0.765	4.834	4,730	145,460	53.84	1713.1	1646.3	1333.1	11174	0215
32.58	28.27	1536.5	0.780	5.949	1,480	144,660	54.88	1759.7	1690.8	1322.3	11174	0345

TABLE X (Cont'd)

G_K	P_{Ko}	T_{Ko}	x_o	$(\Delta P_B)_G$	$\bar{h}_B$	$\bar{q}''_B$	Q_T	T_{Na1}	T_{Nao}	T_{K1}	Date	Time
48.28	30.15	1547.2	0.623	8.751	4,340	178,110	65.46	1716.4	1676.5	1366.6	11014	1400
50.07	32.46	1565.1	0.086	1.563	1,070	26,480	13.52	1608.1	1598.9	1370.3	11024	2130
49.51	32.03	1560.2	0.213	2.401	3,370	64,800	26.02	1622.8	1605.9	1362.8	11034	0030
48.91	29.20	1541.0	0.334	4.585	4,870	99,500	37.68	1631.9	1608.4	1348.2	11034	0300
48.22	29.78	1544.8	0.442	5.460	9,590	130,360	47.92	1649.3	1619.6	1344.6	11034	0430
48.19	28.92	1539.0	0.504	6.395	8,430	147,700	54.06	1660.6	1627.1	1340.9	11034	0550
49.42	36.37	1590.0	0.591	6.599	8,760	174,530	63.40	1725.3	1686.2	1394.0	11034	1000
49.09	31.81	1561.1	0.544	6.534	6,480	161,870	58.49	1725.7	1653.0	1375.3	11174	0700
49.12	32.58	1566.8	0.606	6.739	5,900	179,120	64.75	1749.0	1668.8	1380.0	11174	0830
49.29	29.63	1552.1	0.604	7.685	3,370	176,460	64.66	1755.4	1675.2	1381.9	11174	0900
49.27	26.61	1525.2	0.647	9.077	2,380	187,280	69.08	1772.3	1686.8	1378.3	11174	0905
50.70	31.29	1555.2	0.705	9.443	1,570	203,270	75.57	1863.6	1771.6	1444.8	11184	1100
89.82	34.00	1572.7	0.350	11.582	8,790	204,170	71.03	1744.3	1701.0	1425.1	11014	0800
63.65	35.54	1583.1	0.474	8.569	8,870	185,460	66.29	1732.2	1691.9	1414.6	11014	1000
275.0	35.36	1573.0	0.120	25.501	24,010	338,480	89.61	1833.2	1778.8	1453.4	11154	1230
162.0	35.34	1573.9	0.239	22.078	7,890	285,010	91.54	1830.8	1775.4	1463.6	11154	1400
114.8	31.97	1555.7	0.352	20.077	7,720	273,300	91.91	1805.4	1749.9	1443.8	11154	1730
89.9	31.72	1558.0	0.464	17.215	7,460	265,810	92.00	1794.1	1738.9	1446.5	11154	1900
73.0	29.72	1544.1	0.577	16.018	4,600	257,400	91.94	1794.8	1739.4	1426.8	11154	2100
252.7	33.02	1551.9	0.152	30.202	17,220	388,260	107.31	1864.2	1800.5	1405.0	11164	0230
161.5	31.78	1550.0	0.274	28.266	7,520	337,540	108.42	1862.9	1798.6	1419.9	11164	0400
126.4	32.74	1560.2	0.383	25.703	8,490	337,640	111.77	1860.9	1794.5	1439.3	11164	0530
100.6	31.91	1558.0	0.490	23.350	5,140	317,130	110.33	1863.7	1798.2	1439.1	11164	0700

TABLE XI

Overall and Average Results
0.67-inch ID Boiler Tube With No Insert
Cocurrent Sodium Flow, Test Plan A

Test Case IV_b

G_K	P_{Ko}	T_{Ko}	x_o	$(\Delta P_B)_G$	$\bar{h}_B$	$\bar{q}''_B$	Q_T	T_{Nai}	T_{Nao}	T_{Ki}	Date	Time
$1650 < T_{Ko} < 1750^oF$												
16.68	58.74	1713.4	0.470	0.825	7,610	43,090	17.27	1743.7	1731.8	1460.2	11134	0230
16.64	61.82	1725.1	0.764	0.777	13,460	69,190	26.78	1769.6	1752.0	1448.4	11134	0400
16.76	52.40	1688.3	0.921	0.856	1,690	83,150	32.05	1780.9	1760.5	1434.3	11134	0700
33.07	51.98	1680.7	0.214	0.985	6,550	41,610	18.30	1712.6	1700.4	1409.6	11054	1700
33.03	52.49	1682.1	0.296	0.846	8,100	56,910	23.65	1722.9	1707.5	1405.7	11054	1900
33.03	52.35	1681.6	0.418	1.410	10,540	79,290	31.42	1735.8	1715.8	1407.9	11054	2100
33.02	52.01	1679.4	0.566	2.224	14,260	106,330	40.93	1749.7	1724.2	1406.3	11054	2230
32.81	53.19	1688.6	0.693	3.312	18,400	128,220	48.56	1771.0	1740.5	1425.9	11064	0200
32.38	51.79	1679.6	0.846	3.488	15,690	153,310	57.53	1779.6	1743.6	1424.0	11064	0300
32.80	49.67	1670.3	0.897	4.264	1,910	162,230	62.51	1851.7	1813.1	1366.4	11064	0515
36.78	58.02	1709.1	0.697	3.117	18,890	145,640	55.44	1801.7	1767.5	1397.1	11064	1800
32.80	57.99	1708.8	0.788	3.077	21,360	145,330	55.17	1800.1	1766.1	1395.1	11064	1930
28.93	57.10	1703.9	0.877	2.636	14,530	141,560	53.88	1795.6	1762.3	1378.6	11064	2100
58.12	56.55	1700.0	0.440	4.773	30,140	152,710	57.63	1799.1	1763.4	1432.8	11064	1400
43.14	57.13	1703.4	0.607	3.681	38,790	151,720	57.76	1797.7	1762.2	1383.6	11064	1530
50.41	59.60	1715.1	0.187	1.053	7,320	57,340	24.49	1758.2	1742.1	1469.3	11074	0100
50.18	52.68	1684.6	0.304	2.558	9,300	90,640	35.73	1749.5	1726.8	1446.8	11074	0230
49.68	53.02	1685.0	0.421	3.347	11,760	122,350	46.73	1769.5	1740.3	1446.4	11074	0400
49.64	54.71	1693.6	0.610	4.965	18,710	174,520	65.05	1807.2	1767.2	1451.5	11074	0530
49.02	54.13	1691.8	0.653	5.403	19,080	183,880	68.42	1811.2	1769.2	1446.4	11074	0700
47.95	55.63	1701.0	0.721	6.283	10,540	196,830	73.44	1836.5	1792.0	1445.5	11074	1000
49.75	54.31	1692.3	0.775	7.281	5,340	217,690	81.41	1864.7	1815.1	1447.9	11074	1130
320.2	55.72	1696.5	0.064	12.096	282,500	187,810	56.63	1826.3	1791.4	1600.4	11064	0900
132.6	57.91	1706.1	0.173	6.763	11,570	150,480	54.59	1816.2	1782.3	1563.4	11064	1030
89.8	54.88	1693.2	0.266	6.369	14,440	150,030	55.87	1799.5	1765.1	1493.4	11064	1230
324.7	59.58	1714.8	0.065	12.671	77,830	189,750	57.45	1846.4	1811.2	1622.3	11134	1030
138.1	59.09	1712.2	0.210	10.224	12,630	187,710	66.77	1849.0	1808.9	1569.8	11134	1200
82.1	58.48	1709.2	0.391	7.992	14,760	193,980	71.23	1843.9	1800.2	1501.5	11134	1300
60.9	59.06	1712.2	0.607	7.319	17,700	215,850	79.80	1855.3	1806.8	1458.0	11134	1430
$1500 < T_{Ko} < 1600^oF$												
16.13	30.55	1549.0	0.488	1.330	4,810	44,500	18.07	1587.9	1576.1	1257.3	11104	0815
16.14	33.57	1568.8	0.754	1.278	13,020	68,420	26.74	1617.2	1600.0	1256.0	11104	1100
16.46	31.66	1555.3	0.930	1.426	25,330	86,040	33.03	1611.8	1591.0	1252.9	11104	1230
16.40	33.78	1573.1	0.683	1.258	6,950	62,440	23.97	1620.0	1604.6	1364.5	11114	0230
16.28	30.86	1552.6	0.538	1.590	3,670	49,150	19.43	1598.1	1585.5	1314.0	11114	0556
33.13	29.72	1527.1	0.230	1.491	17,640	46,340	19.59	1570.7	1558.0	1270.1	11044	2200
32.50	29.57	1526.4	0.296	2.048	27,400	57,900	23.48	1577.5	1562.3	1271.8	11044	2330
32.12	32.83	1550.1	0.496	3.008	-24,210	94,920	36.62	1617.6	1594.2	1259.4	11054	0200
31.38	32.15	1544.2	0.597	3.410	-62,540	110,340	41.89	1623.8	1597.3	1276.1	11054	0330
31.28	27.53	1512.6	0.772	4.904	21,610	141,180	53.08	1621.8	1589.1	1255.5	11054	0630
29.86	31.08	1541.2	0.881	5.602	3,620	150,080	57.27	1690.4	1654.7	1261.6	11054	0930
35.64	28.76	1521.5	0.762	5.891	2,520	155,690	59.49	1697.5	1660.5	1284.7	11054	1030
39.03	32.28	1562.5	0.779	6.993	5,390	174,920	65.70	1712.6	1672.2	1336.7	11084	0300
34.43	27.01	1526.8	0.901	8.205	1,570	174,170	65.95	1759.3	1719.0	1364.2	11084	0530
33.30	33.63	1578.7	0.719	4.617	1,330	138,010	52.52	1685.4	1642.3	1298.0	11084	1400
33.20	30.83	1553.0	0.731	4.906	7,350	139,610	53.43	1691.3	1625.5	1276.6	11084	1730
33.27	28.70	1539.4	0.728	5.169	5,810	138,410	52.89	1698.2	1611.0	1298.3	11084	2000
32.47	26.79	1528.7	0.756	6.055	4,910	139,180	53.34	1726.0	1593.7	1303.5	11084	2200
47.28	33.66	1572.8	0.641	7.139	11,410	177,160	65.75	1706.5	1666.1	1373.4	11084	0130
49.76	30.49	1551.6	0.127	1.842	2,140	38,290	16.94	1597.0	1585.9	1380.0	11094	0200
49.27	29.66	1547.0	0.223	2.888	3,530	65,740	26.24	1610.7	1594.0	1380.7	11094	0400
49.31	31.69	1560.3	0.287	3.244	8,710	84,960	32.74	1627.0	1606.3	1386.0	11094	0500
48.07	32.00	1560.0	0.417	4.928	10,310	118,540	44.51	1652.8	1625.2	1385.9	11094	0845
48.62	32.68	1564.5	0.622	7.645	16,050	177,410	65.29	1696.5	1656.3	1394.5	11094	1830
48.52	31.08	1553.5	0.692	9.554	5,280	194,820	72.39	1727.3	1683.1	1382.5	11094	2200
48.78	27.96	1534.2	0.762	12.536	2,170	212,680	80.14	1789.0	1739.3	1374.2	11104	0100
52.49	28.95	1536.8	0.718	12.392	3,330	221,540	83.61	1766.4	1715.7	1303.5	11124	0300

TABLE XI (Cont'd)

G_K	P_{Ko}	T_{Ko}	x_o	$(\Delta P_B)_G$	h_B	q''_B	Q_T	T_{Na1}	T_{Nao}	T_{K1}	Date	Time
158.7	32.25	1552.7	0.226	21.696	8,670	256,090	88.88	1795.3	1741.3	1406.9	11114	1800
114.5	31.97	1554.8	0.316	18.591	7,650	237,930	85.47	1777.2	1725.4	1389.1	11114	2030
88.0	32.55	1561.4	0.427	15.676	9,210	236,510	85.87	1765.9	1713.8	1377.6	11114	2230
71.2	31.41	1555.1	0.538	13.902	8,580	234,900	86.32	1755.1	1702.6	1347.6	11124	0000
60.5	30.89	1550.6	0.624	12.771	5,580	226,180	84.34	1756.7	1705.3	1322.6	11124	0130
267.6	35.15	1568.7	0.130	27.080	12,200	302,190	95.15	1845.8	1788.2	1440.1	11124	1030
161.2	34.62	1568.2	0.269	27.552	7,810	302,610	104.23	1855.3	1792.4	1439.0	11124	1200
97.0	32.49	1558.1	0.526	22.768	6,770	318,720	114.46	1846.8	1777.5	1426.9	11124	1315
122.0	36.49	1584.8	0.408	23.914	12,700	321,750	112.09	1851.1	1783.5	1466.1	11124	1545
323.1	32.06	1552.8	0.063	17.681	48,640	226,950	65.56	1748.4	1708.4	1422.5	11074	1730
156.6	30.95	1549.6	0.164	15.219	6,410	182,460	66.08	1733.1	1692.7	1397.5	11074	2000
88.5	31.38	1555.4	0.314	11.548	7,840	177,140	65.78	1714.2	1674.0	1358.7	11074	2230
61.9	31.57	1557.2	0.459	9.274	10,150	173,940	65.18	1700.6	1660.5	1319.6	11084	0000
284.6	33.20	1555.9	0.106	23.566	31,260	295,120	88.63	1808.4	1754.6	1412.2	11114	1500

TABLE XII

Overall and Average Results
0.67-inch ID Boiler Tube With P/D = 6 Helix Insert
Countercurrent Sodium Flow, Test Plan B

Test Case III

G_K	P_{Ko}	T_{Ko}	x_o	$(\Delta P_B)_G$	$(\Delta P_B)_T$	Φ	$\bar{h}_B$	$\bar{q}''_B$	Q_T	T_{Nai}	T_{Nao}	T_{Ki}	Date	Time
$650 < T_{Ko} < 1750^oF$														
09.1	54.1	1684.6	0.089	25.9	23.8	33.7	12,210	196,880	52.0	1853.4	1820.9	1624.1	10144	0500
53.5	54.7	1690.0	0.188	19.8	20.8	48.5	11,670	179,900	56.8	1848.5	1813.6	1576.6	10144	1000
07.5	54.1	1689.5	0.286	16.4	16.6	68.9	8,040	162,540	56.5	1835.9	1801.0	1518.8	10144	1200
71.7	57.2	1702.3	0.441	13.2	13.7	98.6	9,310	157,620	57.1	1836.0	1800.9	1458.5	10144	1500
52.3	57.3	1703.6	0.634	10.4	11.7	117.9	11,210	159,230	58.4	1831.0	1795.3	1422.8	10144	1900
15.2	57.4	1702.0	0.757	9.3	10.9	125.2	12,590	161,470	59.4	1828.8	1792.4	1415.9	10144	2230
38.5	55.3	1695.8	0.879	8.4	9.8	141.9	12,270	158,080	58.5	1818.6	1782.0	1387.8	10154	0130
35.6	55.4	1697.6	0.990	8.8	8.9	164.5	5,310	160,630	59.9	1837.3	1800.7	1414.7	10154	0330
54.6	37.3	1654.5	60*	15.5		341.1	1,670	148,660	55.9	1842.8	1808.4	1489.1	10104	2050
$500 < T_{Ko} < 1600^oF$														
02.6	34.9	1570.8	0.424	28.9	29.8	115.8	6,210	228,920	77.2	1840.6	1778.4	1467.2	10164	1500
30.8	35.0	1571.7	0.566	27.1	27.8	147.3	6,430	232,800	80.6	1839.6	1774.7	1438.1	10164	1730
39.5	34.1	1566.2	0.708	25.9	27.9	165.4	7,700	246,680	86.0	1842.3	1773.2	1423.2	10164	2030
31.3	33.0	1560.1	0.820	25.4	27.2	188.4	6,480	247,230	87.4	1842.7	1772.3	1418.2	10174	0030
30.1	26.1	1538.9	26*	28.8	26.4	310.6	4,370	240,250	87.1	1847.6	1777.6	1405.6	10174	0230
14.7	17.0	1632.8	211*	34.5	9.5	483.9	2,080	218,860	81.8	1869.7	1803.5	1339.5	10174	0400
00.6	34.0	1564.9	0.116	31.5	32.8	55.5	-71,550	304,380	67.3	1808.4	1766.5	1486.2	10124	2400
02.6	33.5	1563.2	0.186	29.2	30.4	57.8	7,070	223,690	67.9	1807.9	1765.7	1473.5	10134	0200
08.1	33.3	1566.5	0.342	23.1	24.6	88.3	6,230	198,170	67.5	1787.7	1745.7	1434.4	10134	0400
75.3	34.1	1573.4	0.510	19.6	21.3	121.4	7,620	195,380	68.8	1777.8	1735.0	1393.5	10134	0544
08.6	34.4	1576.2	0.647	17.2	19.6	152.6	6,740	186,040	67.2	1772.3	1730.9	1359.6	10134	0730
15.9	34.1	1576.2	0.810	16.1	17.4	205.5	4,910	177,300	65.5	1769.2	1728.9	1319.8	10134	0850
10.6	32.1	1561.3	0.880	16.6	17.6	261.2	3,510	167,590	62.4	1763.0	1725.2	1331.9	10134	1130

*Degrees of Vapor Superheat at Potassium Exit

TABLE XIII

Overall and Average Results
0.67-inch ID Boiler Tube With No Insert
Countercurrent Sodium Flow, Test Plan B

Test Case IV_a

G_K	P_{Ko}	T_{Ko}	x_o	$\bar{h}_B$	$\bar{q}''_B$	Q_T	T_{Nai}	T_{Nao}	T_{Ki}	$(\Delta P_B)_G$	Date	Time
$1650 < T_{Ko} < 1750^{\circ}F$												
315.1	59.4	1712.6	0.071	-30,750	242,720	59.5	1847.7	1811.5	1619.0	13.3	11144	1200
136.6	59.1	1713.4	0.218	10,740	202,990	68.1	1857.0	1815.9	1572.6	10.1	11144	1400
84.5	58.7	1710.9	0.387	10,930	204,460	71.9	1853.4	1810.0	1520.4	8.2	11144	1530
62.0	57.3	1704.9	0.563	11,630	209,740	75.2	1847.9	1802.5	1473.4	7.1	11144	1700
47.9	53.2	1687.3	0.726	4,180	200,850	74.9	1854.1	1808.8	1396.7	6.3	11144	1830
88.6	56.9	1701.4	0.298	11,630	168,130	59.0	1817.6	1781.1	1532.3	6.1	10304	0830
58.3	58.2	1709.4	0.428	10,380	151,090	55.1	1813.4	1779.0	1483.7	4.8	10304	1030
44.1	57.6	1704.6	0.579	12,760	150,100	55.3	1804.0	1770.2	1442.9	3.8	10304	1130
36.0	52.9	1681.7	0.715	5,020	146,770	54.9	1797.1	1763.5	1421.1	3.4	10304	1330
$1500 < T_{Ko} < 1600^{\circ}F$												
252.7	33.0	1551.9	0.152	17,220	388,260	107.3	1864.2	1800.5	1405.0	30.2	11164	0230
161.5	31.8	1550.0	0.274	7,520	337,540	108.4	1862.9	1798.6	1419.9	28.3	11164	0400
126.4	32.7	1560.2	0.383	8,490	337,640	111.8	1860.9	1794.5	1439.3	25.7	11164	0530
100.6	31.9	1558.0	0.490	5,140	317,130	110.3	1863.7	1798.2	1439.1	23.4	11164	0700
275.0	35.4	1573.0	0.120	24,010	338,480	89.6	1833.2	1778.8	1453.4	25.5	11154	1230
162.0	35.3	1573.9	0.239	7,890	285,010	91.5	1830.8	1775.4	1463.6	22.1	11154	1400
114.8	32.0	1555.7	0.352	7,720	273,300	91.9	1805.4	1749.9	1443.8	20.1	11154	1730
89.9	31.7	1558.0	0.464	7,460	265,810	92.0	1794.1	1738.9	1446.5	17.2	11154	1900
73.0	29.7	1544.1	0.577	4,600	257,400	91.9	1794.8	1739.4	1426.8	16.0	11154	2100
32.4	32.7	1554.8	0.068	12,010	189,180	67.3	1755.0	1713.9	1440.0	20.1	11014	0430
16.3	32.4	1558.3	0.170	6,290	184,980	67.8	1752.7	1711.4	1446.6	16.6	11014	0545
89.8	34.0	1572.7	0.350	8,790	204,170	71.0	1744.3	1701.0	1425.1	11.6	11014	0800
63.7	35.5	1583.1	0.474	8,870	185,460	66.3	1732.2	1691.9	1414.6	8.6	11014	1000
48.3	30.2	1547.2	0.623	4,340	178,110	65.5	1716.4	1676.5	1366.0	8.6	11014	1400

TABLE XIV

Overall and Average Results
0.67-inch ID Boiler Tube With No Insert
Cocurrent Sodium Flow, Test Plan B
Test Case IV_b

G_K	P_{Ko}	T_{Ko}	x_o	$\bar{h}_B$	$\bar{q}''_B$	Q_T	T_{Nai}	T_{Nao}	T_{Ki}	$(\Delta P_B)_G$	Date	Time
$1650 < T_{Ko} < 1750^oF$												
320.2	55.7	1696.5	0.064	282,500	187,810	56.6	1826.3	1791.4	1600.4	12.1	11064	0900
132.6	57.9	1706.1	0.173	11,570	150,480	54.6	1816.2	1782.3	1563.4	6.8	11064	1030
89.8	54.9	1693.2	0.266	14,440	150,030	55.9	1799.5	1765.1	1493.4	6.4	11064	1230
58.1	56.6	1700.0	0.440	30,140	152,710	57.6	1799.1	1763.4	1432.8	4.8	11064	1400
43.1	57.1	1703.4	0.607	38,790	151,720	57.8	1797.7	1762.2	1383.6	3.7	11064	1530
36.8	58.0	1709.1	0.697	18,890	145,640	55.4	1801.7	1767.5	1397.1	3.1	11064	1800
32.8	58.0	1708.8	0.788	21,360	145,330	55.2	1800.1	1766.1	1395.1	3.1	11064	1930
28.9	57.1	1703.9	0.877	14,530	141,560	53.9	1795.6	1762.3	1378.6	2.6	11064	2100
$1500 < T_{Ko}$		1600^oF										
284.6	33.2	1555.9	0.106	31,260	295,120	88.6	1808.4	1754.6	1412.2	23.6	11114	1500
158.7	32.3	1552.7	0.226	8,670	256,090	88.9	1795.3	1741.3	1406.9	21.7	11114	1800
114.5	32.0	1554.8	0.316	7,650	237,930	85.5	1777.2	1725.4	1389.1	18.6	11114	2030
88.0	32.6	1561.4	0.427	9,210	236,510	85.9	1765.9	1713.8	1377.6	15.7	11114	2230
71.2	31.4	1555.1	0.538	8,580	234,900	86.3	1755.1	1702.6	1347.6	13.9	11124	0000
60.5	30.9	1550.6	0.624	5,580	226,180	84.3	1756.7	1705.3	1322.6	12.8	11124	0130
52.5	29.0	1536.8	0.718	3,330	221,540	83.6	1766.4	1715.7	1303.5	12.4	11124	0300
323.1	32.1	1552.8	0.063	48,640	226,950	65.6	1748.4	1708.4	1422.5	17.7	11074	1730
156.6	31.0	1549.6	0.164	6,410	182,460	66.1	1733.1	1692.7	1397.5	15.2	11074	2000
88.5	31.4	1555.4	0.314	7,840	177,140	65.8	1714.2	1674.0	1358.7	11.5	11074	2230
61.9	31.6	1557.2	0.459	10,150	173,940	65.2	1700.6	1660.5	1319.6	9.3	11084	0000
47.3	33.7	1572.8	0.641	11,410	177,160	65.7	1706.5	1666.1	1373.4	7.1	11084	0130
39.0	32.3	1562.5	0.779	5,390	174,920	65.7	1712.6	1672.2	1336.7	7.0	11084	0300
34.4	27.0	1526.8	0.901	1,570	174,170	65.9	1759.3	1719.0	1364.2	8.2	11084	0530

TABLE XV

Critical Heat Flux Results

Test Case I: 0.92-inch ID Boiler Tube With P/D = 2.2 Helix Insert, Countercurrent Sodium Flow

Date	Time	G_K	T_{Kc}	x_c	q''_c	a_{Rc}
05274	0005	18.8	1655.0	0.839	412,500	116.7
05274	0020	16.4	1624.0	0.827	532,300	96.2
07014	2120	16.1	1541.3	0.664	285,600	80.3
07014	2130	16.0	1550.5	0.680	340,100	81.6

Test Case II: 0.92-inch ID Boiler Tube With P/D = 6 Helix Insert, Countercurrent Sodium Flow

Date	Time	G_K	T_{Kc}	x_c	q''_c	a_{Rc}
07254	0100	19.1	1674.5	0.864	386,150	15.8
07254	0120	19.1	1675.0	0.727	401,500	11.2
07254	0145	18.1	1637.7	0.667	457,900	9.6
07284	0017	37.1	1563.2	0.793	341,700	74.2
07284	0100	33.5	1563.5	0.739	437,400	52.5
07284	1740	19.8	1543.5	0.722	269,100	18.9
07284	1845	18.4	1521.9	0.788	438,300	21.0

Test Case III: 0.67-inch ID Boiler Tube With P/D = 6 Helix Insert, Countercurrent Sodium Flow

Date	Time	G_K	T_{Kc}	x_c	q''_c	a_{Rc}
10104	2150	38.6	1686.2	0.758	298,900	65.3
10114	0230	40.5	1686.7	0.736	395,000	67.8
10124	0800	34.1	1603.7	0.759	261,400	68.4
10124	1200	38.1	1615.2	0.801	287,100	90.7
10124	1220	38.0	1618.6	0.731	302,600	74.5
10124	1240	37.0	1615.7	0.709	277,500	66.9
10174	0400	44.7	1655.0	0.696	446,200	82.4

TABLE XV (Cont'd)

Test Case IVa: 0.67-inch ID Boiler Tube With No Insert, Countercurrent Sodium Flow

Date	Time	G_K	T_{Kc}	x_c	q''_c	a_{Rc}
10294	1130	31.7	1694.8	0.533	187,000	0
10304	1330	36.0	1688.9	0.602	193,200	0
10314	0300	50.6	1690.9	0.540	269,800	0
11014	0030	31.7	1556.3	0.670	221,950	0
11014	1730	38.0	1569.4	0.562	427,000	0
11014	2100	32.5	1576.6	0.556	275,900	0
11014	2330	31.7	1562.0	0.557	341,700	0
11024	0100	32.4	1555.5	0.548	244,900	0
11024	0230	32.1	1553.4	0.632	280,700	0
11144	1830	47.9	1702.7	0.505	274,100	0
11154	2100	73.0	1597.2	0.486	355,100	0
11164	0700	100.6	1643.2	0.398	428,600	0
11174	0215	32.6	1566.8	0.708	221,000	0
11174	0345	32.6	1558.9	0.607	370,000	0
11174	0900	49.3	1563.0	0.549	295,000	0
11174	0905	49.3	1554.1	0.524	360,800	0
11184	0215	33.3	1705.0	0.617	191,100	0
11184	1000	50.8	1630.7	0.500	377,700	0

Test Case IVb: 0.67-inch ID Boiler Tube With No Insert, Cocurrent Sodium Flow

Date	Time	G_K	T_{Kc}	x_c	q''_c	a_{Rc}
11054	0930	29.9	1573.4	0.686	178,600	0
11054	1030	35.6	1558.5	0.559	200,300	0
11064	0515	32.8	1677.1	0.703	210,400	0
11074	1130	49.8	1703.5	0.687	219,600	0
11084	0530	34.4	1563.5	0.597	269,400	0
11104	0100	48.8	1584.1	0.585	287,500	0
11124	0300	52.5	1583.1	0.576	235,300	0

TABLE XVI

Transition Boiling Heat Transfer Coefficients

Test Case I: 0.92-inch ID Boiler Tube With P/D = 2.2 Helix Insert, Countercurrent Sodium Flow

Date	Time	G_K	T_{KTB}	x_{TB}	ΔT_{TB}	h_{TB}	a_{RTB}
05274	0005	18.8	1677.5	0.920	174	279	140.0
05274	0020	16.4	1654.3	0.914	215	175	117.2
07014	2120	16.1	1523.4	0.832	121	650	125.9
07014	2130	16.0	1525.8	0.840	153	359	124.5

Test Case II: 0.92-inch ID Boiler Tube With P/D = Helix Insert, Countercurrent Sodium Flow

Date	Time	G_K	T_{KTB}	x_{TB}	ΔT_{TB}	h_{TB}	a_{RTB}
07254	0100	19.1	1680.0	0.932	161	177	18.4
07254	0120	19.1	1682.8	0.864	154	334	15.7
07254	0145	18.1	1649.9	0.833	201	267	15.1
07284	0017	37.1	1541.0	0.897	77	3966	94.8
07284	0100	33.5	1551.5	0.869	205	699	72.7
07284	1740	19.8	1527.4	0.861	137	596	27.0
07284	1845	18.4	1512.2	0.894	230	174	27.0

Test Case III: 0.67-inch ID Boiler Tube With P/D = 6 Helix Insert, Countercurrent Sodium Flow

Date	Time	G_K	T_{KTB}	x_{TB}	ΔT_{TB}	h_{TB}	a_{RTB}
10104	2150	38.6	1669.6	0.879	115	842	87.8
10114	0230	40.5	1664.2	0.868	136	743	94.3
10124	0800	34.1	1582.4	0.880	107	1215	91.9
10124	1200	38.1	1576.4	0.901	139	678	114.8
10124	1220	38.0	1590.7	0.866	104	1326	104.6
10124	1240	37.0	1587.1	0.855	96	1690	97.3
10174	0400	44.7	1621.1	0.848	154	989	122.3

TABLE XVI (Cont'd)

Test Case IVa: 0.67-inch ID Boiler Tube With No Insert, Countercurrent Sodium Flow

Date	Time	G_K	T_{KTB}	x_{TB}	ΔT_{TB}	h_{TB}	a_{RTB}
10294	1130	31.7	1691.1	0.648	58	1736	0
10304	1330	36.0	1685.3	0.659	66	1612	0
10314	0300	50.6	1685.4	0.617	75	2136	0
11014	0030	31.7	1550.0	0.745	78	1259	0
11014	1730	38.0	1551.9	0.652	155	385	0
11014	2100	32.5	1566.2	0.641	98	565	0
11014	2330	31.7	1551.0	0.683	112	612	0
11024	0100	32.4	1545.4	0.671	106	884	0
11024	0230	32.1	1543.0	0.713	142	471	0
11144	1830	47.9	1695.0	0.616	90	1695	0
11154	2100	73.0	1570.6	0.532	120	1952	0
11164	0700	100.6	1600.6	0.444	127	2394	0
11174	0215	32.6	1563.9	0.736	98	1034	0
11174	0345	32.6	1547.7	0.693	178	292	0
11174	0900	49.3	1557.5	0.576	158	474	0
11174	0905	49.3	1539.6	0.586	183	462	0
11184	0215	33.3	1703.5	0.688	63	2305	0
11184	1000	50.8	1618.4	0.591	172	608	0

Test Case IVb: 0.67-inch ID Boiler Tube With No Insert, Cocurrent Sodium Flow

Date	Time	G_K	T_{KTB}	x_{TB}	ΔT_{TB}	h_{TB}	a_{RTB}
11054	0930	29.9	1557.2	0.784	63	1428	0
11054	1030	35.6	1540.0	0.661	85	1115	0
11064	0515	32.8	1673.7	0.800	109	750	0
11074	1130	49.8	1697.9	0.731	66	1957	0
11084	0530	34.4	1545.2	0.749	137	749	0
11104	0100	48.8	1559.1	0.673	136	849	0
11124	0300	52.5	1559.9	0.647	83	2183	0

TABLE XVII

Superheated Vapor Results

Date	Time	Tube I.D. inches	Insert P/D	T_{KSH} °F	ζ_{SH} °F	q''_{SH} Btu/(hr-ft^2)	G_K lb/ft^2-sec	L_{SH} inches	h_{SH} (experimental) Btu/(hr-ft^2-°F)
05274	0005	0.92	2.2	1638.8	54	6,620	18.8	22.5	33.4
05274	0020	0.92	2.2	1671.7	215	28,170	16.4	24.5	200.8
07014	2120	0.92	2.2	1552.4	141	20,920	16.1	17.5	173.9
10114	0230	0.67	6.0	1649.1	55	7,050	40.5	10.5	34.7
10124	0800	0.67	6.0	1576.6	133	8,850	34.1	13.8	49.1
10124	1220	0.67	6.0	1569.7	119	4,190	38.0	14.5	20.9
10124	1240	0.67	6.0	1572.0	150	6,810	37.0	16.5	34.4
10174	0400	0.67	6.0	1610.0	211	14,480	44.7	15.5	57.4

APPENDIX C

Derivation of Helix Equations

Definition of Helix

The cylindrical helix is the path of a point which moves around the surface of a right circular cylinder with a constant angular velocity w and at the same time moves parallel to the axis of the cylinder with a constant linear or axial velocity V_a. The pitch (P) of the helix is the axial distance traveled for an angular displacement of 2π radians.

Derivation of Helical Path Length and Helical Velocity:

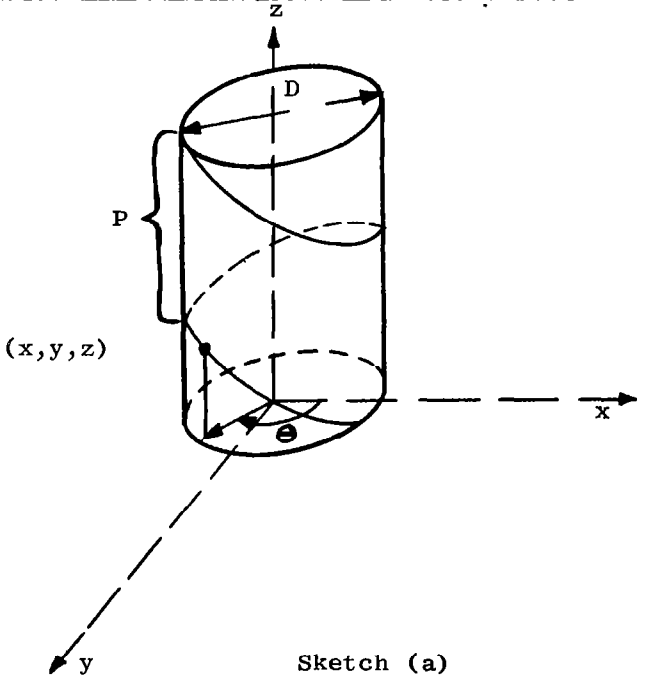

Sketch (a)

Sketch (a) above illustrates the helical path. From the drawing, the co-ordinates x, y and z are given as follows in terms of the angular displacement θ the time t and the helix diameter D:

$$x = D/2 \cos\theta \tag{C1}$$

$$y = D/2 \sin\theta \tag{C2}$$

$$z = V_a t \tag{C3}$$

$$\theta = wt \tag{C4}$$

From equations (3) and (4):

$$t = z/V_a = \theta/w \tag{C5}$$

The arc length s along a three dimensional curve is given as follows:

$$s = \int \sqrt{dx^2 + dy^2 + dz^2} \tag{C6}$$

In terms of the parameter θ,

$$s = \int \sqrt{\left(\frac{dx}{d\theta}\right)^2 + \left(\frac{dy}{d\theta}\right)^2 + \left(\frac{dz}{d\theta}\right)^2}\, d\theta \tag{C7}$$

From equations (C1) and (C2):

$$\frac{dx}{d\theta} = -D/2 \sin\theta \tag{C8}$$

$$\frac{dy}{d\theta} = D/2 \cos\theta \tag{C9}$$

$$\left(\frac{dx}{d\theta}\right)^2 + \left(\frac{dy}{d\theta}\right)^2 = \frac{D^2}{4}(\sin^2\theta + \cos^2\theta) = D^2/4 \tag{C10}$$

From equation (C5)

$$z = \frac{V_a}{w} \tag{C11}$$

In the time required for 2π angular displacement, an axial length $z = P$ is traveled, therefore from equation (C5):

$$P = \frac{2\pi V_a}{w}, \text{ or } \frac{V_a}{w} = \frac{P}{2\pi} \qquad \text{(C12)}$$

From equations (C11) and (C12):

$$\frac{dz}{d\theta} = P/2\pi \qquad \text{(C13)}$$

Combining equations (C7), (C8), (C9) and (C13) to obtain the helical path length L_H:

$$s = \int \sqrt{D^2/4 + \frac{P^2}{4\pi^2}}\, d\theta = L_H \qquad \text{(C14)}$$

Upon integrating equation (C14) over the angular displacement 0 to 2π radians, and recognizing that the axial length L traversed for a 2π angular displacement is P, we obtain:

$$\frac{L_H}{L} = \frac{L_H}{P} = \sqrt{1 + \left(\frac{\pi D}{P}\right)^2} \qquad \text{(C15)}$$

The helical velocity V_H is obtained by dividing the helical path length for 2π revolutions by the time required by 2π revolutions as follows, using equations (C5) and (C15):

$$V_H = \frac{L_H}{\frac{2\pi}{w}} = \frac{P\sqrt{1 + \left(\frac{\pi D}{P}\right)^2}}{(P/V_a)} \qquad \text{(C16)}$$

$$\frac{V_H}{V_a} = \sqrt{1 + \left(\frac{\pi D}{P}\right)^2} \qquad \text{(C17)}$$

Tangential Velocity:

In the time P/V_a required for 2π revolutions, a circumferential distance of πD is traversed. The circumferential or tangential component of the helical velocity V_T is therefore given as follows:

$$V_T = \frac{\pi D}{P/V_a} \tag{C18}$$

$$V_T/V_a = \frac{\pi D}{P} \tag{C19}$$

Axial Flow Area and Equivalent Diameter:

The axial flow area A_F perpendicular to the axis of a tube containing a helical insert is given as follows, where D_i is the tube inside diameter, D_{cb} the helix centerbody diameter and Δ_T is the thickness of the tape wound around the centerbody.

$$A_F = \frac{\pi}{4}\left[D_i^2 - D_{cb}^2\right] - \frac{\left[D_i - D_{cb}\right]\Delta_T}{2.0} \tag{C20}$$

The wetted perimeter P_w encountered by the axial flow is as follows:

$$P_w = \pi(D_i + D_{cb}) + D_i - D_{cb} - 2\Delta_T \tag{C21}$$

The equivalent diameter, D_e, of the tube containing helical insert is obtained as follows from the flow area and wetted perimeter:

$$D_e = \frac{4A_F}{P_w} = \frac{D_i\left[1 - \left(\frac{D_{cb}}{D_i}\right)^2 - \frac{2\Delta_T}{\pi}\left(\frac{1}{D_i} - \frac{D_{cb}}{D_i^2}\right)\right]}{1 + \frac{D_{cb}}{D_i} + \left(1 - \frac{D_{cb}}{D_i} - \frac{2\Delta_T}{D_i}\right)\frac{1}{\pi}} \tag{C22}$$

Neglecting the tape width Δ_T, equation (C23) following is obtained:

$$D_e/D_i = \frac{1 - \left(\frac{D_{cb}}{D_i}\right)^2}{1 + \frac{D_{cb}}{D_i} + \frac{1}{\pi}\left(1 - \frac{D_{cb}}{D_i}\right)} \qquad \text{(C23)}$$

Radial Acceleration Developed by the Insert:

A parameter of interest in the analysis of the experimental boiling data is the radial acceleration developed by the insert in two phase flow in the thin liquid film at the tube wall. An expression for this radial acceleration a_R, expressed as a multiple of the standard gravitational acceleration g, is obtained as follows. Assuming that the liquid fraction in two phase potassium flow occupies a negligible fraction of the flow area*, the axial vapor velocity V_{ag} is given by equation (C24) in terms of the total mass flow rate W, or axial mass velocity G_a:

$$V_{ag} = \frac{xW}{\rho_g A_F} = \frac{xG_a}{\rho_g} \qquad \text{(C24)}$$

Using the ratio of vapor to liquid velocities K and equation (C19), the tangential liquid velocity at the tube wall V_{fT} is obtained as follows:

$$V_{fT} = \frac{V_{ag}}{K} \frac{\pi D_i}{P} = \frac{xG_a}{\rho_g K} \frac{\pi D_i}{P} \qquad \text{(C25)}$$

The radial acceleration a_R in the liquid film at the tube wall is the square of the tangential velocity divided by the radius, as follows:

$$a_R = \frac{2V_{fT}^2}{D_i g} = \frac{2}{D_i g}\left(\frac{xG_a}{\rho_g K} \frac{\pi D_i}{P}\right)^2 \qquad \text{(C26)}$$

* If the liquid fraction is not neglected, equation C24 is modified by substitution of (x/α) for x in equation C24, where α is the void fraction.

APPENDIX D

Correlation of Single-Phase Pressure Drop and Heat Transfer With Inserts

It is useful in the analysis and evaluation of the boiling potassium heat transfer and pressure loss data obtained from the experiments to compare the two-phase results with the corresponding single-phase values. In order to do this, methods for prediction of the single phase pressure drop and vapor phase heat transfer coefficients in tubes containing helical inserts were sought.

Gambill (Reference 33) has assembled single-phase heat transfer and pressure drop data for flow in tubes containing twisted tapes, and has found that the friction factors obtained under these conditions could be correlated within approximately $\pm$ 20% by employing the equivalent diameter and maximum helical path length and velocity in the calculation of the friction factors and Reynolds Numbers.

This procedure was employed in an attempt to correlate the water pressure drop data presented in Figure 31 of this report for the flow of water in tubes containing helical inserts. The data obtained by Greene (Reference 33) with tubes containing helical inserts were also treated.

Figure 41 shows the friction factor data of Greene together with the data obtained in the present investigation. The experimental data are represented by smooth curves in Figure 41 for ease of comparison. Figure 42 compares this data with the prediction obtained by use of the helical velocities and lengths (V_H and L_H) together with the equivalent diameter (D_e). The definitions of these quantities, based upon the derivations given in Appendix C, are given by the following equations along with the equations for the equivalent friction factor f_e and the equivalent Reynolds Number $(N_{Re})_e$,

$$V_H = V_a \sqrt{1 + \left(\frac{\pi D_i}{P}\right)^2} \qquad \text{(D1)}$$

$$L_H = L \sqrt{1 + \left(\frac{\pi D_i}{P}\right)^2} \qquad \text{(D2)}$$

$$D_e = \frac{D_i \left[1 + \left(\frac{D_{cb}}{D_i}\right)^2\right]}{1 + \frac{D_{cb}}{D_i} + \frac{1}{\pi}\left(1 - \frac{D_{cb}}{D_i}\right)} \qquad \text{(D3)}$$

$$f_e = \frac{\Delta P}{\frac{L_H}{D_e} \frac{\rho_f V_H^2}{2g_c}} \qquad \text{(D4)}$$

$$(N_{Re})_e = \frac{D_e V_H \rho_f}{\mu_f} \qquad \text{(D5)}$$

It can be seen from Figure 42 that the single-phase pressure drop data are correlated to the empirical expression for smooth tubes quite well through use of equations D1 - D5, with the exception of the data obtained by Greene for the very tight twist ratio P/D = 0.56. The recommended correlation, which is the smooth tube equation (Reference 47), is given below. It should be noted that the friction factors employed in Reference 47 are the Fanning friction factors, which are smaller by a factor of four than the Darcy-Weisbach friction factor utilized in Equation (D6).

$$f_e = \frac{0.316}{(N_{Re})_e^{\frac{1}{4}}} \qquad \text{(D6)}$$

A plot of the ratio of experimental to predicted friction factor, employing Equation (D6), is shown in Figure 43, where the maximum, minimum

and average ratios are given as a function of P/D. The analytical technique described is seen to be valid within approximately 20% in the range $1 < P/D < 6$. At P/D = 0.56 the friction factor is apparently over-estimated.

Additional, more recent single-phase friction factor data for water flowing in tubes with helical inserts (P/D = 2) are reported by Bond (Reference 60). This data is also correlated reasonably well by Equation D6 using the helical flow parameters (Reference 60).

Greene also measured the single-phase heat transfer coefficient in his experiments with helical inserts. The data of Greene, (Reference 33), are plotted in Figure 44 as the swirl flow Nusselt Number (N_{Nu_i}) divided by the cube root of the Prandtl Number (N_{Pr}) versus the Reynolds Number (N_{Re_i}), the dimensionless groups being based upon the axial velocity V_a and the tube inside diameter D_i. The prediction of the Colburn equation (Reference 47) for smooth tubes is shown for comparison.

Figure 45 shows the correlation of heat transfer data by use of the helical velocities and lengths (V_H and L_H) together with the equivalent diameter (D_e). Equations (D1), (D2), (D3), and (D5) were employed, as in the correlation of the single-phase pressure drop data, for V_H, L_H and $(N_{Re})_e$ respectively. Equation (D7), following, defines the equivalent Nusselt Number $(N_{Nu})_e$ that was used.

$$(N_{Nu})_e = \frac{h\, D_e}{k} \qquad \text{(D7)}$$

It can be seen from Figure 45 that the experimental heat transfer data correlate among themselves quite well with the approach employed, but the agreement with the smooth tube prediction is not as good as was obtained in the single-phase friction factor correlation. An empirical line, shown in Figure 45, was drawn through the correlated values. This line is recommended

for the prediction of single-phase heat transfer coefficients in tubes containing helical inserts. The correlation is recommended for fluids having Prandtl Numbers within an order of magnitude of the water test data used in the derivation; that is, a Prandtl Number within an order of magnitude of 1.0. The equation for the empirical single-phase heat transfer correlation is given as follows:

$$(N_{Nu})_e = 0.359\ (N_{Re_e})^{0.563}\ (N_{Pr})^{1/3} \qquad \text{(D8)}$$

Equation D8 was derived to provide a means for the prediction of the heat transfer coefficient for potassium vapor flowing in tubes containing helical inserts. Gambill (Reference 33) points out that heat transfer coefficients obtained with vortex generator inserts are different with liquids than with gases due to differences in natural circulation effects caused by the radial acceleration developed by the inserts. Because of this, there may be some error in the heat transfer coefficients calculated using equation D8 for potassium vapor in helical flow. Unfortunately, no heat transfer data for gases in tubes containing helical inserts with the twist ratios of interest could be found in the literature.

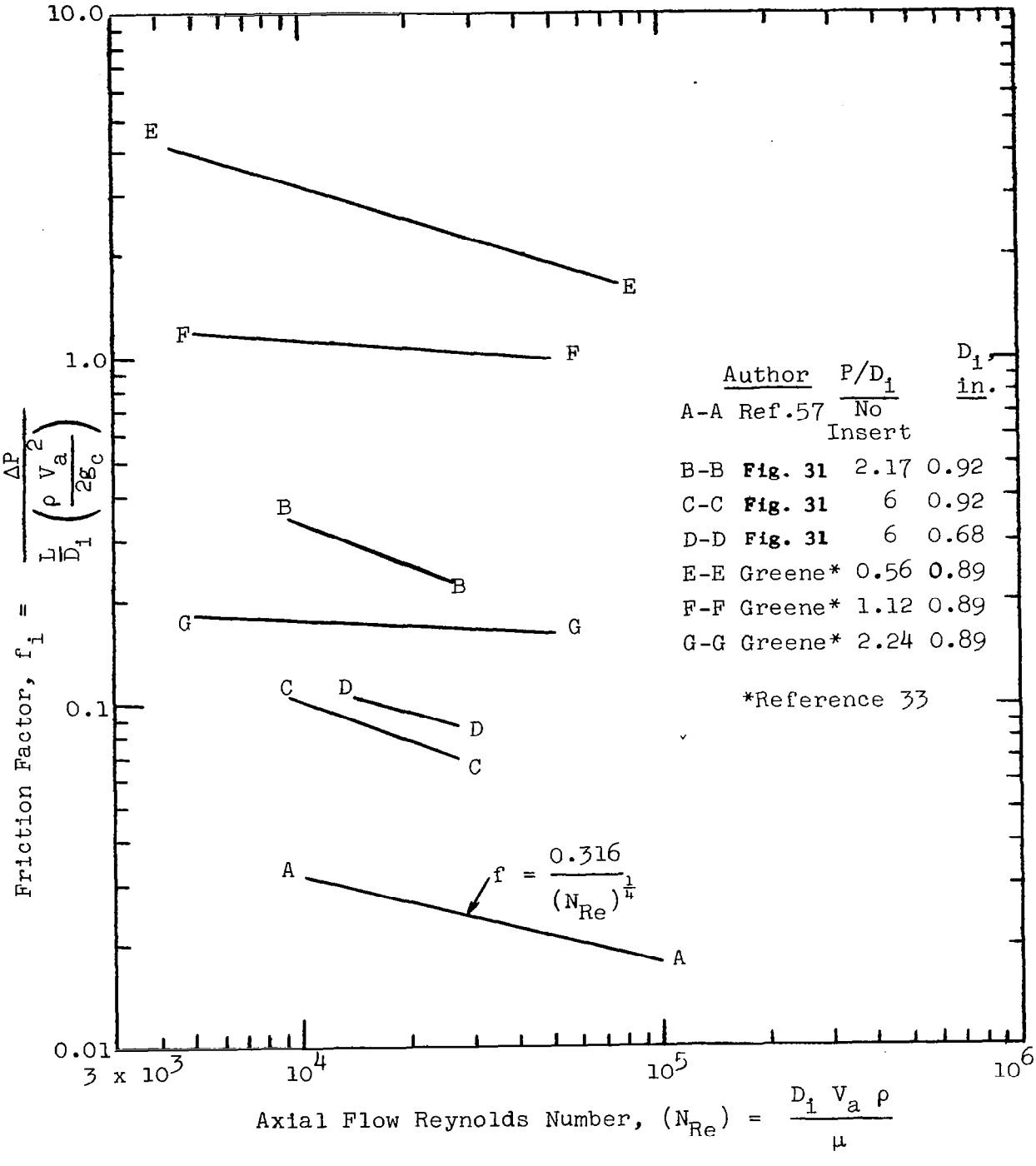

Figure 41. Summary of Single Phase Friction Factor Measurements From The Literature For Water Flowing In Straight Tubes Containing Helical Inserts

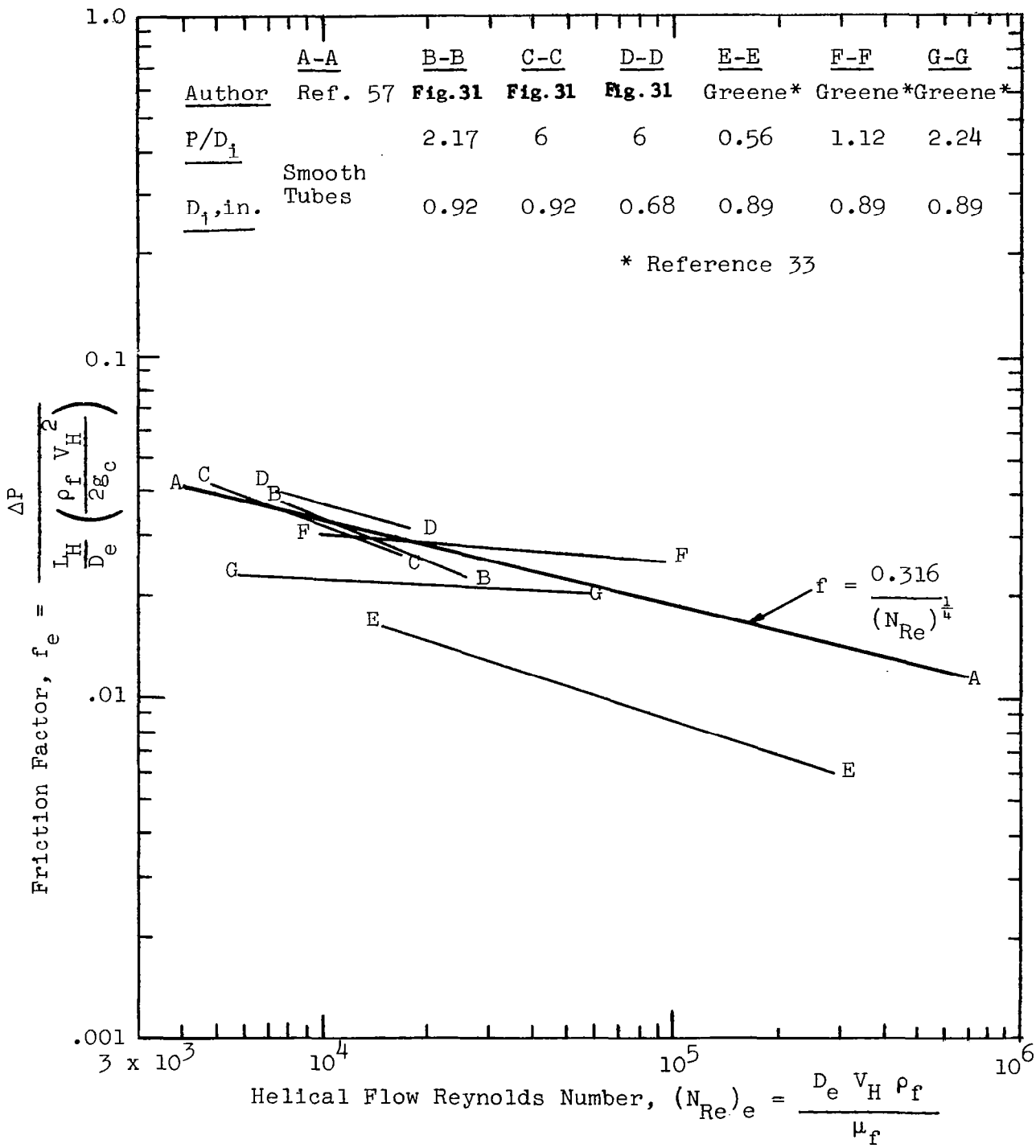

Figure 42. Correlation of Helical Flow Water Pressure Drop Data of Figure 41 Using Helix Equations

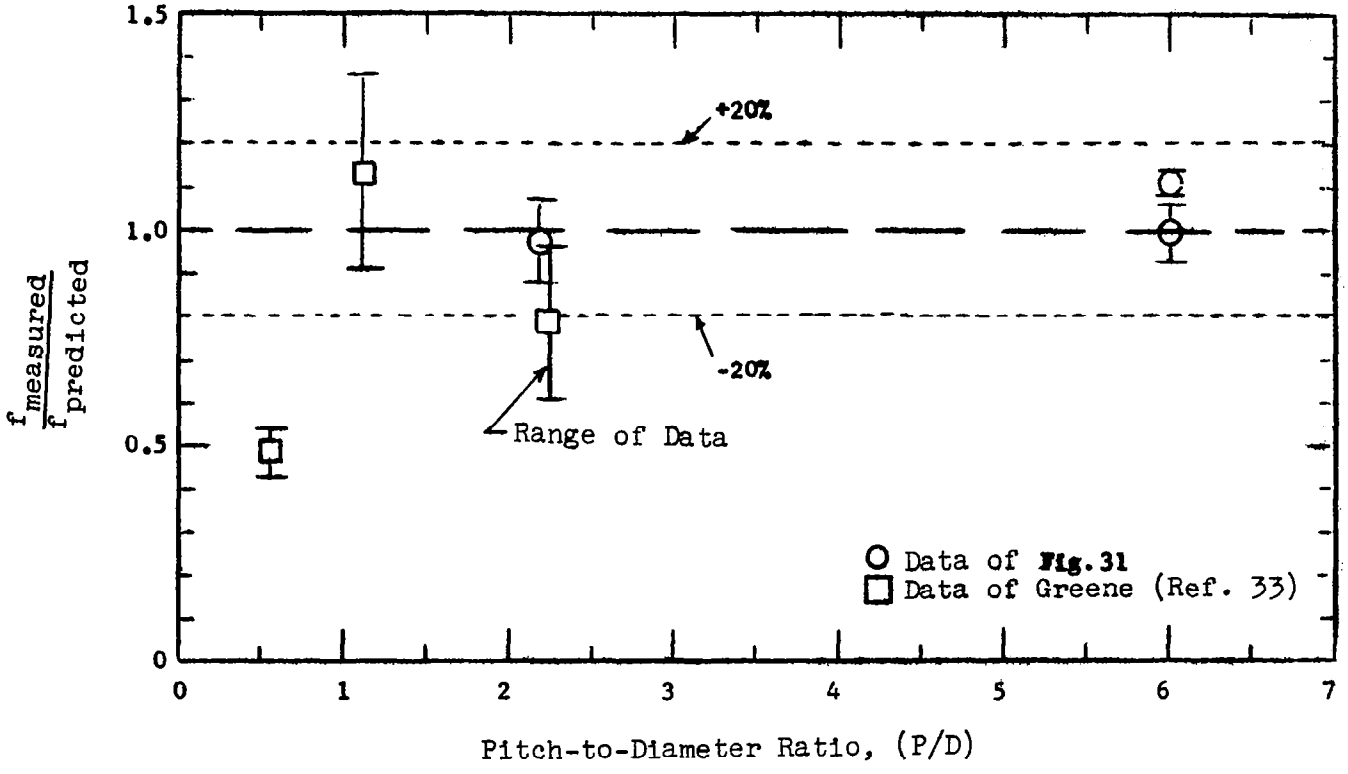

Figure 43. Comparison of Predicted and Measured Single Phase Friction Factors For Helical Flow

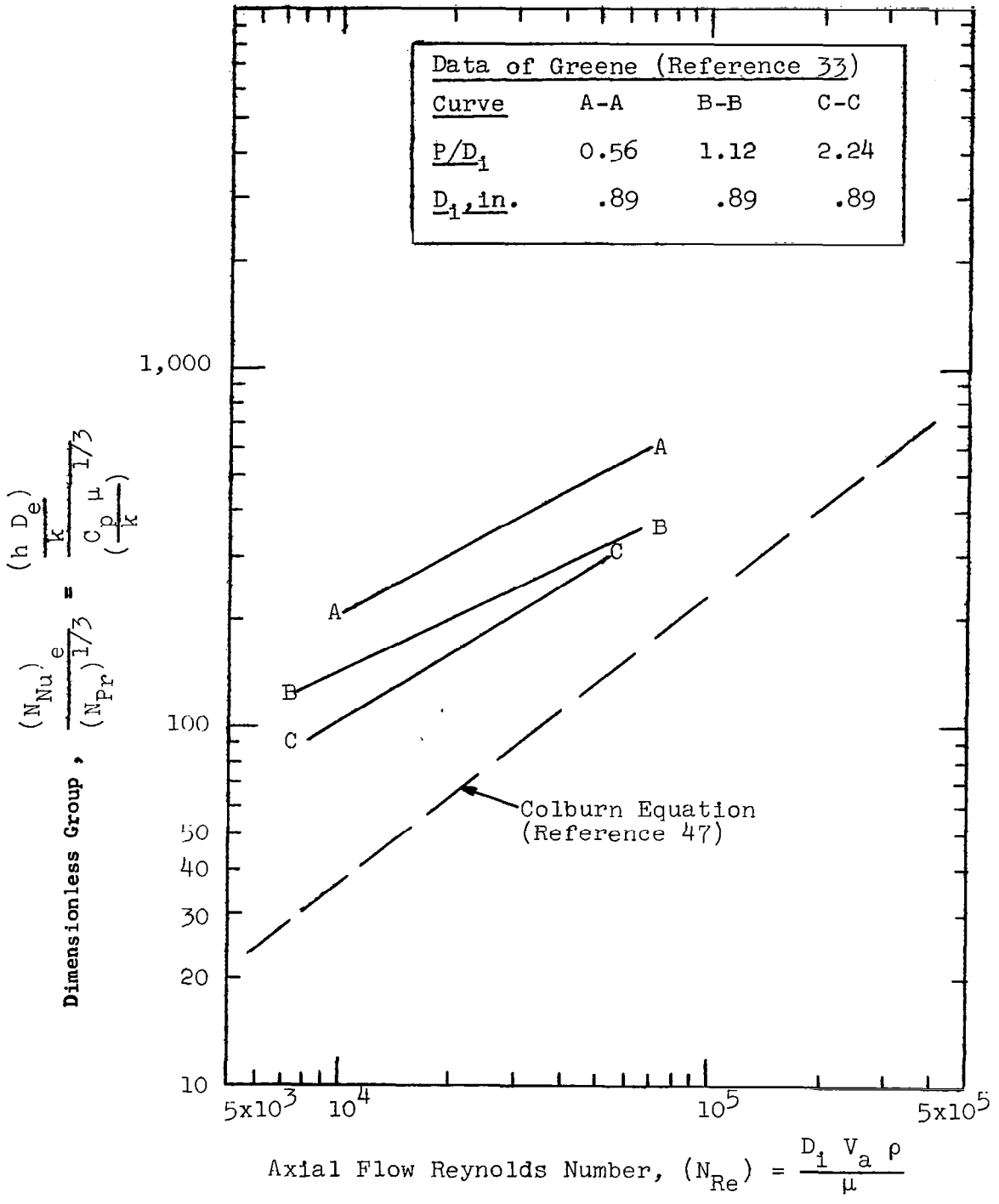

Figure 44. Heat Transfer Data of Greene (Reference 33) for Water Flowing in Straight Tubes Containing Helical Inserts

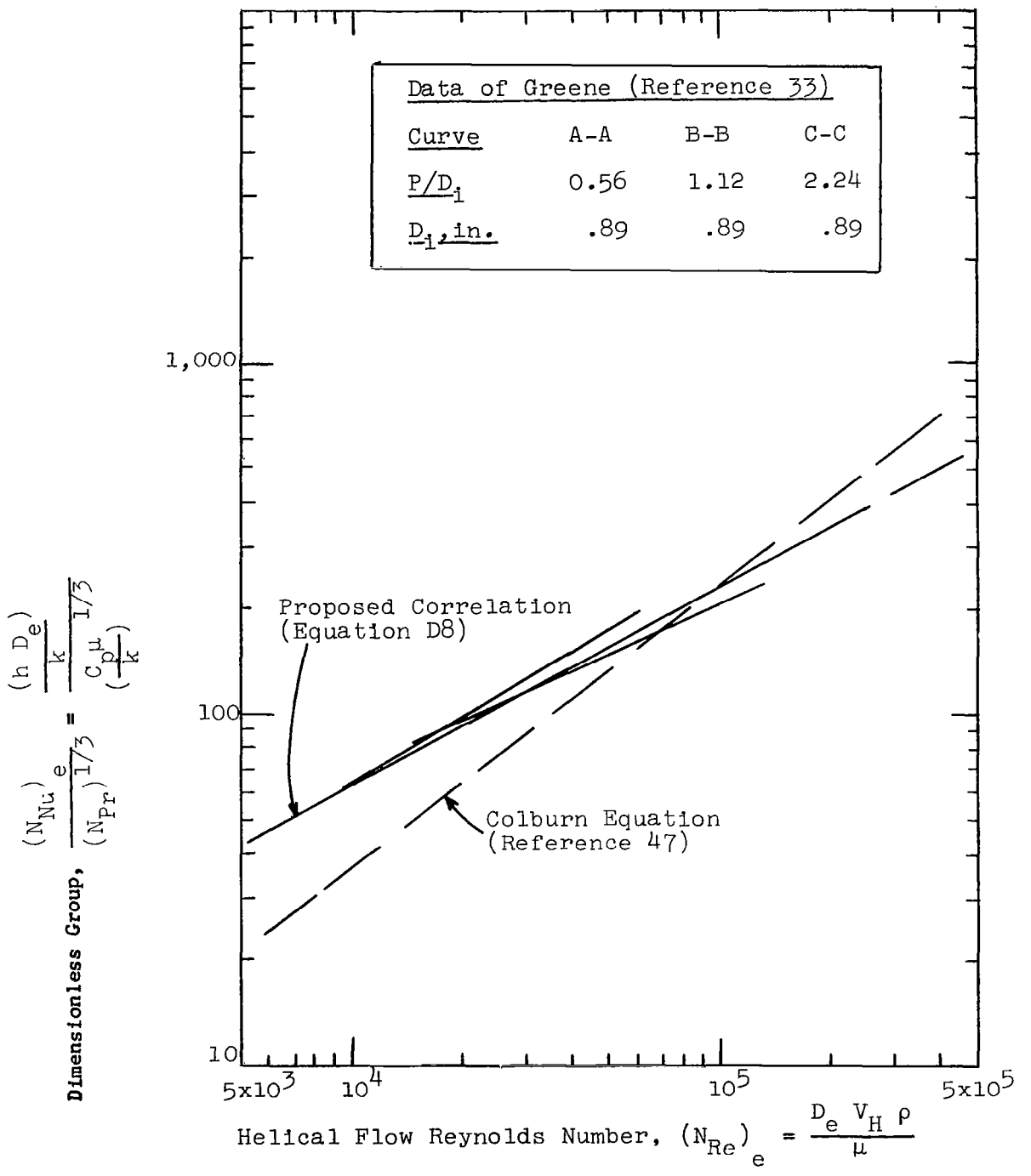

Figure 45. Correlation of Helical Flow Water Heat Transfer Data of Greene (Reference 33) Using Helix Parameters

APPENDIX E

Thermal Design Procedures For "Once-Through" Forced Convection Potassium Boilers

The local and average thermal design procedures, given in this Appendix, require fixed values of the following parameters for each thermal design point calculated:

Total Thermal Power
Potassium Inlet Temperature
Potassium Exit Temperature and Pressure
Primary Fluid Inlet Temperature
Primary Fluid Temperature Change (or Flow Rate)
Boiler Tube Diameter and Wall Thickness
Number of Tubes and Tube Material
Tube Spacing
Insert Twist Ratio and Configuration

For each set of fixed parameters, the boiler tube length required to meet the specified conditions is provided by the thermal design calculational procedures. Each fixed variable can be studied parametrically to determine its effect upon the required tube length and resulting boiler weight, thereby providing information which can be used with similar information from other components of a space power system for optimization of the system. The insert twist ratio is almost entirely determined by the boiler specifications alone, since the relatively small variations in boiler pressure drop in the working fluid caused by changes in twist ratio have little effect upon the system. The optimum boiler tube diameter and number of tubes are partially determined by boiler weight and reliability considerations and also partially determined by system requirements regarding boiler shape. The tube spacing is set by boiler weight and the system weight penalties paid for primary fluid boiler pressure drop. The primary fluid temperature change is determined by an

optimization of the reactor and boiler pressure losses in relation to their weights with respect to the weight and power requirements of the primary pump. The primary fluid boiler inlet temperature is determined by the reactor temperature limitations.

Local Thermal Design Procedure

A local calculational procedure, proceeding from the known conditions at the potassium exit end of the boiler, provides the local temperature distributions in both the primary and secondary fluids, the local heat flux distribution and the required tube length for the specified operating conditions. This is accomplished through a solution of general thermal and hydraulic equations over successive increments (Δz) of the tube length. The length of the increments can be set according to the accuracy required. Positive length along the boiler tube (z) is in the direction of potassium flow and heat added to the potassium is taken as positive. The incremental change (Δ) in a parameter is the potassium downstream value minus the upstream value. The subscript (i) denotes upstream values and the subscript (i + 1) denotes downstream values. Parameters without subscripts are averaged over the length increment. The general equations are as follows:

HEAT TRANSFER

$$q'' = U\,(T_p - T_K) \tag{E1}$$

$$\Delta Q = q''\,\pi\,D_i\,\Delta z \tag{E2}$$

PRESSURE LOSS

$$\Delta P_K = \Delta P_{KM} + \Delta P_{KF} \tag{E3}$$

$$\Delta T_K = \Delta P_K \left(\frac{dT_K}{dP_K}\right)_{sat} \tag{E4}$$

The parameter $\left(\frac{dT_K}{dP_K}\right)_{sat}$ is the derivative of temperature with respect to the pressure for the potassium in thermodynamic equilibrium at saturation. Equation (E4) is used only in two-phase regions.

ENERGY BALANCE

$$\Delta T_p = \frac{\Delta Q}{W_p C_p} \tag{E5}$$

$$\Delta x = \frac{\frac{\Delta Q}{W_K} - \Delta T_K C_{Kf} - \frac{\Delta \bar{V}_{Hg}^2}{2Jg_c}}{h_{fg}} \tag{E6}$$

$$\Delta T_K = \frac{\Delta Q}{W_K C_{Kf}} \tag{E7}$$

$$\Delta T_K = \frac{\Delta Q}{W_K C_{Kg}} \tag{E8}$$

Equation (E7) is used only in the subcooled liquid region and Equation (E8) is used only in the superheated vapor region.

The overall heat transfer coefficient U is given as follows in terms of the primary fluid heat transfer coefficient (h_p), the boiler tube thermal conductivity (k_w) and the potassium heat transfer coefficient (h_k):

$$U = \left\{ \frac{1}{\frac{D_o}{D_i} h_p} + \frac{D_i \ln\left(\frac{D_o}{D_i}\right)}{2k_w} + \frac{1}{h_k} \right\}^{-1} \tag{E9}$$

The prediction of Dwyer and Tu (Reference 54) given following, is recommended for computation of the primary fluid heat transfer coefficient under conditions of parallel flow in tube bundles.

$$\frac{h_p D_{es}}{k_p} = 0.93 + 10.81\,(P/D)_t - 2.01\,(P/D)_t^2 + .0252\,(P/D)_t\,(N_{Pe})_p^{0.8} \qquad \text{(E10)}$$

The potassium heat transfer coefficient and the expressions for the potassium pressure drop are different for the various regions of the boiler tube. In the superheated vapor region, the recommended prediction for the heat transfer coefficient is given by equation (E11), which is derived from available single phase helical insert heat transfer data in Appendix D.

$$\frac{h_v D_e}{k_g} = 0.359 \left[\frac{D_e V_H \rho_g}{\mu_g}\right]^{0.563} (N_{Pr})_g^{1/3} \qquad \text{(E11)}$$

There is a momentum pressure loss in the superheated vapor region due to density change, as given following:

$$\Delta P_{MSH} = -\frac{\left[G_{KH}\right]^2}{g_c}\,\Delta\left(\frac{1}{\rho_g}\right) \qquad \text{(E12)}$$

The following prediction, derived in Appendix D from water pressure drop data with inserts, is recommended for calculation of the frictional pressure loss in the superheated vapor region.

$$\Delta P_{FSH} = -f_{eg}\,\frac{\Delta z}{D_e}\,\frac{(G_K)^2}{2\rho_g g_c}\,\left(\frac{L_H}{L}\right)^3 \qquad \text{(E13)}$$

The friction factor f_e is defined in Appendix D.

The potassium heat transfer coefficient in the transition boiling region can be calculated from the correlation developed from the experimental data in Section V as follows:

$$h_{KTB} = h_v \left[1 + \frac{2.55 \times 10^5 \, (1 + a_R)^{1/5} \, \left(\frac{x}{1-x}\right)^{0.7}}{(\Delta T_{TB})^2} \right] \qquad \text{(E14)}$$

The nucleate boiling coefficient is indicated by the available data to be large and thus is a small portion of the thermal resistance in the nucleate boiling region. Therefore, it can be taken as constant with little error. A value of the nucleate boiling heat transfer coefficient (h_{NB}) of 10,000 Btu/(hr-ft^2-°F) was assumed for the example boiler design presented in this report.

The expressions recommended for the computation of the boiling pressure losses are the same for both the nucleate boiling region and the transition boiling region. The frictional pressure drop in both regions is given by equation (E15), where Ø is the local two-phase frictional pressure gradient multiplier, obtained from the curves shown in Figure 2 at the local temperature and quality.

$$\Delta P_{FTP} = - f_{ef} \frac{\Delta z}{D_e} \frac{(G_K)^2}{2 \rho_f g_c} \left(\frac{L_H}{L}\right)^3 \phi \qquad \text{(E15)}$$

The momentum pressure loss in both the nucleate and transition boiling regions is given by equation (E16), which is derived in Reference 11 from the analysis of Converse (Reference 6). It is recommended that the square root of the fluid-to-vapor density ratio be used for the slip ratio (K), since this was the procedure employed in the reduction of the experimental two-phase pressure loss data presented in Section V.

$$\Delta P_{MTP} = - \frac{\Delta x (G_K \frac{L_H}{L})^2}{\rho_g g_c} \left\{ \left[1+x(K-1) \right] \left[\frac{1}{K} - \frac{\rho_g}{\rho_f} \right] + \left[(1-x) \frac{\rho_g}{\rho_f} + \frac{x}{K} \right] \left[K-1 \right] \right\} \qquad \text{(E16)}$$

At the present there is no prediction available for the liquid potassium heat transfer coefficient applicable to a tube containing a helical insert. As discussed previously, however, the magnitude of the liquid potassium heat transfer coefficient has very little influence on the size of a once-through boiler, due to the small fraction of the total power transferred in the liquid region and the large temperature differences available in the region. An approximate prediction of the liquid coefficient magnitude is therefore satisfactory. The equation given by Rohsenow (Reference 57) for liquid metal heat transfer coefficients without inserts is recommended. The work of Stein (Reference 59), however, indicates that liquid metal heat transfer coefficients considerably lower than predicted by equation (E17), or other relations, can be obtained under certain conditions in a two-fluid heat exchanger. Stein's analysis should be considered if the length of the liquid region in a particular boiler design is significant, which is not usually the case for once-through boilers with saturated or superheated vapor conditions at the exit. Rohsenow's equation is:

$$\frac{h_f D_e}{k_f} = 6.7 + 0.0041 \left(N_{Pe}\right)_f^{0.793} e^{41.8 \left(N_{Pr}\right)_f} \qquad \text{(E17)}$$

It is pointed out that the value of the liquid heat transfer coefficient can be increased significantly, if necessary, by employing tubular inserts in the subcooled heating region in order to form an annulus. The proper diameter (D_e) to use in equation (E17) for an annulus is the equivalent diameter of the annulus, which is twice the annular gap. As can be seen from equation (E17), reduction of the annular gap in such an arrangement increases the liquid heat transfer coefficient.

The pressure drop in the subcooled liquid region does not significantly affect the thermal design. If desired, the liquid pressure drop may be computed from equation (E13), employing liquid rather than vapor properties. The momentum pressure drop in the liquid region may be neglected.

The local calculational procedure yields local heat fluxes, local potassium temperature and pressure and local potassium vapor quality as a function of distance along the boiler tube. The change from the heat transfer and pressure loss equations applicable to the superheated vapor region to those appropriate for the transition boiling region is made when the calculated local potassium vapor quality is 1.0.

The change from use of the transition boiling heat transfer coefficient to use of the nucleate boiling heat transfer coefficient is made when the local heat flux is equal to the critical heat flux calculated from the local quality with equation (E18) following, which is the critical heat flux correlation established from the experimental potassium data in Section V.

$$q''_c = \frac{(1 + a_R)^{\frac{1}{4}} \, 10^6}{1 + 2\left(\frac{x}{1-x}\right)} \, , \quad \frac{\text{Btu}}{\text{hr-ft}^2} \qquad \text{(E18)}$$

The equations appropriate to the subcooled heating region are substituted for the equations appropriate to the nucleate boiling region when the local vapor quality is equal to 0. The thermal design calculations for a particular case are completed when the local potassium temperature yielded by the incremental calculations in the subcooled heating region is equal to the specified potassium temperature at the boiler inlet. The total boiler length is the sum of the incremental lengths Δz.

Design Procedure Employing Average Parameters

The average potassium heat transfer coefficients and pressure drop multipliers can be employed for boiler designs having tube lengths, tube material and wall thickness, primary fluids, boiling pressure losses and helical inserts different from those tested if reasonable judgement is employed. It is recommended that the radial acceleration developed by the insert be employed to generalize the

average heat transfer coefficients, since this parameter is indicated to be significant with respect to the local data obtained. This implies tighter insert twist ratios at low mass velocities and higher boiling temperatures, since the radial acceleration decreases both with decreasing mass velocity and increasing temperature. Figure 46 shows the average boiling heat transfer coefficients at 100% potassium exit quality (obtained from Figures 18, 20, 21, 22 and the additional data in Appendix B) plotted versus the radial acceleration developed by the inserts utilized. An exact correlation is not obtained, since the heat transfer coefficient plotted is averaged over the nucleate and transition boiling regions, which are affected differently by the various variables. Trends with temperature, insert twist ratio and tube diameter are indicated in the data, as discussed in Section V; thus a design line closest to the conditions of a specific application should be selected. Above an acceleration of 80 g's however, the data lie between approximate values of 3,000 Btu/(hr-ft^2-°F) and 6,000 Btu/(hr-ft^2-°F) for the average coefficient, which is within $\pm$ 33% of a mean value of 4,500 Btu/(hr-ft^2-°F), as indicated by the design range shown in Figure 46.

Figure 46, is recommended, in conjunction with the integrated Martinelli two-phase frictional pressure drop multipliers of Figure 33, for calculation of the length required in the 0 to 100% vapor quality region of a once-through boiler. The superheat and liquid regions of the boiler can be sized separately, employing conventional single phase design procedures. The same general equations employed in the local design procedure are applicable, except they are applied over three increments: the subcooled heating length, the 0-100% quality boiling length, and the vapor superheating length. The average boiling potassium heat transfer coefficients and integrated Martinelli friction pressure loss multipliers are used in the boiling region; the equations in the subcooled heating and superheated vapor regions remain the same as in the local design procedure.

The design procedure based upon the average heat transfer coefficient is less complex than the local procedure but is also more limited. In particular, it should not be employed at average boiling heat fluxes above those obtained experimentally, approximately 200,000 Btu/(hr-ft^2) at the conditions represented by Figure 46. Application of the average boiling heat transfer coefficient data at heat fluxes higher than those obtained experimentally would result in an actual boiler performance that would be lower than predicted using Figure 46, due to early onset of the critical heat flux.

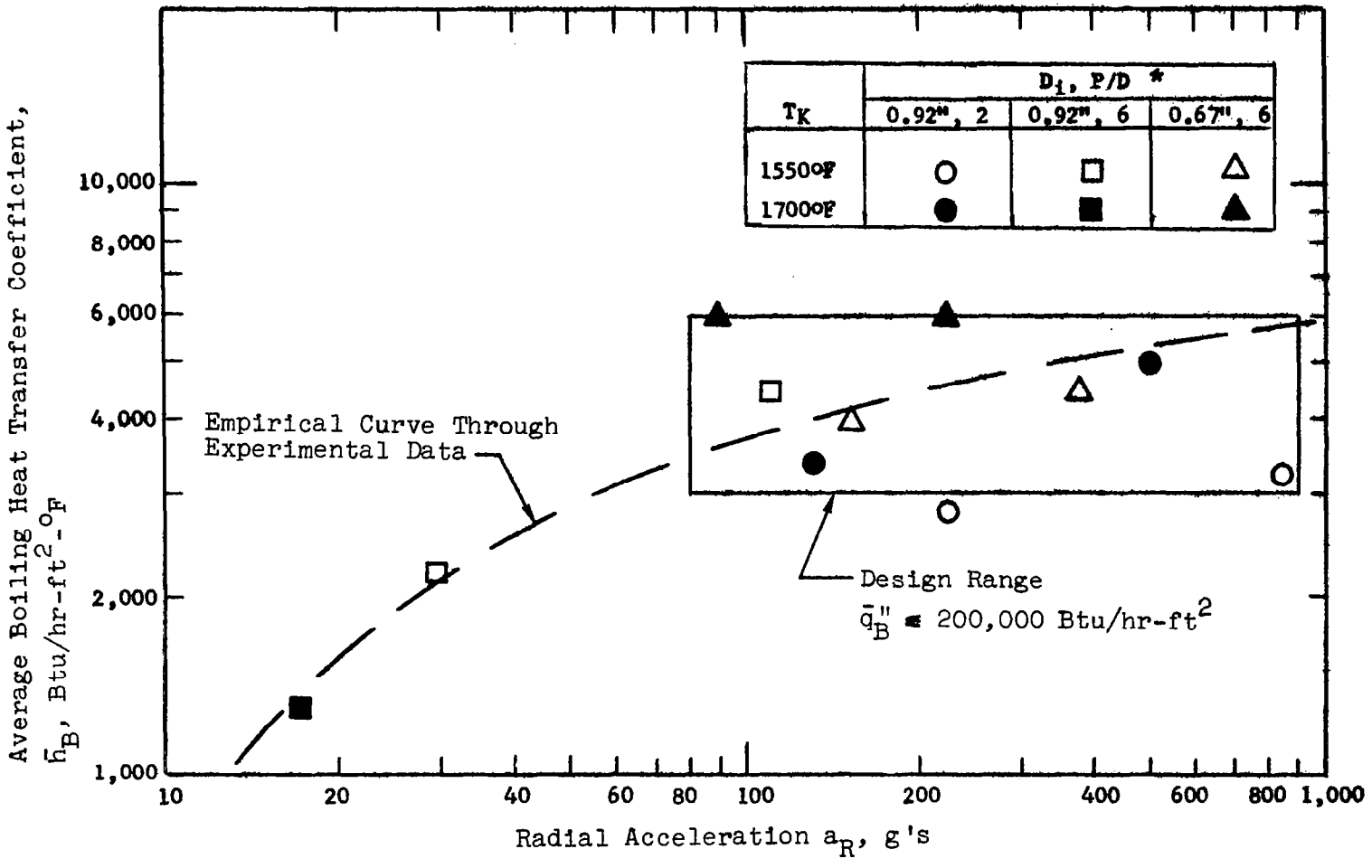

Figure 46. Potassium Heat Transfer Coefficients Averaged Over Boiling Length From 0 to 100% Quality As Function of Radial Acceleration Developed By Helical Insert

* 100% exit quality was not achieved for test sections without inserts.

BIBLIOGRAPHY

1. Brooks, R.D., "Alkali Metals Boiling and Condensing Investigations", Volume I, Final Report, Contract NAS 5-681, SPPS, MSD, General Electric Company, June, 1964, NASA CR-54050.

2. Longo, J., "Alkali Metal Boiling and Condensing Investigations", Quarterly Progress Report No. 1, Contract NAS 3-2528, SPPS, MSD, General Electric Company, September 30, 1962.

3. Longo, J., "Alkali Metal Boiling and Condensing Investigations," Quarterly Progress Report Numbers 2 and 3, Contract NAS 3-2528, SPPS, MSD, General Electric Company, April 20, 1963.

4. Longo, J., "Alkali Metal Boiling and Condensing Investigations", Quarterly Progress Report No. 4, Contract NAS 3-2528, SPPS, MSD, General Electric Company, July 25, 1963.

5. Longo, J., "Alkali Metal Boiling and Condensing Investigations", Quarterly Progress Report No. 5, Contract NAS 3-2528, SPPS, MSD, General Electric Company, January 6, 1964.

6. Longo, J., "Alkali Metal Boiling and Condensing Investigations", Quarterly Progress Report No. 6, Contract NAS 3-2528, SPPS, MSD, General Electric Company, April 20, 1964, NASA CR 54037.

7. Tippets, F.E., "Alkali Metal Boiling and Condensing Investigations", Quarterly Progress Report No. 7, Contract NAS 3-2528, SPPS, MSD, General Electric Company, April 20, 1964, NASA CR 54038.

8. Tippets, F.E., "Alkali Metal Boiling and Condensing Investigations", Quarterly Progress Report No. 8, Contract NAS 3-2528, SPPS, MSD, General Electric Company, October 20, 1964, NASA CR 54138.

9. Tippets, F.E., Converse, G.L., "Alkali Metal Boiling and Condensing Investigations", Quarterly Progress Report No. 9, Contract NAS 3-2528, SPPS, MSD, General Electric Company, October 20, 1964, NASA CR 54215.

10. Tippets, F.E., Converse, G.L., "Alkali Metal Boiling and Condensing Investigations,"Quarterly Progress Report No. 10, Contract NAS 3-2528, SPPS, MSD, General Electric Company, January 20, 1965, NASA CR 54308.

11. Tippets, F.E., Converse, G.L., "Alkali Metal Boiling and Condensing Investigations", Quarterly Progress Report No. 11, Contract NAS 3-2528, SPPS, MSD, General Electric Company, April 23, 1965, NASA CR 54405.

12. Tippets, F.E., Converse, G.L., "Alkali Metal Boiling and Condensing Investigations", Quarterly Progress Report No. 12, Contract NAS 3-2528, SPPS, MSD, General Electric Company, July 23, 1965, NASA CR 54739.

13. Tippets, F.E., Ferguson, D.R., "Alkali Metal Boiling and Condensing Investigations", Quarterly Progress Report No. 13, Contract NAS 3-2528, SPPS, MSD, General Electric Company, October 29, 1965, NASA CR 54890.

14. Balzhiser, R.E. "Literature Survey on Liquid Metal Boiling", Final Report, Phase I, Contract AF33(616)-8277-Item IIa, Univ. of Michigan, College of Engineering, December, 1961.

15. Collier, J.G., "A Review of Two-Phase Heat Transfer, 1935-1957", AERE Report C E/R 2496, Harwell, Berkshire, England, 1958.

16. Griffith, P. and Gouse, S.W., "Two-Phase Gas-Liquid Flow", Special Summer Program, Massachusetts Institute of Technology, July 27, 1964.

17. Parker, J.D., and Grosh, R.J., "Heat Transfer to a Mist Flow", ANL-6291, January, 1961.

18. Krakoviak, A.I., "Superheat Requirements with Boiling Liquid Metals", Proceedings of 1963 High-Temperature Liquid Metal Heat Transfer Technology Meeting, Oak Ridge National Laboratory, ORNL-3605, November, 1963.

19. Hoffman, H.W., and Krakoviak, A.I., "Convective Boiling With Liquid Potassium", Proc. of the 1964 Heat Transfer and Fluid Mechanics Institute, Stanford University Press, 1964.

20. Bergles, A.E., and Rohsenow, W.M., "The Determination of Forced Convection Surface Boiling", ASME Paper 63-HT-22.

21. Berenson, P.J., "Forced-Convection Vaporization of Potassium in a Single Tube", Technical Documentary Report No. APL TDR 64-115, November, 1964.

22. Colver, P.C., "Saturated Pool Boiling of Potassium Up to Burnout Heat Fluxes", Final Report, "Investigation of Liquid Metal Boiling Heat Transfer", Balzhiser, R.E., Director, Preliminary Final Report, Contract No. AF33(616)-8277, Univ. of Michigan, College of Engineering, October, 1963.

23. Tippets, F.E., "Critical Heat Fluxes and Flow Patterns in High Pressure Boiling Water Flows", Trans. ASME, J.Ht. Trans. 86-C, pp. 12-22, February 1964.

24. Janssen, E., and Kervinen, J.A., "Burnout Condition For Single Rod in Annular Geometry, Water at 600 to 1400 psia" GEAP-3899, February, 1963 (OTS).

25. Tippets, F.E., "Analysis of the Critical Heat Flux Condition in High-Pressure Boiling Water Flows", Trans. ASME, J. Ht. Trans. 86-C, pp. 23-33, February, 1964.

26. Bishop, A.A., Sandberg, R.O., and Tong, L.S., "Forced Convection Heat Transfer at High Pressure After the Critical Heat Flux", ASME Publication 65-HT-31, 1965.

27. Hench, J.E., "Transition and Film Boiling Data at 600, 1000 and 1400 psia in Forced Convection Heat Transfer to Water", GEAP-4492, February, 1964 (OTS).

28. Hench, J.E., "Forced Flow Transition Boiling Experiments in a Two-Rod Test Section at High Pressures", ASME Publication 64-WA/HT-44, 1964.

29. Polomik, E.E., Levy, S., and Sawochka, S.G., "Heat Transfer Coefficients with Annular Flow During "Once-Through" Boiling of Water to 100% Steam Quality at 800, 1100, and 1400 psia," GEAP-3703.

30. Drew, T.B., and Mueller, A.C., "Boiling", Trans. AIChE, Vol. 33, (1937) p. 449.

31. Poppendiek, H.F., et al., "Quarterly Technical Report on High Accelration Field Heat Transfer for Auxiliary Space Nuclear Power Systems", AEC Contract No. AT (04-3)-409, September 1 to November 30, 1964, Geoscience Limited, LaJolla, California.

32. Gambill, W.R., Bundy, R.D., and Wansbrough, R.W., "Heat-Transfer, Burnout, and Pressure Drop for Water in Swirl Flow Through Tubes With Internal Twisted Tapes", ORNL-2911, March 28, 1960. Also Chem. Engr. Prog. Symp. Series, Vol. 57, No. 32, 1961, pp. 127-137.

33. Gambill, W.R., and Bundy, R.D., "An Evaluation of the Present Status of Swirl Flow Heat Transfer", ORNL 61-4-61, April 24, 1961. Also ASME Paper No. 62-HT-42, 1962.

34. Viskanta, R., "Critical Heat Flux for Water in Swirling Flow", Nuclear Science and Engineering, Vol. 10, 1961, pp. 202-203.

35. Blatt, T.A., and Adt, R.R., Jr., "The Effects of Twisted Tape Swirl Generators on the Heat Transfer Rate and Pressure Drop of Boiling Freon 11 and Water", ASME Paper No. 63-WA-42, 1963.

36. Lockhart, R.W., and Martinelli, R.C., "Proposed Correlation of Data for Isothermal Two-Phase, Two-Component Flow in Pipes", Chemical Engineering Progress, Vol. 45, 1949, p. 39.

37. Martinelli, R.C., and Nelson, D.B., "Prediction of Pressure Drop During Forced-Circulation Boiling of Water," Trans. ASME, Vol. 70, 1948, p. 695.

38. Fauske, H.K., "Contribution to the Theory of Two-Phase, One-Component Critical Flow," ANL-6633, October, 1962.

39. Polomik, E.E., "Vapor Voids in Flow Systems from a Total Energy Balance," GEAP 3214, General Electric Company, August, 1959.

40. Levy, S., "Steam Slip-Theoretical Prediction from Momentum Exchange Model", Journal of Heat Transfer, Vol. 82, p. 113, May, 1960

41. Wesling, G.C., and McCarthy, M.E., "Thermodynamic Properties of Potassium Vapor from 1300°R - 2700°R - Using Naval Research Laboratory Experimental Data", GE Report R64SD3012, SPPS, MSD, General Electric Company, October 6, 1964.

42. Lyon, R.N., "Liquid Metal Heat Transfer Coefficients", Trans. AIChE, 47, pp. 75-79.

43. Haynes Stellite Corporation, "Haynes High Temperature Alloys", June, 1962.

44. Costello, C.P., and J.M. Adams, "Burnout Heat Fluxes in Pod Boiling at High Accelerations", Paper No. 30, 1961 International Heat Transfer Conference, Boulder, Colorado, August, 1961.

45. Usiskin, C.M., and R. Siegel, "An Experimental Study of Boiling in Reduced and Zero-Gravity Fields", Trans. ASME, J. Ht. Trans., 83-C pp. 243-253, August, 1961.

46. Beers, Y.F., Introduction to the Theory of Error, Addison-Wesley, Reading, Mass., 1957.

47. McAdams, W.H., Heat Transmission, McGraw-Hill, New York, 1954.

48. Poppendiek, H.F., et al., "Annual Technical Report on High Acceleration Field Heat Transfer for Auxiliary Space Nuclear Power Systems," AEC Contract No. AT (04-3)-409. September 1, 1962 through August 31, 1963, Geoscience Limited, LaJolla, California

49. Weatherford, W.D., Jr., J.C. Tyler and P.M. Ku, "Properties of Inorganic Energy Conversion and Heat Transfer Fluids for Space Applications" WADD Technical Report 61-96.

50. Gottlieb, M., and R.J. Zollweg, "Thermal Conductivity of Alkali Metal Vapors", J. Chem. Phys., Vol. 39, No. 10, (1963), p. 2773.

51. Stiel, L.I., and Thodos, G., "The Prediction of the Transport Properties of Pure Gaseous and Liquid Substances", Progress in International Research on Thermodynamic and Transport Properties, Academic Press, 1962.

52. Macbeth, R.V., "Burnout Analysis, Part 4: Application of a Local Conditions Hypothesis to World Data for Uniformly Heated Round Tubes and Rectangular Channels", AEEW-R-267, 1963.

53. Merte, H., Jr., and J.A. Clark, "Pool Boiling in an Accelerating System", ASME Paper No. 60-HT-22.

54. Dwyer, O.E., and P.S. Tu, "Analytical Study of Heat Transfer Rates for Parallel Flow of Liquid Metals Through Tube Bundles", Chem. Eng. Symposium Series, Vol. 56, No. 30, 1960.

55. Friedland, A.J., M.W. Maresca, C.F. Bonilla and O.E. Dwyer, "Heat Transfer to Mercury in Parallel Flow Through Bundles of Circular Rods," Part III International Developments in Heat Transfer, ASME, New York, 1961.

56. Borishanskiy, V.M., and E.V. Fursova, "Heat Transfer in Longitudinal Flow of Sodium Through A Bank of Tubes", Atomnoya Energiya, Vol. 14, No. 6, (1963) p. 584.

57. Rohsenow, W.M. and H.Y. Choi, Heat, Mass, and Momentum Transfer, Prentice-Hall, Inc., Englewood Cliffs, N.J., 1961.

58. Jackson, C.B., editor, Liquid Metals Handbook (Sodium-NaK Supplement), Atomic Energy Commission, Third Edition, 1955.

59. Stein, R.P., "Heat Transfer Coefficients in Liquid Metal Cocurrent Flow Double Pipe Heat Exchangers", Proceedings of 1963 High Temperature Liquid-Metal Heat Transfer Technology Meeting, Vol. 1, p. 194, ONRL-3605, 1964.

60. Bond, J.A., and Converse, C.L., "Vaporization of High-Temperature Potassium in Forced Convection At Vapor Temperatures From 1800°F To 2100°F", Topical Report, Contract NAS 3-2528, SPPS, MSD, General Electric Company, 1966.

61. Affel, R.G., Burger, G.H. and Pearce, C.L., "Calibration and Testing of 2-inch and 3½-inch Magnetic Flowmeters for High Temperature NaK Service", ORNL-2793, March 4, 1960.

"The aeronautical and space activities of the United States shall be conducted so as to contribute . . . to the expansion of human knowledge of phenomena in the atmosphere and space. The Administration shall provide for the widest practicable and appropriate dissemination of information concerning its activities and the results thereof."

—NATIONAL AERONAUTICS AND SPACE ACT OF 1958

NASA SCIENTIFIC AND TECHNICAL PUBLICATIONS

TECHNICAL REPORTS: Scientific and technical information considered important, complete, and a lasting contribution to existing knowledge.

TECHNICAL NOTES: Information less broad in scope but nevertheless of importance as a contribution to existing knowledge.

TECHNICAL MEMORANDUMS: Information receiving limited distribution because of preliminary data, security classification, or other reasons.

CONTRACTOR REPORTS: Scientific and technical information generated under a NASA contract or grant and considered an important contribution to existing knowledge.

TECHNICAL TRANSLATIONS: Information published in a foreign language considered to merit NASA distribution in English.

SPECIAL PUBLICATIONS: Information derived from or of value to NASA activities. Publications include conference proceedings, monographs, data compilations, handbooks, sourcebooks, and special bibliographies.

TECHNOLOGY UTILIZATION PUBLICATIONS: Information on technology used by NASA that may be of particular interest in commercial and other non-aerospace applications. Publications include Tech Briefs, Technology Utilization Reports and Notes, and Technology Surveys.

Details on the availability of these publications may be obtained from:

SCIENTIFIC AND TECHNICAL INFORMATION DIVISION

NATIONAL AERONAUTICS AND SPACE ADMINISTRATION

Washington, D.C. 20546